Unraveling the complex signaling behavior of neurotransmitters and their receptors in the brain

Tomasz Maciej Stepniewski

TESI DOCTORAL UPF / ANY 2019

DIRECTOR DE LA TESI

Dra. Jana Selent

DEPARTAMENT DE CIÈNCIES EXPERIMENTALS I DE LA SALUT

Maybe the real PhD is the friends we made long the way.

Acknowledgements

I would like to acknowledge funding from Fundación Instituto Mar de Investigaciones Médicas (beca predoctoral Javier Lamas Miralles).

Carrying out and writing this thesis had multiple great moments, however at the same time was a long and sometimes painful process for me as well as for my surroundings who had to listen about long rants about my inability to do anything and the bleakness of human existence in general, as such there is a lot of people to thank.

First and foremost, I would like to thank my supervisor dr Jana Selent. Who is truly extraordinary as a scientist, a mentor, and a person. She took me in when I knew really little (despite me thinking otherwise) and with patience helped me work on the worst stuff in me, while further developing the best, all the while going to great lengths whenever me or anybody else in the group needed help. Last but not least, seeing how much she pushes herself in work is always a motivation to do the same.

I would also like to thank multiple collaborators who gave me the pleasure to look at their data from a structural perspective, helped verify our hypothesis and with whom I had multiple stimulating discussions. Special thanks are due to Billy Breton, Arturo Mancini, Arun Shukla, Marta Sommer, Dimitri Veprintsev, Enrico Dainese, Mette Rosenkilde, Ulrik Henriksen, Viktorija Daugvilaite, Patrick Giguere, Johanna Tiemann and Kristoffer Sahlholm. On this note I would also like to thank the whole GLISTEN (currently ERNEST) community, especially the management body for organizing amazing meetings, where a lot of those collaborations were formed.

One thing, that really made my work here much easier is the great atmosphere I had in the group. Sometimes the world of science can feel like a cutthroat place, but here all of us were dedicated to helping each other out, and having each other's back rather than stabbing it. Everybody was extremely friendly, not making fun of my misshapen scripts and going to great lengths to make me feel included despite me being the only foreigner. During my PhD there was no government for almost a year, then the government fell down, and

finally Catalonia declared independence, but despite all of this and choppers flying constantly above our heads (one of the perks of working close to the parliament), the lab always felt like a stable place.

Special thanks are warranted for Ismael who worked with me during the lab “night-shift”, helped me get more into programming, explain to me all of the technical intricacies which I still do not understand, and is the only reason why my paperwork here is done or my thesis has a functional list of contents. Mariona always politely laughed at my awful jokes, made python a bit more accessible to me, shared #gossip as well as a time-zone with me for some time. Only thanks to her do I know who is Sara Borrell, and that she does not come from Brazil. It was always a pleasure to “talk science” with Adrian who probably was the most low-maintenance master student in history. With Maria my stay had only a very short overlap, however she always had a supportive ear for me either from Marburg or Cambridge, and our hangouts provided me with much needed emotional release. Finally, Juanma was always a welcomed guest in the evening, encouraging us to look away from the computers.

I would also like to thank Ramon, Alejandro, Aida, David, Aina, Nathalie, Alessandro and Judith. All of You put a little brick in constructing my extremely pleasant stay in this group.

I am also very gratefully for the excellent team at PRBB, Alfons and Miguel the computer magicians, Carina, Chus who helped me with a smile with all my weird grant problems, as well as the whole Intervals team, that were extremely helpful during the time I worked here.

Przed wyjazdem do Barcelony miałem przyjemność pracować w laboratorium w Polsce, w którym nauczyłem się podstaw chemii obliczeniowej. Specjalne podziękowania należą się prof. Sławomirowi Filipkowi, który zawsze okazywał mi życzliwość, wsparcie i był/jest naprawdę świetnym szefem i naukowcem, dr Ani Modzelewskiej która opiekowała się mną podczas mojej pracy magisterskiej, która jak się okazuje zostanie zakończona po pracy doktorskiej, dr Przemysławowi Miszcie, Jakubowi Jakowieckiemu, Krzysztofowi Młynarczykowi oraz Pawłowi Pasznikowi, którego stale irytowałem banalnymi technicznymi pytaniami. Słuchając wszystkim historii o okropnych laboratoriach i szefach, uważam się

za niezwykle szczęśliwego ze dwa razy trafiłem do tak sympatycznych i przyjacielskich grup.

Wyjazd za granice jest świetną lekcją tego, jak ważni w życiu są przyjaciele i znajomi. W tej kwestii, z pewnością bardzo poszczęściło mi się w życiu. Jestem absolutnie pewien, ze bez wsparcia i zrozumienia bliskich mi osób, nie byłbym w stanie dotrzeć do momentu w którym jestem. Szczególnie dziękuje (bez ustalonego porządku) Dagmarze która miała swoja równoległa Barcelońska przygodę, Kasi K., Konradowi, Piotrkowi M, Kasi Sz., Elizie, Izie, Marcie K oraz wszystkim znajomym z CNK (tak Magda i Martyna, głównie mowa o was), Julce, Dorocie, Radkowi, Marcie D wraz z żona, Rodnyemu, my fantastic flatmates Ona and Oscar oraz Oli którą poznałem pod koniec pobytu ale która stała się dla mnie jedna z bliższych osób w Barcelonie. Jeszcze raz ogromne dzięki dla wszystkich, znoszenie mojego jęczenia przez tyle czasu, zasługuje na imienne wyróżnienie. Chciałbym też wyrazić ogromna wdzięczność mojej grupie z Rasztowa oraz p Kasi, bez których nie umiałbym się sobą zajmować tak jak się zajmuje. Dziękuje także dr Annie Serafin, z którą miałem przyjemność pracować i która jest dla mnie niedoścignionym przykładem społecznika/idealisty.

Idąc chronologicznie, chciałbym podziękować mojej rodzinie. Tylko i wyłącznie dzięki ich wsparciu mogłem koniec końców wybrać cos na kształt swojej drogi życiowej. Mimo różnorakich trudnych sytuacji, jedna rzecz była niezmienna, czyli to ze stale wspieraliśmy siebie w realizacji swoich planów i marzeń. Szczególne podziękowania należą się mojej matce chrzestnej oraz cioci Teresie, mojej najlepszej nauczycielce chemii i stałemu wsparciu naszej rodziny.

Y por último, quisiera dar las gracias a Nacho, mi pololo chileno por ser tan paciente y comprensivo durante el rollecaster emocional de mi doctorado, soportandome cuando fui la persona más insoportable en mi vida - este tiempo cuando estaba escribiendo mi tesis, llorando y gritando "soy un fracaso humano " cada 10 min. Además quiero agradecer a la familia de Nacho y todos sus amigos, que a pesar de todas mis peculiaridades y de mi deformado castellano, siempre me tratan con amabilidad y me hacen sentir bienvenido.

Abstract

G protein-coupled receptors (GPCRs) are the main acceptors of neurotransmitters, and thus play an important role in communication between neurons. Because of this they are an attractive drug target for multiple neurodegenerative and neuropsychiatric disorders.

The primary function of GPCRs is to initiate diverse intracellular signaling cascades in response to extracellular events, like neurotransmitter binding. Despite the wealth of available biochemical data, the structural foundations of GPCR activity remain poorly understood. Such insights would not only expand our knowledge of those receptors, but also facilitate the design of safer and more efficient drugs.

Here, using several computational approaches, we propose structural mechanisms that explain GPCR in vitro data. We unravel features GPCR functionality at multiple levels of action including ligand-receptor interactions, allosteric signal transmission as well as post-translational modifications. Our results identify phenomena potentially conserved among GPCRs that advance our understanding of this relevant receptor family.

Resumen

Los receptores acoplados a proteína G (en ingles GPCRs) son los principales receptores de neurotransmisores, teniendo un papel importante en la comunicación neuronal. Por esto, se los considera una atractiva diana farmacológica en múltiples trastornos neurodegenerativos y neuropsiquiátricos.

El rol primario de los GPCRs es iniciar múltiples cascadas de señalización intracelular en respuesta a eventos extracelulares. A pesar de la vasta información bioquímica disponible, los fundamentos estructurales de la actividad de GPCRs no se comprenden totalmente. Estos fundamentos, no sólo podrían expandir nuestro conocimiento de los receptores, sino que podrían facilitar el diseño de farmacos más seguros y eficaces.

Utilizando varios enfoques computacionales, proponemos mecanismos estructurales que explican los resultados in vitro de los GPCRs. Desciframos elementos de la funcionalidad de GPCRs en múltiples niveles, incluyendo interacciones ligando-receptor, transmisión de señales alostérica y modificaciones post-traduccionales. Nuestros resultados identifican fenómenos potencialmente conservados entre los GPCRs, ampliando nuestro conocimiento de esta relevante familia de receptores.

Prologue

Recent years have dramatically expanded our knowledge about neurotransmission, and multiple proteins that mediate this complex process. Among them, one of the most important players are G protein-coupled receptors (GPCRs), a family of transmembrane receptors that in response to extracellular stimuli initiate intracellular signaling cascades. GPCRs in the brain are among the main targets of neurotransmitters, enabling communication between billions of neurons. As such they present an exciting gateway to better understand the functionality of the central nervous system and in a larger scheme treat multiple neuropsychiatric and neurodegenerative disorders. Interestingly, despite variation in sequence, the GPCR structural fold is highly conserved, and as such functional insight from one receptor is likely transferable to others.

One of the remarkable features of GPCRs is the diversity of the signaling responses they can initiate. A single receptor interacts with multiple downstream intracellular partners, each linked to a different physiological effect. Such interaction promiscuity is possible due to the flexibility of GPCRs and their ability to assume multiple conformations, each with different affinity towards downstream effectors. The specific receptor conformation is governed by an intrinsic allosteric communication network and depends on multiple factors like the bound ligand, the membrane environment or post-translational modifications. A structural understanding how those factors contribute to the GPCR structure and signaling response would shed more light on the functionality of this family of receptors, as well as the process of neurotransmission. For this it is necessary to employ methods that not only can visualize the GPCR structure at a high resolution, but also follow it´s dynamic fluctuations for extended periods of time.

In this thesis we combined *in silico* methods with *in vitro* results to interrogate structural features of GPCR function, focusing on receptors involved in neurotransmission.

First, combining data from enhanced sampling techniques, live-cell bioassays and mutagenesis, we dissected the structural features of dopamine signaling (**publication 3.1**). The obtained data allowed us

to identify an interaction pattern within the dopamine 2 receptor, linked to specific recruitment of downstream effectors. Furthermore, the discovered mechanism, appears to be conserved amongst other monoaminergic receptors.

In the next part of this thesis, we study allosteric communication in the δ-opioid receptor, trying to rationalize how several mutations, distributed near the sodium allosteric binding site, induce alter the signaling response of antagonist naltrindole (**publication 3.2**). Using multiple short simulations, we are able to identify structural events that appear to be linked to a specific response, as well as are in line with NMR data,

In the next part, we studied GPCRs at the level of interactions with intracellular proteins. Specifically, we investigated how the unique phosphorylation pattern of the intracellular C-tail contributes to the recruitment and signaling behavior of an important downstream effector – β-arrestin (**publication 3.3**). By using classical molecular dynamic simulations, we were able to decipher how a distinct change in the phosphorylation pattern results in the change of β-arrestin structure, which can be linked to an altered signaling response

Lastly, we investigated the impact on palmitoylation of the cannabinoid receptor 1 on its trafficking and function (**publication 3.4**). Our results show that this modification stabilizes distinct parts of the receptor, possibly facilitating interactions with caveolin 1. Furthermore, this modification promotes the interaction between the receptor and cholesterol, which can explain why the palmitoylated receptor is primarily found in cholesterol-rich lipid rafts.

All in all in this thesis, we expand the understanding of GPCR involved in neurotransmission. The combination of *in vitro* and *in silico* data provides important insight on the signaling of this family on multiple levels of action.

List of contents

Chapter 1
Introduction

1.1. Neurotransmitters and their receptors in the brain

The function of the brain is dependent on the communication of billions of neurons connected to each other in complex circuits. Neurons maintain a voltage gradient along their membrane, which predisposes them to their role in receiving and propagating signals. In response to extracellular stimuli the neuronal membrane can become hyper- or depolarized. Local depolarization, if strong enough, creates a depolarization wave called the action potential that is propagated across the cell. In response to such an event, the neuron can initiate its own signaling mechanisms to affect the behavior of other cells including other neurons, myocytes or cells forming endocrine organs.

Information exchange between neurons occurs at cell interfaces called synapses. Neuronal synapses can be divided into two groups:

- electrical synapses in which two neurons are physically connected through protein complexes, called gap-junctions. In such a synapse, the electrical current is passed from one neuron to another, and the resultant communication is bidirectional.[1]

- chemical synapses that depend on the release and recognition of chemical molecules (neurotransmitters) in the synaptic cleft, which modify the physiology of the pre- and postsynaptic terminal.[2] Thus in such a synapse, the electrical signal is briefly transformed into a chemical one. These synapses are unidirectional and typically slower than electrical synapses. In mammals this is the main type of synapse in the brain.[3]

Neurotransmitters are diverse in their structure as well as in mediated physiological processes. These molecules are primarily stored in vesicles in the presynaptic terminal. In response to depolarization of the neuron, the vesicles fuse with the membrane, releasing stored neurotransmitters into the synaptic cleft. Similarly to synapses, those molecules can be grouped into several subtypes[4]:

- classical neurotransmitters which are small molecules and include molecules like the γ-butyric acid, glycine and acetylcholine

- monoamine neurotransmitters, that contain a charged amino group and include molecules like dopamine, adrenaline, noradrenaline, serotonin and histamine

- neuropeptides, which are easily the biggest and most structurally diverse group of neurotransmitters

- membrane permeable neurotransmitters like cannabinoids or nitric oxide, which are not stored in presynaptic vesicles, but rather synthesized and released directly in response to neuron depolarization

The presynaptic terminal possesses an active re-uptake mechanism for classical neurotransmitters, where there is no such mechanism for neuropeptides.[5] The action of neurotransmitters is dependent on their recognition by two types of membrane receptors: ionotropic receptors or metabotropic receptors.

Ionotropic receptors (or ligand-gated ion channels) form a permeable pore in the post-synaptic membrane. In response to neurotransmitter binding, they undergo a structural rearrangement, allowing the flow of ions through the now open channel, consequently altering the voltage potential of the membrane.[6]

The function of metabotropic receptors is more complex (Fig. 1). In response to neurotransmitter binding they initiate downstream signaling cascades that affect the post-synaptic as well as to a lesser degree the presynaptic cell. Those cascades frequently culminate in changing the membrane potential. However, they are not limited to this outcome as they also affect multiple aspects of the cell physiology like gene transcription[7] or the cytoskeletal architecture.[8] This receptor group includes proteins like guanyl cyclases, tyrosine kinases and G protein-coupled receptors (GPCRs).[9]

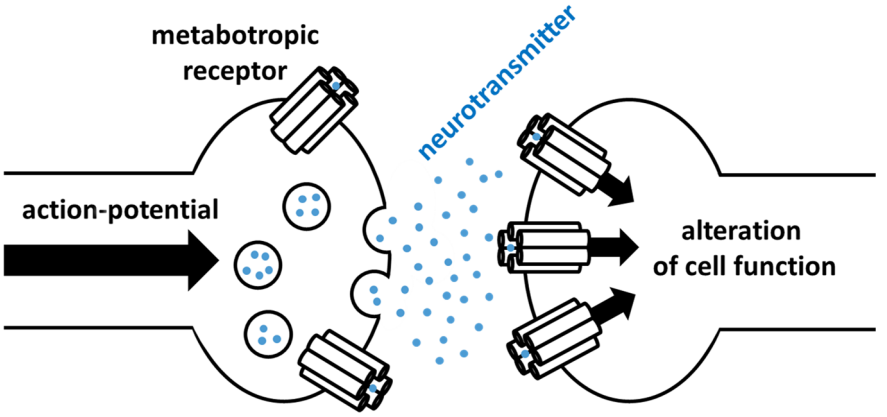

Figure 1 A schematic representation of metabotropic receptors in the synapse In the figure we present a general model of neurotransmission mediated by metabotropic receptors

Out of all the metabotropic receptors, GPCRs are the class with most experimental data, and conversely the greatest amount of open research questions.

1.2. G protein-coupled receptors

GPCRs are the largest family of membrane proteins in the human genome, with over 800 known members.[10] Their primary function is to react to extracellular chemical or physical stimuli, and in response initiate intracellular signaling cascades, which alter the cell physiology. Although, GPCR primarily exist in the cell-membrane, functional GPCRs have been also found in the nucleic and mitochondrial membranes, as well as in the endoplasmic reticulum.[11]

Despite sequence variability, all GPCRs share a common structural fold, which consists of seven transmembrane (TM) α-helixes connected with extracellular and intracellular loops. The residues directly after TM7 adopt the structure of an amphipathic helix, localized in the interface between the membrane and the cell environment. Posterior residues often adopt a disordered polar C-terminal tail of varying length (Fig. 2).[12]

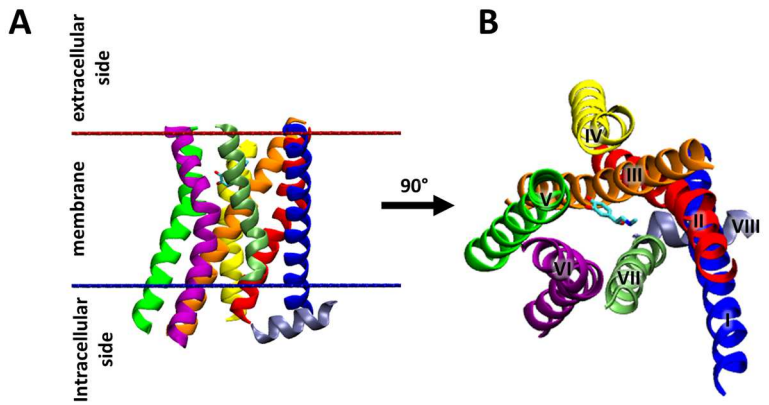

Figure 2 The conserved GPCR structural fold
In panel A we show the structure of the β2-adrenergic receptor in complex with noradrenaline (PDB code: 4LDO). For clarity we occult non-helical fragments of the receptor. The conserved transmembrane helixes are labelled using roman numerals, noradrenaline is depicted in licorice. The placement of the membrane is delimited with red (extracellular side) and blue (intracellular side) dots. In panel B we show the same structure, rotated by 90° in the X-axis and enlarged. This allows to better appreciate the localization of noradrenaline within the receptor.

Based on sequence similarity, GPCRs can be classified into six classes, ranging from A to F, with class A being by far the largest and encompassing most of the GPCRs involved in neurotransmission.[13] Although research efforts have focused on studying those receptors in humans, GPCRs or GPCR-like proteins are expressed in multiple eukaryotic organisms, not just in animals but also plants[14], fungi[15] and even single-cell organisms.[16]

In humans GPCRs are present in almost every type of cell and are involved in the regulation of most know physiological processes. As such they are attractive drug targets, with over 30% of currently available drugs targeting this family of receptors.[17] In fact, when looking at drugs sales per target, GPCRs are among the top 20 proteins with the highest number of sales(Tab. 1).[18]

Receptor	2011-15 sales in USA [$]	Examples of drugs	Main location in the body	Natural agonist
angiotensin receptor 1	100 billion	valsartan, olmesartan	blood vessels, smooth muscles	peptide hormone
β2-adrenergic receptor	90 billions	salmeterol, salbutamol	lungs, heart	monoamine neurotransmitter
μ-opioid receptor	88 billions	oxycodone, fentanyl	brain	peptide neurotransmitter
dopamine 2 receptor	75 billions	aripiprazole, quetiapine	brain	monoamine neurotransmitter
muscarinic receptors	64 billions	tiotropium, solifenacin	brain	classical neurotransmitter
serotonin 2A receptor	58 billions	aripiprazole quetiapine	brain	monoamine neurotransmitter
histamine 1 receptor	54 billions	olopatadine cetirizine	smooth muscles brain	monoamine neurotransmitter

Table 1 Drugs targeting GPCRs are a significant part of the medical market Above we show GPCR targets extracted from the list of top 20 protein targets according to drug sales[18]

Some GPCRs have sensory functions; mediating olfaction, taste, light perception and pheromone signaling. Contrarily, non-sensory receptors mediate signaling by recognizing small peptides and other ligands. Interestingly, within non-sensory GPCRs, an excessively large number (close to 90%) are expressed within the central nervous system (CNS), primarily in the brain.[19] Considering the quantity of different GPCRs present there, it is not surprising that they are one of the most successful targets, to address CNS disorders - mainly neuropsychiatric and neurodegenerative in nature.[20] The popularity of such drugs can be underlined by their yearly sales, easily reaching billions of dollars (Tab. 1). In fact, as of now, the GPCRs targeted by most drugs are the histamine, serotonin, dopamine, adrenergic and opioid receptors, all of which are expressed primarily in the brain.[17]

1.3. Structural determinants of GPCR activity

In the majority of class A GPCRs the extracellular side of the helical bundle forms a pocket that is able to recognize and bind a diverse range of ligands. We can differentiate between three basic types of ligands: agonists which promote GPCR-dependent signaling, antagonists which do not initiate a signaling response and prevent agonist binding, and inverse agonists which lower GPCR-dependent signaling below the level of the receptor in the apo-state.[21]

To understand how a relatively small ligand can engage the whole GPCR into signaling activity, it is important to look at the receptor from a mechanistical perspective. GPCRs are not rigid structures, but rather exist in an equilibria between different conformations.[22] The binding of agonists in the orthosteric site can stabilize certain receptor conformations and/or induce local structural changes. Those induced changes are propagated and amplified by the movements of residues within the transmembrane hydrophobic core. Correlated changes in those residues alter the dynamic equilibria of the receptor, pushing it into a subset of potential conformations.[22–24] Agonist stabilized conformations, called "active", have a higher propensity to couple intracellular signaling partners, forming GPCR complexes and in turn initiating various signaling pathways within the cell.[25]

We currently know of multiple intracellular proteins that interact with GPCRs, and there is no doubt that their number will be expanding[26]. However, the most prominent ones are guanine nucleotide-binding proteins (G-proteins).[27] The majority of G-proteins are macro-complexes, consisting of three subunits called α, β and γ. One exception is the Ras family G-proteins, that consist only of the α subunit.[28] In all G-proteins, the α subunit contains an ATPase domain, and in its ground-state is bound to guanosine diphosphate (GDP).

In the canonical model of GPCR signaling, when the G-protein is bound to the receptor, a structural change is promoted in the α subunit, that induces the exchange of the bound GDP into guanosine triphosphate (GTP). This exchange stabilizes the α-subunit in a conformation with a lower affinity to the βγ-dimer, promoting the dissociation of the α-subunit, and later the βγ-dimer from the receptor. Both dissociated components interact with other proteins,

modulating their activity and propagating the agonist initiated signaling cascade.[29] Importantly, the α-subunit can exist both in the membrane and cytoplasm, while the βγ dimer is primarily membrane-bound.[30]

After some time, the inherent GTP-ase activity of the α-subunit results in the hydrolysis of the bound GTP into GDP. This mechanism can be compared to a timer, and likely protects the cell from prolonged α-subunit-dependent signaling in the absence of ligand. The GDP-bound α-subunit returns to an inactive-like conformation, regaining high-affinity for the βγ dimer. Thus the heterotrimeric G-protein is reformed, and can again bind to GPCRs in active conformations.

Studies of the human genome revealed multiple isoforms of each G-protein subunit with at least 16 different genes coding the α-subunit, 5 the β-subunit and 12 the γ-subunit (Fig 3).[31] It appears that certain subunit isoforms cannot assemble to form a G-protein. However, the shear amount of possible subunit combinations allows for the existence of multiple different G-proteins, each with potentially varying signaling properties.[32]

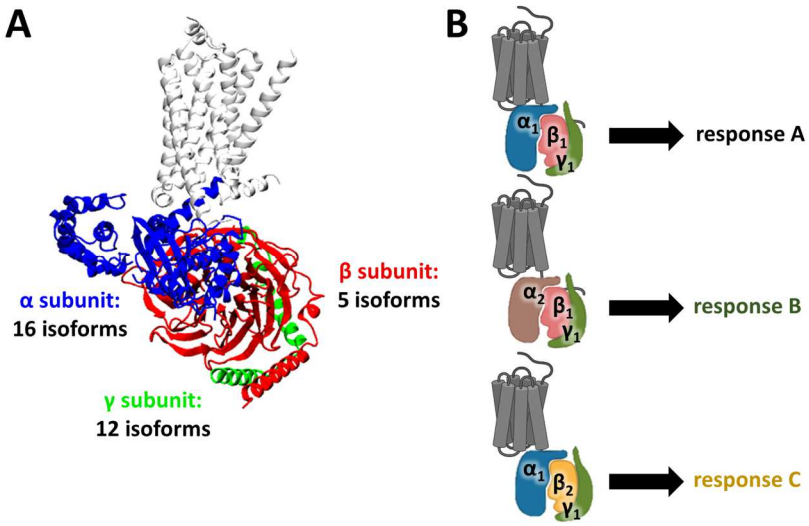

Figure 3 Diversity of G protein isoforms allows diverse intracellular responses In panel A we show the structure of the β2 adrenergic receptor in complex with a G protein (PDB code: 3SN6). The Receptor is colored in white, and different subunits of the G protein are denoted in blue, red and green. For each subunit we present the number of isoforms identified in the human genome. In panel B we schematically explain how the signaling response depends on the coupled G protein isoforms (variability of isoforms is highlighted by coloring)

Currently we possess the largest amount of data on the α-subunits. Based on sequence similarity, α-subunits can be grouped into four classes: G_s, $G_{i/o}$, G_q and $G_{12/13}$.[33] Members of all classes can overlap in their downstream effect. However, there are some functions, that are specific to each of them:

- G_s proteins stimulate the production of cyclic adenosine monophosphate (cAMP), one of the main secondary messengers related to GPCR signaling. This leads to the activation of protein kinase A[34]

- $G_{i/o}$ proteins appear to have an antagonistic function to G_s, inhibiting cAMP production[35]

- G_q stimulates the formation of two secondary messenger: inositol phosphate (IP3) and diacylglycerol. This leads to the

activation of protein kinase C, as well as the release of calcium ions from the endoplasmatic reticulum[36]

- $G_{12/13}$ primarily interact with Rho GTPases, modifying the cytoskeleton[37]

Within the presynaptic terminal G_s and G_q can be linked with neurotransmitter release (and as such signal propagation), whereas G_i acts antagonistically to G_s inhibiting this process.[38]

GPCRs after activation do not permanently remain in the same conformation, and after some time the ligand dissociates, and the receptor returns to a state, where it no longer binds G-proteins. However, the cell uses mechanisms to attenuate G-protein coupling much before this natural inactivation occurs. After varying amounts of time, the active receptor is phosphorylated on the C-terminal tail and intracellular loops by G protein receptor kinases (GRK).[39] This modification promotes the coupling of another family of proteins – the arrestins[40] (named so because of their ability to "arrest" GPCR activity). Arrestins first form a low-affinity complex with the GPCR, which later rearranges to a high-affinity complex where arrestin is tightly bound to the receptor core.[41] The interaction of arrestin with GPCRs primarily leads to the desensitization and internalization of those receptors, preventing excessive G-protein dependent signaling.

Apart from their canonical function, arrestins can also serve as signaling scaffolds, forming a surface that facilitates contacts between certain proteins. This function promotes the activity of multiple proteins, among which are mitogen-activated protein kinases (MAPK), tyrosine kinases (discussed here previously for their metabotropic receptor function), and multiple phosphatases.[42] However, it is still under debate which of those pathways are independent of G-protein coupling.[43]

In contrast to the diversity of G-proteins, only four types of arrestin have been identified up to date. Furthermore, two of those types exist exclusively in the visual system. Arrestin-1 and arrestin-4 are primarily expressed in the rod and cone cells respectively, and involved in photoreception.[44] GPCRs not involved in sight (including those involved in neurotransmission), are regulated by β-arrestin 1 and 2.[45]

All in all, it can be considered that GPCRs are in a constant equilibrium between signaling and inactivity, and this equilibrium is maintained by ligand binding as well as interaction with multiple downstream effectors (Fig. 4).

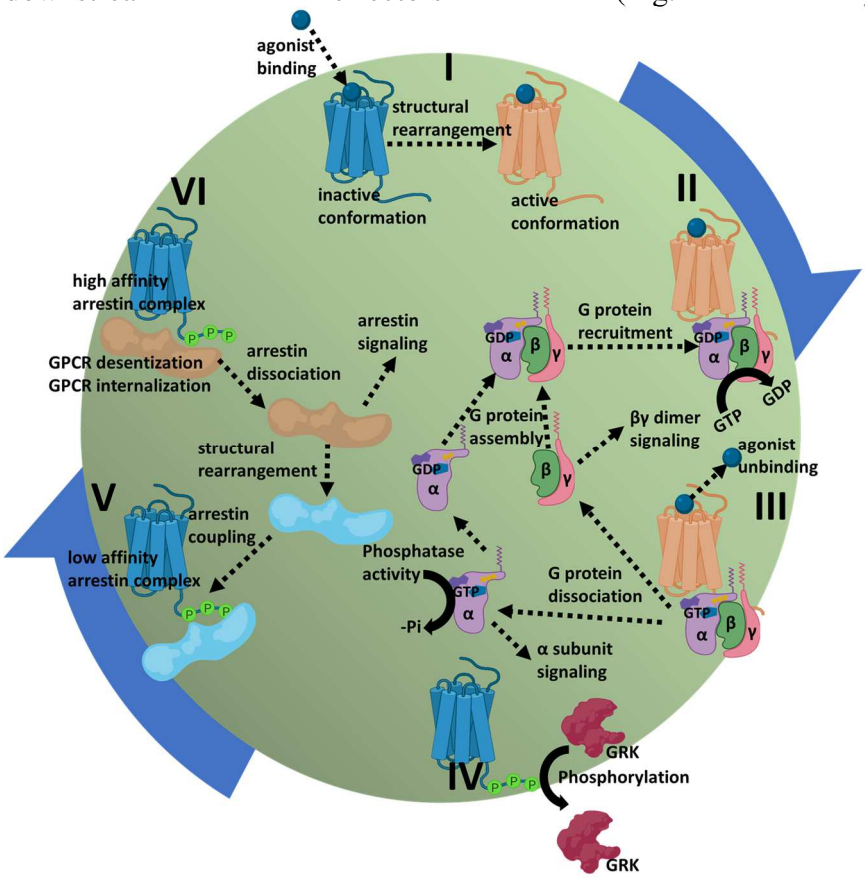

Figure 4 The canonical GPCR signaling cycle
Above we present a simplified representation of the GPCR activity within the cell. The subsequent steps GPCR functional states are denoted in roman numerals.

1.4. GPCR-regulated pathways in the brain

As mentioned before GPCRs are one of the main mediators of neurotransmission. These proteins in contrast to ionotropic receptors depend on the formation of secondary messengers to modulate neuron function. As such, their response is usually slower than ionotropic receptors. However, the response mediated by metabotropic receptors is amplified within the cell, and because of

this produces more long-lasting effects in the neural system. In this sense, binding of neurotransmitters to ionotropic receptors is primarily involved in fast reactions like reflexes, while GPCRs participate in "higher" brain functions, like love[46], mood[47], fear[48] and cognitive functions.[49]

Neurons are limited to the types of neurotransmitters they release or react to. Cells processing the same neurotransmitter are organized in systems e.g. the dopamine, noradrenaline or serotonin system. Each one is present in different structures of the brain and regulates different processes. Discussing the intricacies of those systems is beyond the scope of this work. However, for the sake of clarity I include a short discussion of neurotransmission pathways investigated in articles included in this thesis

a) Dopamine neurotransmission

Nerves expressing dopamine are the most prominent within the CNS.[50] Dopamine is recognized by five different receptor subtypes, all of which are GPCRs. D1 and D5 primarily couple to G_s and are localized post-synoptically, while D2, D3 and D4 primarily couple to G_i and are placed both in the pre- and post-synaptic terminal. Among all the receptors D1 has the highest occupancy in the brain, followed by D2.[51] D1 and D2 are mainly localized within the striatum, olfactory bulb and *substantia nigra* of the brain.[52] Dopamine neurotransmission modulates motion and motor control[53], feelings of pleasure and reward[54] as well as memory and learning.[55] Due to their involvement in the reward system, this family of receptors has long been implicated in addiction, which can be underlined by the fact, that all known addictive drugs directly or indirectly stimulate dopamine receptors.[56]

Dopamine receptor are pharmacologically explored as drug targets for Parkinson's disease.[57] Furthermore all drugs that attenuate manic episodes in bipolar disorder either bind to the D2 receptor, or modulate downstream pathways governed by it.[58] Similarly, all known antipsychotic bind to the D2 receptor, and more specifically antagonize its interaction with β-arrestin 2.[59]

b) Adrenaline neurotransmission

Adrenaline and noradrenaline are recognized by 5 subtypes of receptors, divided into α and β class families. α1 couples to G_q, and

α2 to G_i, while β-adrenergic receptors couple primarily to G_s. Adrenergic receptors are expressed both in the brain as well as in peripheral regions. In the brain they are spread heterogenicaly, found in most regions, with high concentrations in the cortex, thalamus, hypothalamus and hippocampus.[60] The physiology and pharmacology of those receptors was first studied outside of the CNS, with adrenergic receptors exploited as drugs for asthma of heart disorders.[61]

In the CNS the noradrenergic system modulates functions like arousal, attention, memory and learning.[62] Dysregulation of this network has been associated with disorders like ADHD, chronic stress and anxiety, depression, addiction, as well as acute inflammation in neurodegenerative disorders.[63,64] Furthermore, within adrenergic receptors, α-adrenergic receptors have been linked to dysregulation of cognition, arousal and motivation observed in depression and schizophrenia.[65]

Conversely, brain adrenergic receptors are investigated as drug targets for the treatment of eating disorders[66], analgesia[67] and depression.[68]

c) Serotonin neurotransmission

In the CNS Serotonin is produce by serotonergic neurons, primarily located in the nine *raphe nuclei* of the brain stem.[69] Those neurons form a fast network, connecting to multiple regions of the brain, like the cortex, hippocampus as well as the mid and hindbrain.[70] In mammals serotonin is recognized by 14 types of receptors, including 13 GPCRs and one ion-gated channel.[71] Those receptors are primarily expressed at the post-synaptic terminal.[72] Due to the sheer number of serotonin receptor, they have been found to control diverse processes like neurogenesis and neurodevelopment[71] modulation of memory[73], cognition[74], fear[75], mood[55] and hunger.[77]

From a pharmacological point of view, multiple serotonin receptors are explored as drug targets against depression, anxiety[78] as well as obsessive compulsive disorder[79] and migraine.[80] Modulation of serotonin receptors (particularly 1A and 2A) has been linked to improved efficacy and less side-effects in antipsychotic medication.[81] Further studies linked the activation of 2A with the onset and progression of schizophrenia.[82,83] Antagonism within this receptor

has an antipsychotic effect, as well as reduces negative symptoms and cognitive impairment associated with this disease.[84]

d) Opioid neurotransmission

Opioid neurotransmission is mediated primarily by opioid peptides: enkephalins, endorphins, endomorphins, dynorphins, nociceptin and melanocortins.[85] Currently four opioid receptors (OR) have been identified: the μ, δ, κ and NOP receptors.[86] All opioid receptors are primarily placed within subcortical structures (e.g. thalamus, hypothalamus), with the δOR also ubiquitously expressed in the cortex, the μOR in the cerebellum and κOR in the frontal lobe.[87] They are expressed both pre- and post-synaptically and primarily couple to G_i proteins.

Opioid receptors are known to be involved in mediating pain reception.[88] The name of this family is derived from opium, a poppy extract with potent analgesic properties, used since ancient times, which was later found to work through this family of receptors (mostly through the μ-receptor).[89,90] Furthermore opioid receptors are known to modulate multiple functions like analgesia, euphoria, anxiety as well as resolution of inflammation, control of bowel movements and respiration.[86]

Based on their function, opioid receptors show major potential as targets for the treatment of pain.[91] The current challenge is engaging this receptors, without initiating multiple adverse effects (addiction, respiratory depression) associated with their activation.[92] Furthermore, they are attractive drug targets for mood and fear disorders (primarily the κ receptor).[87]

e) Cannabinoid neurotransmission

Endocannabinoids are recognized by two types of cannabinoid receptors: cannabinoid receptor (CB) type 1 and 2. The cannabinoid receptor type 1 is the most abundantly expressed receptor in the human brain. CB 2 is less present, and can also be expressed in peripheral tissues. CB1 and 2 are located primarily on the presynaptic terminal. Topographically, high concentration of cannabinoid receptors are present it in the cortex, midbrain, hippocampus and cerebellum.[93] CB receptors couple mainly to G_i and as such their activation in the presynaptic terminal inhibits the release of multiple other neurotransmitters.[94]

CB receptors participate and modulate multiple processes like memory[95], stress[96] as well as pain.[97] Due to their anti-excitatory role they show promise as drug targets in epilepsy[98,99], as well as other conditions related to increased neuron excitability like manic episodes or schizophrenia.[100,101] Conversely deletion of CB2 results in a schizophrenic-like phenotype in mice.[102]

1.5. Signaling preference in GPCRs

Initially it was thought, that agonists engage all downstream pathways equivocally. In such a model, a GPCR would exist only in two conformations: an active one with high affinity towards intracellular partners, and an inactive one with none or little affinity. However, two simultaneous publications in 2003 demonstrated, that GPCR agonists can show preference towards certain signaling pathways.[103,104] The phenomena of preferential signaling is called biased agonism (e.g. preference of coupling to G-proteins over arrestin, or one G-protein subtype), and ligands that demonstrate it – biased agonists (Fig 5).

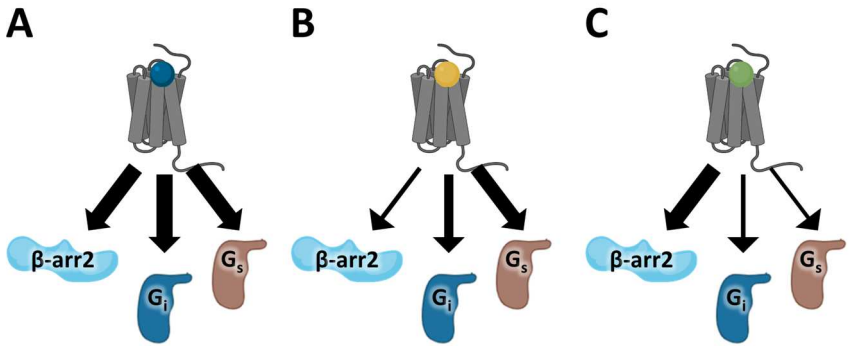

Figure 5 Biased agonists show preference for certain downstream signaling partners.
GPCR agonists can show signaling preference towards certain pathways in a phenomenon called biased signaling. In panel A we show an agonist that couples three downstream effectors with similar efficiency. Such an agonist is considered balanced. In panel B we show an agonist biased towards G_s and partially biased towards G_i. In panel C we show an agonist biased towards βarr2.

Considering the hypothesis that GPCRs can exist in multiple conformations, agonists that show signaling preference, stabilize the receptor in a subset of active conformations (that can be referred to

as “biased” conformations).[105,106] Although this is not the only model that tries to explain biased signaling, it is the one supported by the largest amount of experimental data.[107]

Biased agonists are molecules of much interest for the scientific community. Such compounds allow to selectively block certain signaling pathways in a cell, while maintaining signaling in others. This allows to interrogate the involvement of this pathway in physiological processes or the development of disease symptoms. Signaling probes like that would be especially important to study CNS diseases, which often involve subtle changes in multiple downstream pathways.[108–111] Furthermore biased agonists show great promise in GPCR pharmacology, as they potentially allow to modulate pathways associated with disease symptoms, while not engaging counter-therapeutic pathways, or those related to debilitating side-effects. This is especially relevant for CNS GPCRs (Tab. 2).

Receptor	Targeted disease	Consequences of lack of bias	Reference
α2-adrenergic receptor	affective disorders	less efficient drugs	68
dopamine 1 receptor	Parkinson’s disease	less efficient drugs	112
dopamine 2 receptor	psychotic disorders	less efficient drugs	59
histamine 1 receptor	affective, psychotic and anxiety disorders	respiratory failure, sedation, allergic reaction	113
muscarinic 3 receptor	cognitive disorders, insulin resistance	less efficient drugs	114,115
μ-opioid receptor	chronic pain	constipation, respiratory distress, addiction	116,117
Δ-opioid receptor	pain, affective and anxiety disorders	seizures	118

κ-opioid receptor	chronic pain	affective disorders, hallucinations, skin irritability	119
serotonin 2A receptor	affective and psychotic disorders	hallucinogenic effects	120

Table 2 Biased agonism can lead to better drugs targeting CNS disorders In the table we show examples of CNS GPCRs in which signaling bias could lead to the development of better drugs. Table adapted from[121]

Within FDA approved drugs, the concept of biased agonism helped rationalize the unique signaling profile of drugs like carvedilol.[122] It also laid the blueprints for the development of the peristaltic - loperamide.[123] Biased agonism is speculated to play a role in the favorable therapeutic profile of the antipsychotic aripiprazole.[124] Other biased agonists, like TRV130 targeting acute pain[125], TRV250 migraines[126] and TRV120027 heart failure[127] are currently in clinical trials phase.

Taking this into account, there is an apparent need for more biased agonists. However, the identification of novel biased molecules remains difficult. When attempting to identify novel ligands of a receptor, the most straightforward approach appears to be extensive experimental testing of large libraries of compounds. However, this is a very costly process with a low success rate. This search can be facilitated by virtual screening techniques, in which using computational models we try to predict the molecules which will form a high-affinity complex with a receptor. Such a process only allows to identify binders and does not predicting the signaling response initiated by the molecule.

Understanding how distinct receptor-ligand interactions translate into a biased/balanced signaling response could guide the discovery of biased agonists, by providing additional guidelines for *in silico* drug discovery. One popular strategy to identify such features is to corelate the pattern of ligand-receptor interactions with the signaling outcomes of structurally close molecules.[111] In such a process we selectively disturb contacts of the ligand with the receptor, identifying the contribution of each interaction for the signaling

response. Such an iterative process, called a structure-activity relationship study (SAR), can potentially reveal interaction patterns related to a biased response. This can be facilitated by mutagenesis.

Monoamine neurotransmitters are an attractive starting point for such endeavors. From a biological point of view, those neurotransmitters regulate a very large group of important CNS GPCRs, which are one of the most important drug targets according to sales (Tab. 1). Fully appreciating how their binding modes translates into a response, would enable us to better understand core physiological processes in the human body, provide important data for drug design as well as partially explain how sequence variability within their orthosteric site predisposes the receptor towards a certain signaling response, and in connection, to a physiological role. Furthermore, despite the diversity of processes their receptors regulate, monoamine neurotransmitters and their binding sites show a surprising degree of structural conservation. Because of this, structural determinants of a biased/balanced response within one receptor, would likely be transferrable to another one. Lastly, those neurotransmitters are small molecules, possessing limited rotatable bonds. Owning to this, their binding mode and kinetics are easier to sample using in silico techniques than most molecules. This is facilitated by the fact that all monoamine neurotransmitters form a salt-bridge with a conserved aspartate in the third transmembrane helix of their receptors.[128]

1.6. Propagation of signaling response within GPCRs

A major part of a ligand's intracellular response can be linked to ligand-receptor interactions, which stabilize the receptor in a distinct state. Thus, to fully grasp GPCR function, it is also important to understand how alterations in the ligand-binding site are transferred within the receptor to impact its structure. As mentioned before, this is mediated primarily by residues in the GPCR hydrophobic core, which communicate with each other within a complex allosteric network. In such a network, the conformation of one residue affect the conformation of others through direct and indirect interactions.

Multiple conserved residues that play an important role in this network have been described.[23,129] Examples include a highly conserved tryptophan in TM6 which alters its rotational state in

active GPCR structures[130], a tyrosine in the intracellular part of TM7 which toggles the access of intracellular water molecules[131], an ionic lock in the intracellular side that opens during receptor activation[132] as well as a cluster of hydrophobic residues close to the orthosteric ligand binding site called the P-I-F motif[133]

Taking into account that allosteric communication governs GPCR conformations, it would be tempting to speculate that biased agonists engage different patterns of communication within this network, resulting in a different receptor conformation, and a different signaling response. NMR experiments verified that the GPCR conformational state is tightly connected with its signaling response (in terms of bias).[134] Additional experiments identified distinct allosteric features, connecting the intracellular part of TM6 with G-protein bias, and the intracellular part of TM7 with β-arrestin bias. A recent NMR study has shed light into allosteric communication between the ligand binding site and intracellular ends of TM5, TM6 and TM7[135]. This data highlighted the complexity of the allosteric network, showing that multiple inter-helical contacts participate in signal transmission. Furthermore a bioinformatic study linked signaling bias within serotonin receptors, with the specific behaviour of the P-I-F motif.[136] Mutation studies enable us to better understand the allosteric GPCR network, as they enable to selectively alter communication between two or more residues. By observing the effect of the disturbance in the mutant, we can speculate on the role of those contacts on the WT response.

Unravelling the differences of allosteric communication between balanced and biased signaling, could provide us another angle to design biased molecules, as well as give us a deeper understanding of GPCRs.

1.7. Impact of phosphorylation patterns on the arrestin response

As mentioned before, the G-protein response is very diverse, due to the number of combinations between the heterotrimeric-G-protein subunits. In comparison the arrestin response appears surprisingly less varied, with only two possible coupling partners (βarr1 and βarr2) in the non-visual system. However, coupling of the arrestin to the same receptor can have multiple functional outcomes, suggesting

the existence of a cellular mechanism of regulation, that mediates the arrestin response.

One of the points of interest when attempting to identify this mechanism was the GPCR C-terminal tail, one of the primary targets of GRKs. Experimental data revealed, that the phosphorylation pattern of this tail, has a high degree of variability[137], and can be influenced by multiple features like the type of bound ligand.[138]

Interestingly, the induced phosphorylation pattern is tightly linked to the specific arrestin response in the cell.[139–142] It is still not clear how this pattern contributes towards a different signaling response. Structures of visual-arrestin bound to Rhodopsin[143] as well as βarr1 bound to the phosphorylated C-tail[144], indicate that the C-tail forms a large part of the arrestin-GPCR interface. As such, changing the properties of this interface would likely alter the structure of the GPCR-arrestin complex, leading to a different arrestin conformation and in turn affect the signaling response. This hypothesis has been confirmed by a BRET-study[145,146], and elaborated upon by further BRET-studies as well as nuclear magnetic resonance (NMR) studies.[147,148]

The notion that the structure and function of arrestin is governed by the unique phosphorylation pattern of the C-tail is currently referred to as the flute-model.[149] It holds, that the phosphorylation of the C-tail pattern is recognized by ten conserved recognition sites on the arrestin structure. Which of those sites are occupied by a phosphate-group determines the conformations and physiological outcome of arrestin coupling, analogous to the tune a flute would make when different holes are covered. (Fig 6)

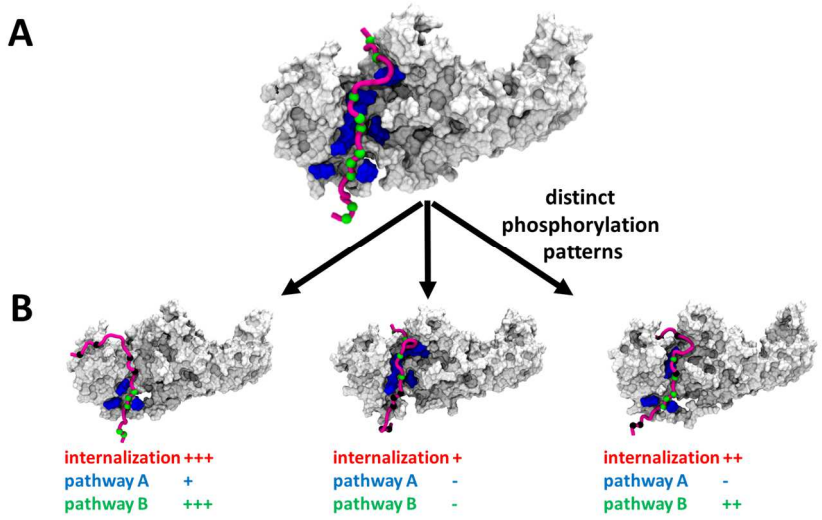

Figure 6. Distinct phosphorylation patterns impact arrestin structure and function.
In panel A we show the crystal structure of arrestin in complex with a phosphorylated C-tail (PDB code: 4JQI). Arrestin is depicted in white, and the C-tail in magenta, we show phosphorylation sites on the C-tail as green orbs, and positively charged residues in arrestin interacting with those sites in blue. In panel B we schematically show that altering the phosphorylation pattern of the C-tail (phosphorylated sites demonstrated in green, unphosphorylated in black) affects the structure of the arrestin C-tail complex, resulting in a different downstream signaling response.

Gaining structural insights into how a phosphorylation pattern translates into a different response and would expand what we know about the functionality of GPCRs (not only those expressed in the brain).

1.8. Palmitoylation as a modulator of CNS receptors

A different example of a posttranslational modification that impact GPCR functionality is the covalent attachment of lipid groups, called lipidation. A prominent example of this process in GPCRs is linking palmitic acid to the intracellular side of GPCRs through formation of an ester bond. Although potentially all residues containing a thiol of hydroxy group can undergo this modification, in GPCRs as of yet we have only observed palmitoylation of cysteines.[150] In GPCR, palmitoylation typically occurs on the 8th amphipathic helix, that is

placed on the interface between the membrane and cell environments. The lipid tail is attached to either one or two cysteine residues, facing the membrane. Multiple GPCRs have been experimentally confirmed to be palmitoylated in this positions[151], and seeing as cysteines in helix 8 are highly conserved (present in more than 70% of GPCRs)[152] it is likely that the number of confirmed palmitoylatable GPCRs will be expanding.

It has been proposed that GPCR palmitoylation can be divided into constitutive (carried out shortly after translation, present during all of the life of the receptor and likely involved in trafficking) and dynamic (in which the receptor is palmitoylated and de-palmitoylated multiple times during its life).[153] In this sense dynamic palmitoylation appears to be a situation-dependent mechanism of GPCR regulation, akin to phosphorylation.

Helix 8 palmitoylation has been confirmed in multiple GPCRs mediating neurotransmission. The effect of this modification varies by receptor, altering the receptor localization, ligand signaling response as well as promoting certain patterns of phosphorylation.[151] Unsurprisingly, dysregulation in palmitoylation of brain GPCRs has been connected to multiple neurodegenerative and neuropsychiatric disorders.[154]

The cannabinoid 1 (CB1) receptor is a prime example of a CNS-expressed GPCR whose functionality is regulated by palmitoylation, altering the receptor function and location.[155] However, we still have limited understanding as to how, palmitoylation induces such changes in the receptor. Discovering would likely present interesting data, applicable not only to the CB_1 receptor.

1.9. Molecular dynamics as a tool to unravel GPCR complexity

In the introduction, we highlighted multiple questions related to GPCRs involved in neurotransmission, which could be at least partially addressed by applying high-resolution structural techniques. Among classical experimental techniques NMR provides the means to study the structure of proteins in solution or in a native-like membrane. However due to multiple technical hurdles with NMR

(primarily the protein size), the method is unsuitable for GPCRs, as it provides data of very low resolution.[156]

As such the method of choice to study GPCRs is X-ray crystallography. In this approach the receptor is immobilized by crystallization. Subsequently X-ray diffraction maps are generated for the molecule, which when resolved reveal the relative locations of atoms of the crystallized complex. The first crystal GPCR crystal structures were obtained in inactive conformations.[157–159] Progress in crystallization techniques provided structures in active conformations bound to G-protein, arrestin or stabilized by nanobodies.

As mentioned before, GPCRs are highly dynamic proteins, and as such a single structural snapshot is not sufficient to fully understand their complexity. A good example of this is ligand dependent signaling. In this process the most prominent structural event is the transition from the inactive into active conformation. However, X-ray crystallography only provides the initial and final conformation, without capturing multiple meta-stable states visited during the transition.

Furthermore, X-ray crystallography requires multiple proteins crystallized in one conformation. However, GPCRs are highly dynamic proteins and multiple experimental procedures are necessary to stabilize them (thermostabilizing mutations, insertion of fusion proteins, truncations, coupling to antibodies, use of detergents to clear out the membrane). Taking into account the degree of experimental modification, it is not clear to what extent the obtained structure is shifted to an artificial conformation by experimental conditions.[160]

In this respect molecular dynamic (MD) simulations are an attractive technique to complement crystallography and NMR data. In a classical MD simulation each atom of a system is represented as a point particle with defined connectivity to other atoms. The impact of bonded and non-bonded interactions affecting each atom is derived from parameter sets called forcefields. Based on those interaction the force vector affecting each atom is obtained which is used to calculate the velocity and subsequent new position of each atom. This process is repeated multiple times in a user defined interval, simulating the

behavior of a biological system in a fixed period of time. Importantly, MD simulations are mechanistic in their nature, and don't consider quantum effects, like changes in atom charges, or dissolution/formation of bonds.

For a GPCR, such a biological system consists usually of a receptor embedded in a user defined membrane and solvated by water and ions. Simulating a receptor with this technique offers spatial and temporal resolution of a process unobtainable by other experimental methods, enabling us to observe the GPCR-signaling machinery at the scale of a single atom. The growing popularity of MD as an experimental methods for GPCRs is underlined by the number of published studies on GPCR using this technique (Fig. 7).

It is possible to simulate receptors without an available experimentally-resolved crystal structure, by using homology modelling. In homology modelling we aim to predict the structure of one protein by aligning its sequence to that of a protein with a resolved 3D structure. This technique has been proven to have high accuracy for GPCRs[161–163], providing valid experimental data even when compared with later obtained X-ray data.[164]

One of the primary limitations of MD techniques is the amount of computational resources necessary to simulate a system for a biologically relevant amount of time. However, our threshold is constantly increased by improvements in simulation algorithms as well as computer hardware. Currently simulations on the millisecond scale are obtainable on scientific computer clusters. In GPCR biology this time is sufficient to sample allosteric rearrangements within the receptor, as well as inactivation and initial stages of GPCR activation.[165]

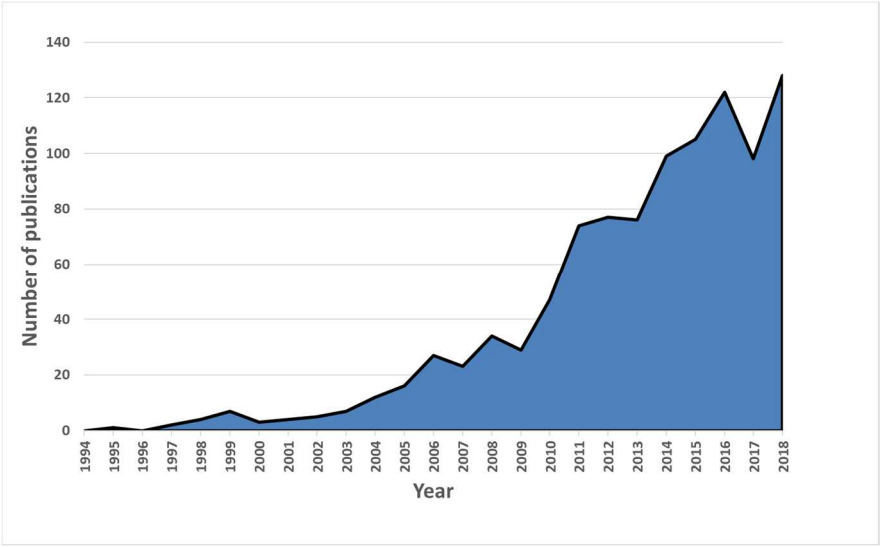

Figure 7. The popularity of molecular dynamics in the study of GPCRs is increasing
Above we plot the number of papers indexed at Thomson Reuters' Web of Science that contain the topics "molecular dynamics" and "GPCR" or "GPCRs".

Although we are now able to reach the millisecond scale, this time is still not enough to appreciate multiple processes related to GPCRs. Enhanced sampling techniques attempt to tackle this problem by expanding the conformational space explored by a system. Within metadynamics we attempt to define a process using one or more collective variables.[166] During a metadynamics run a biasing potential is calculated on the fly. This potential is history-dependent, and as such it aims to prevent the system from re-entering already visited conformations. Conformations are defined by the value of one or more collective variables, which are structural variables best defining the studied process. Multiple types of collective variables have been proposed depending on the studied process including the distance between two atoms, an angle or the number of contacts between protein segments.[167]

Every time the protein returns to an already visited state, an additional bias is deployed, further forcing the system to visit different conformations. Thus, after a certain number of steps the algorithm enables the protein to cross-high energy barriers. The applied bias is stored within the algorithm. Summing up the energy

used to progress the system along the colvar or colvars allows us to identify energetical barriers as well as intermittent meta-stable states of the studied process (Fig 8).

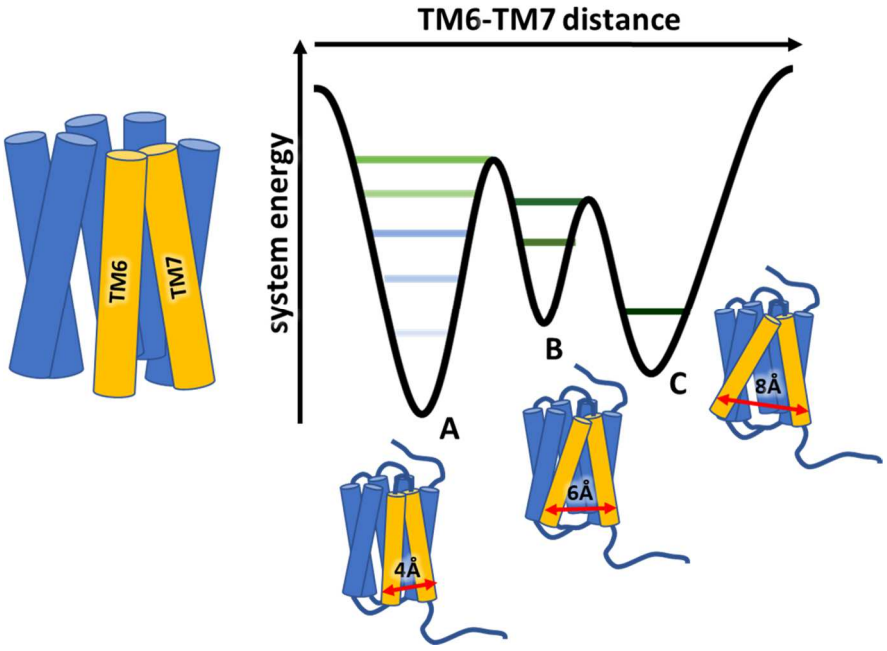

Figure 8. A schematic representation of GPCR metadynamics. Above we show a process of sampling the distance between TM6 and TM7 (the collective variable, depicted as a red arrow). The energy landscape of this movement (which we aim to study with metadynamics) is depicted as a black curve. The metadynamics protocol adds additional bias (shown as lines going from light blue into dark green) trying to move the system into conformations with different values of the colvar. The system starts in conformation A, the bias allows it to obtain conformation B, and then conformation C. By summing up the bias added along the way, it is possible to assess the energetic landscape of this transition.

One of the difficulties associated with metadynamics is that the system seldomly reaches a converged state, furthermore in extended simulations we run the risk of pushing it into non-physiological high energy conformations due to the massive amount of accumulated bias. A modified version of the classical algorithm, well-tempered metadynamics addresses this problems.[168] In this algorithm, the amount of bias applied for a certain conformation is time-dependent. The more time a system spends in a distinct conformation, the less

bias each time will be applied to try to force into a different one. In simpler terms, each time the system revisits a conformation, the algorithm tries less and less to force it into a different one. This modification reduces the risk, of forcing the protein into unnatural high-energy states, and also facilitates the convergence of the energy landscape.

A popular application of metadynamics in GPCRs is the study of ligand binding where this protocol can be used to efficiently sample the affinity[169] as well as the binding mode of ligands.[170] Ifs run using appropriate collective variables, this technique offers much more information on the dynamic process of ligand-receptor interactions, than static techniques like docking. Furthermore, it enables us to sample the conformational landscape much faster than unbiased MD. This method is especially viable for ligands that can interact with the GPCR in more than one binding mode.

The binding mode of small molecules, such as monoamine neurotransmitters is an attractive problem to tackle with metadynamics, as they form a small number of receptor interactions. Because of this, each of those interactions can be used as a collective variable, efficiently sampling the conformational space of a neurotransmitter.

Chapter 2
Objectives

This PhD thesis aimed at understanding the structural basis of GPCR functioning, focusing on receptors involved in neurotransmission. To obtain a comprehensive understanding, we investigated various GPCRs at multiple levels of action: the orthosteric binding site, the allosteric network, interactions with downstream effectors as well as the level of post-translational modifications. We anticipated, that the obtained data would not only be useful in basic research, but also for the development of novel pharmacological strategies to target disorders related to GPCRs. To reach this overarching goal, the following specific goals were established:

- To dissect the structural determinants of monoamine neurotransmitter signaling, and by using this knowledge decipher the contribution of distinct receptor-ligand interactions to a balanced/biased response within aminergic GPCRs

- To understand how specific alterations within receptor-receptor contacts contribute to β-arrestin bias within the δ-opioid receptor

- To understand how a distinct phosphorylation pattern of the C-terminal tail contributes towards GPCR-arrestin interactions, as well as downstream arrestin signaling.

- To investigate how palmitoylation of the CB1 receptor, modifies its function and localization.

Chapter 3
Publications

3.1 A common mechanism drives the coupling response to dopamine and other monoamine neurotransmitters

In this chapter, we present our work in form of a journal article

Summary:
In this article, we attempted to dissect the balanced coupling response of the monoamine neurotransmitter dopamine within the dopamine 2 receptor. We did so by studying the binding mode of dopamine and its close structural analogues and correlate the obtained data with experimental assays from live cell biosensor assays.

By integrating the gained insight, we observed that simultaneous polar interactions with TM5 and TM6, contribute towards a balanced signaling response, while exclusive TM5 polar interactions result in G-protein bias, primarily G_{ob}. Using mutagenesis, we confirm that our findings are transferrable to other monoamine neurotransmitter receptors.

The results of this study help us better understand the functionality of aminergic GPCRs, as well as suggest how sequence variability observed in the orthosteric binding site of studied receptors (e.g. lack of polar residues in the upper part of TM6) promotes a specific coupling pattern.

The PhD candidate was responsible for all the computational work carried out in this paper, computing bias factors as well as planning the *in vitro* experiment strategy. He was involved in writing the manuscript.

A common mechanism drives the coupling response to dopamine and other monoamine neurotransmitters

Tomasz Maciej Stepniewski[1#], Arturo Mancini[2#*], Mariona Torrens-Fontanals[1], Billy Breton[2] and Jana Selent[1*]
[#]Both authors contributed equally to this work.

[1]*Research Programme on Biomedical Informatics (GRIB), Hospital del Mar Medical Research Institute (IMIM) - Pompeu Fabra University (UPF), Dr. Aiguader 88, E-08003, Barcelona, Spain*
[2]*Domain Therapeutics NA Inc. 7171 Frederick-Banting, Local 3209, Saint-Laurent (QC) H4S 1Z9, Canada*

*Corresponding authors:
e-mail: jana.selent@upf.edu
e-mail: amancini@domaintherapeutics.com

Abstract
The function of the brain relies on neurotransmitters which mediate communication between billions of neurons. Disruption of this communication results in psychiatric and neurological disorders. In this work, we investigate the action of the neurotransmitter dopamine on the D2 receptor (D2R) combining molecular dynamics simulations and live-cell biosensor assays. The study of dopamine and closely related chemical probes allowed us to dissect how neurotransmitter binding translates into a distinct coupling profile (i.e. to G_i, G_{oB}, G_z and β-arrestin 2). We find that interaction with key residues in TM5 (S5.42) and TM6 (H6.55) in the receptor binding pocket yields a balanced dopamine-like signaling signature, whereas exclusive TM5 interaction is typically linked to G protein bias (in particular G_{oB}). Most importantly, studies on serotonin 1A (5HT1AR), 2A (5HT2AR) and β2-adrenergic receptor (β2AR) indicate that the reported mechanism is common for other monoaminergic neurotransmitter receptors. Ultimately, we suggest that sequence variation in position 6.55 is used by nature to fine-tune β-arrestin recruitment and in turn receptor internalization and β-arrestin-mediated signaling in neurotransmitter receptors.

Key words
neurotransmission**,** G protein coupled receptor, signaling bias, live-cell biosensor assays, metadynamics

Introduction

Neurotransmitters are chemical messengers which mediate communication between billions of neurons within an enormous network that constitutes the central nervous system (CNS). Disruptions in the regulation of this system are known to result in disorders such as depression, psychosis, bipolar disorder, general anxiety disorder and Parkinson's disease, among many others.[1] Main acceptors of neurotransmitters are G protein coupled receptors (GPCRs) which are the largest family of human cell surface receptors.[2] Herein, we focus on the dopamine D2 receptor (D2R) and its native agonist dopamine - a neurotransmitter with a catecholamine structure[3] that is also common to other signaling molecules (e.g. adrenaline, noradrenaline or serotonin). As a natural agonist of the D2R, dopamine is considered to be a functionally balanced agonist for G protein- (i.e., $G_{i1\text{-}3}$, $G_{oA\text{-}B}$, G_z) and β-arrestin-(βarr2)-mediated signaling pathways. This coupling profile modulates important processes in the brain related to memory, learning, attention, mood and movement. The concept of balanced agonism holds that ligands display similar efficacies for various signaling pathways linked to a given GPCR. An emerging concept for more efficient CNS drugs is to selectively engage therapeutic pathways and inhibit those responsible for deleterious side-effects.[4-6] This discovery has initiated the quest for ligands with a tailored signaling signature for the D2R. Despite first insights[7,8], the rational design of drugs with a desired signaling profile remains complicated as it is difficult to pinpoint ligand-receptor interactions responsible for a distinct coupling profile. Even subtle changes in ligand-receptor interactions can result in a dramatic change of the signaling profile.[9] We envisage that dissecting the balanced signaling signature of dopamine at the D2R can contribute to a wider understanding of neurotransmission and guide the development of ligands with a tailored coupling profile. During the last decades, several research groups have studied the binding and functional outcome for dopamine and its analogues.[10-13] Unfortunately, the results are not always consistent between studies which is likely due to different experimental setups. In addition, the atomistic resolution of how dopamine binding translates into the recruitment of distinct intracellular signaling proteins (G_{oB}, G_z, G_{i2}, βarr2) remains largely unclear. To address this knowledge gap, we carried out all-atom molecular dynamics simulation (classical and enhanced sampling techniques) accumulating ~40μs of simulation time (Table S1). The

power of enhanced sampling techniques for capturing biologically relevant events has been shown in previous studies.[14,15] Here, we use this approach to construct the complete energetic binding landscape of dopamine and closely related signaling probes. The small size and low number of rotatable bonds of studied compounds allows for an exhaustive sampling of their binding. The signaling signature of each ligand was characterized by assessing receptor coupling to several intracellular signaling proteins (G_{oB}, G_z, G_{i2}, βarr2) using live-cell BRET-based biosensors. Ultimately, this approach allowed us to detect a common signaling mechanism for GPCRs that is critical for neurotransmission.

Results

Simultaneous TM5 and TM6 contacts contribute to the dopamine-like coupling outcome

In a first step, we evaluated the ability of dopamine to engage different Gi proteins (G_{oB}, G_z, G_{i2}) and βarr2 at the D2R using the live-cell BRET-based biosensors. The BRET-based assay confirmed robust coupling to all tested intracellular effector proteins upon dopamine binding (Figure 1A-D, blue lines). As an approximation of the signaling response, we use the area under the curve (AUC) which takes into account potency (EC50), efficacy (Emax) and the Hill slope. The AUCs are further used to obtain the coupling ratios for all combinations of individual effector proteins (e.g. $AUC_{\beta arr2}$ vs AUC_{Gz}, $AUC_{\beta arr2}$ vs AUC_{GoB} etc.). As a natural agonist, dopamine is considered to have a balanced coupling profile at the D2R. Thus, all obtained coupling ratios are normalized to 1 (Figure 1S) and used as reference for other studied compounds (see method for more details).

Next, we probed the general binding mode of dopamine using classical unbiased molecular dynamics simulations. We were able to reproduce known binding characteristics including polar contacts of the meta (m-OH) and the para (p-OH) hydroxyl groups of dopamine to TM5 and TM6 (Figure S1). In particular, polar interactions with TM5 are in agreement with site directed mutagenesis[10-13,16] and computational[17] studies. Despite the structural insights provided by different mutational studies, specific contributions of the individual p- and m-OH groups to the binding and functional outcome of dopamine or its analogues remain unclear (Table S2A-B). To address this question, we used metadynamics (Figure S2) to construct the energetic map of dopamine binding focusing on its p-

/m-OH groups and their preferred binding contacts to residues in TM5 (S5.42 and S5.46).

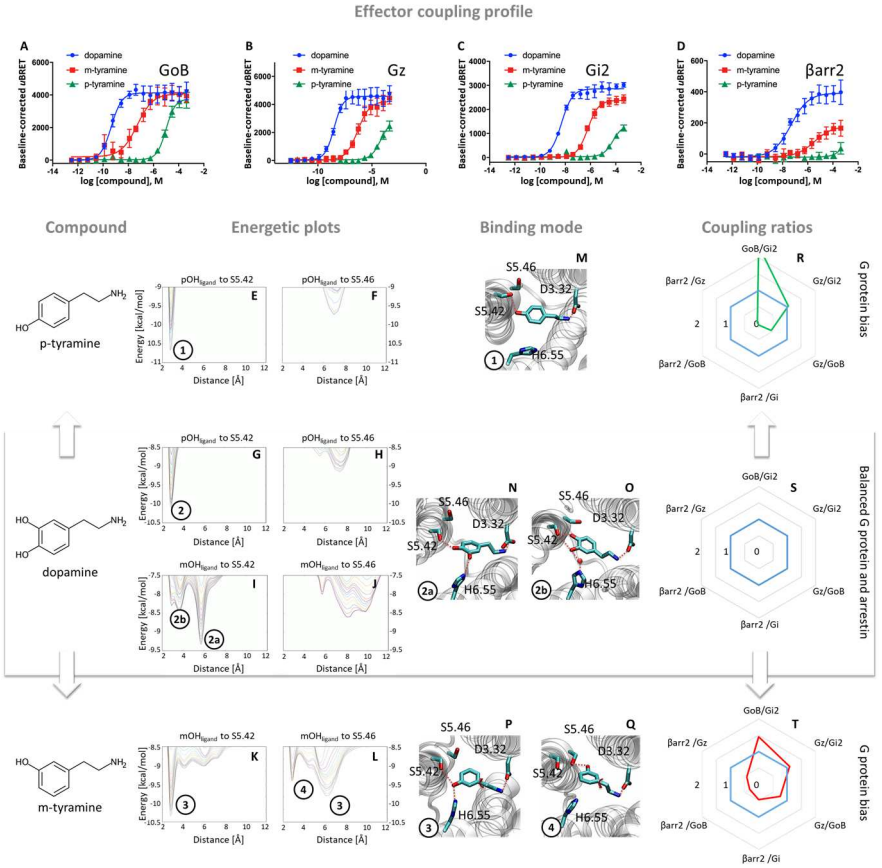

Figure 1 *Coupling and binding profile of dopamine, p-tyramine and m-tyramine. The corresponding chemical structures are depicted on the left.* ***A-D****: Coupling curves for G protein (G_{i2}, G_z, G_{oB}) and β-arrestin 2 (βarr2) at the D2R in response to dopamine (blue), p-tyramine (green) and m-tyramine (red) have been monitored using bioSensAll™ technology. For corresponding pEC50 and Emax values see Table S3.* ***E-L****: Energetic plots of ligand binding obtained by metadynamics using as metrics the distance of the m- and/or p-OH groups to S5.42 and S5.46. An energetic well at ~2.8 Å indicates a favorable distance for binding contacts with the corresponding residue. To ensure convergence of binding energetics, we monitored free energy profiles along simulation by plotting the profile every 20000 deposited Gaussians (graphs shown in different colors).* ***M-Q****: Representative structures of the binding mode corresponding to the*

energetic wells identified in the energetic plots. ***R-T****: Coupling ratios were approximated using the curve (AUC) and its ratio for individual signaling effectors (e.g. βarr2 vs G_z, βarr2 vs G_{oB} etc.). To eliminate observational bias linked to differences within different biosensor assays (e.g. βarr2 vs G_i), we use dopamine as internal standard for analyzing the areas under the curve (AUC). A balanced coupling profile of dopamine (reference ligand) is denoted by a coupling ratio of 1 for all pathway combinations and highlighted in all plots as blue line. Preferential or disfavored coupling are indicated by ratios > 1 or < 1, respectively. Dose-response curves were generated using data obtained from 3 independent experiments. Baseline uBRET values were subtracted from dose-response curves.*

Regarding the m-OH group, we observe two binding modes with respect to S5.42 (peaks 2a and 2b, Figure 1I). Despite their small difference in binding, both modes (Figure 1N-O) allow for simultaneous interaction with TM5 (via p-OH) and TM6. It is worth noting that TM6 interaction can be direct (2a) or indirect via a water molecule (2b), as also suggested by unbiased simulation (Figure S1). All in all, our data indicate that simultaneous interaction between TM5 and 6 likely contribute to the balanced signaling outcome of dopamine.

Exclusive TM5 interaction results in preferential G_{oB} over βarr2 coupling

To elucidate the relevance of the m-OH group for the coupling outcome, we studied p-tyramine, a molecule that lacks this specific group (Figure 1, left side). Not surprisingly, at the level of p-tyramine binding, energetic maps indicate that the p-OH group interacts with S5.42 in TM5 (Figure 1E-F) similar to dopamine (Figure 1G-H). Due to the lack of m-OH, no simultaneous interactions are formed with TM5 and 6 (Figure 1M vs 1N-O). Importantly, this alters significantly the coupling signature as seen in the corresponding dose-response curves (Figure 1A-D, green lines). We observe a reduction in potency and efficacy for all effector proteins (G_{oB}< G_z < G_{i2} << βarr2) in which G_{oB} is least affected along with an almost entire shutdown of βarr2 recruitment. The strong preference of G_{oB} coupling over βarr2 could not be validated by the operational model[18,19] as the flat dose-response curve of βarr2 impedes the calculation of the bias factor. Alternatively, the preferential G_{oB} coupling can be appreciated when comparing the AUC ratios for

individual pathways to those of our reference compound dopamine (Figure 1R). The resulting plot reveals a strong coupling preference of G_{oB} over βarr2. All in all, our findings suggest that exclusive TM5 interaction is primarily linked to G_{oB} recruitment, whereas additional interactions with TM6 via the m-OH promotes in particular βarr2.

Co-existence of two binding modes with different coupling signatures

To further test this hypothesis, we studied m-tyramine, a molecule that lacks the p-OH group. Following the theory that m-OH interaction with TM6 promotes βarr2 coupling (p-tyramine vs dopamine Figure 1A-D), we expected to recover in particular βarr2. Surprisingly, βarr2 was only partially regained as seen in the dose-response curves (Figure 1D, red line) and corresponding coupling ratios (Figure 1T). Analyzing the binding of m-tyramine to the D2R, however, provides a plausible explanation and indicates the co-existence of two different binding modes. One binding mode is characterized by a binding peak to S5.42 (Figure 1K). The corresponding state (Figure 1P) allows for simultaneous interaction with S5.42 in TM5 as well as H6.55 in TM6 similar to dopamine. The second binding mode (peak 4 in Figure 1L) involves a rotation of the aromatic ring directing its m-OH group to the bottom of the binding pocket. Such structural constellation allows only for TM5 contacts (Figure 1Q) which corresponds to a p-tyramine like binding mode (Figure 1M). The co-existence of these two binding modes should result in a coupling outcome that is between the ones of dopamine and p-tyramine. In fact, this is observed for all tested effector proteins (Figure 1A-D). According to the energetic plots, the energetic barrier between both binding modes (Figure 1L, peaks 3 and 4) is approximately 1.3 kcal/mol which should allow frequent interconversion. Due to the low energetic barrier, the interconversion was also observed in classical unbiased simulations (Figure S3). Such a ligand rotation is not surprising and captured in several X-ray structures (Table S5).

Proof of concept using rigid signaling probes

According to our previous data, the coupling profile of m-tyramine (Figure 1T) is the result of the co-existence of two binding modes. We predict that impeding the rotation of the hydroxylated aromatic ring, and in consequence locking the compound in one or the other state (Figure 1P or Q), will yield two different coupling outcomes

driven either by simultaneous TM5/6 interaction or exclusive TM5 contacts. To test this hypothesis, we used the rigid S and R enantiomers of 7-hydroxy-2-(di-n-propylamino)tetralins (7-OH-DPAT).[20] Similar to m-tyramine, the OH-group of 7-OH-DPATs is separated by 5 carbons from the amine group (Figure 2, see chemical structures). However, a main difference is that the bond that links the aromatic ring with the amine group has no rotational freedom due to ring condensation. As a consequence, we predict that the R and S enantiomers adopt only one m-tyramine-like binding mode at a time. In fact, the observed energetic landscape shows that (R)-7-OH-DPAT interacts with S5.42 via its OH group (Figure 2G). The corresponding binding mode allows for simultaneous interaction with H6.55 in TM6 (Figure 2P). In contrast, the related enantiomer (R)-7-OH-DPAT binds in an inverted position directing its OH group towards the bottom of the binding pocket interacting either with S5.42 or S5.46 (Figure 2I-J). This is due to steric requirements and comprehensively described in the supplementary material (Figure S4). As a consequence of the downwards orientation of the aromatic hydroxyl groups, (S)-7-OH-DPAT forms polar contacts only with TM5 (Figure 2Q-R). All in all, our simulation data indicate that by blocking the rotational freedom of m-tyramine, we are able to favor one binding mode at a time either with exclusive TM5 or simultaneous TM5/TM6 contacts. According to our previous findings (Figure 1), the DPAT with exclusive TM5 contacts should show preferential coupling of G_{oB} over βarr2 compared to the one with simultaneous TM5 and 6 interactions. Indeed, this is supported by our BRET experiments (Figure 2A and D) and the corresponding coupling ratios for individual pathways (Figure 2V and W). Whereas the resulting coupling ratios for (R)-7-OH-DPAT (Figure 2V, black line) is similar to dopamine (blue line), for (S)-7-OH-DPAT we find a general preference of G_{oB} over all tested effector proteins, in particular for βarr2 (Figure 2W, orange line).

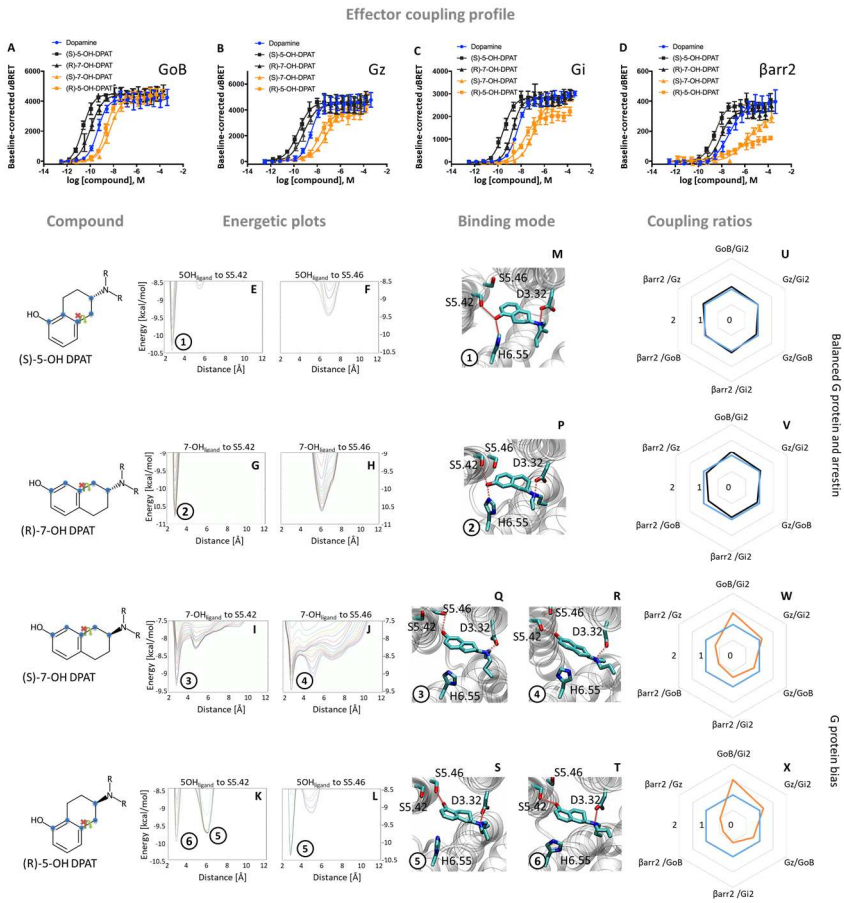

Figure 2 *Coupling and binding profile of (R)- and (S)-7-OH-DPATs. The chemical structures of studied compounds are depicted on the left. Blue points indicated 5 carbon distance between OH group and amine group.* ***A-D****: Coupling curves for G protein (G_{i2}, G_z, G_{oB}) and β-arrestin 2 (βarr2) at the D2R in response to (R)- 7-OH-DPAT (black) and (S)-7-OH-DPAT (orange) have been monitored using bioSensAll™ technology. Dopamine (blue) is plotted as reference ligand. For corresponding plogEC50 and Emax values see Table S3.* ***E-H****: Energetic plots of ligand binding obtained by metadynamics using as metrics the distance of the m- and/or p-OH groups to S5.42 and S5.46. An energetic well at ~2.8 Å indicates a favorable distance for binding contacts with the corresponding residue. To ensure convergence of binding energetics, we monitored free energy profiles along simulation by plotting the profile every 20000 deposited Gaussians (graphs shown in different colors).* ***I-K****: Representative structures of the binding mode corresponding to the energetic wells*

identified in the energetic plots. ***L-M****: Coupling ratios were approximated using the curve (AUC) and its ratio for individual signaling effectors (e.g. βarr2 vs G_z, βarr2 vs G_{oB} etc.). To eliminate observational bias linked to differences within different recruitment assays (e.g. βarr2 vs G_i), we use dopamine as internal standard for analyzing the areas under the curve (AUC). A balanced coupling profile of dopamine (reference ligand) is denoted by a coupling ratio of 1 for all pathway combinations and highlighted in all plots as blue line. Preferential or disfavored coupling are indicated by ratios > 1 or < 1, respectively. Dose-response curves were generated using data obtained from 3 independent experiments. Baseline uBRET values were subtracted from dose-response curves.*

This is supported by the operational model[18,19] (Table S4) in which (S)-7-OH-DPAT shows an approximately 12-fold bias of G_{oB} over βarr2 ($\Delta\Delta\log(\tau/KA)$ = 1,09, bias factor 12,27). To further confirm our structural model, we tested additional DPAT derivatives (5-OH-DPATs) which maintain a 5-carbons distance between the OH-group and the amine group. Intriguingly, we find that they follow the same tendency. The (S)-5OH-DPAT with exclusive S5.42 contacts (Figure 2E-F) and simultaneously interaction to H6.55 (Figure 2M) results in a balanced coupling profile similar to dopamine (Figure 2U). In contrast, the (R)-5OH-DPAT adopts an inverted position with binding contacts to S5.42/S5.46 (Figure 2K-L) and exclusive TM5 interactions. This alters the coupling response (Figure 2A-D) yielding a strong preference of G_{oB} over βarr2 (Figure 2X) which is supported by the operational model with a more than 200-fold bias ($\Delta\Delta\log(\tau/KA)$ =2,44, bias factor 274,16) (Table S4).

Relevance of H6.55 for the coupling outcome

Our structural model reveals that (in)direct polar interactions with the key residue H6.55 in TM6 is an important determinant for efficient coupling to G_{oB}, G_z, G_{i2} and primarily βarr2 that results in a balanced coupling profile as seen for dopamine and (R)-7-OH-DPAT. Based on our data, we predict that mutating this position into an alanine should block polar TM6 and favor exclusive TM5 interaction, thus promoting G_{oB} over G_z, G_{i2} and particularly βarr2 coupling. In fact, this coupling shift is observed in our BRET experiments for both compounds when comparing the coupling ratios in the H6.55A mutant (Figure 3C-D) to the WT D2R (Figure 3A-B). A bulkier hydrophobic phenylalanine in position 6.55 (H6.55F) shifts their

profile even further to preferential G protein coupling (Figure 3E-F) indicating the importance of a polar residue in this position for βarr2 recruitment. We further demonstrate this by introducing, instead of a nonpolar, a polar residue (H6.55N) which partially recovers βarr2 recruitment yielding a more balanced coupling profile (Figure 3G-H).

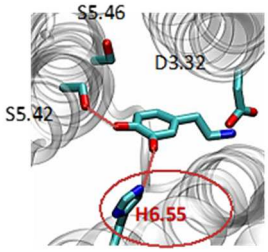

dopamine

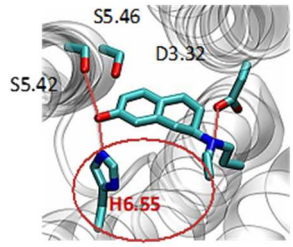

(R)-7-OH DPAT

WT

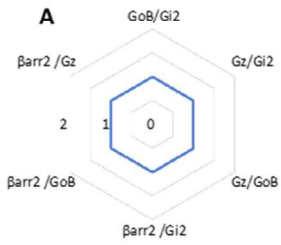

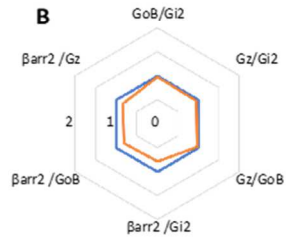

H6.55A

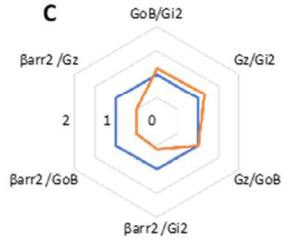

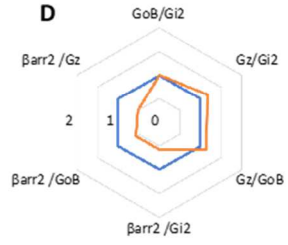

H6.55F

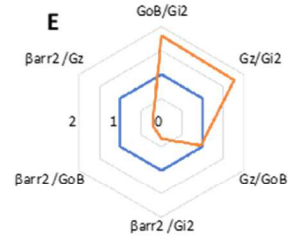

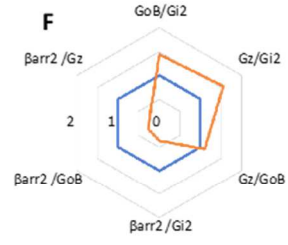

H6.55N

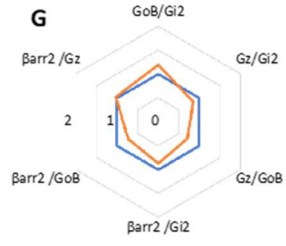

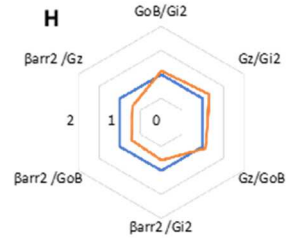

Figure 3 *Site directed mutation of position 6.55 (H6.55A, H6.55F and H6.55N) and its impact on the coupling outcome at the D2R receptor.*
Coupling response was approximated using the ratios of the AUC of corresponding response curves (Figure S5) for individual signaling effectors (e.g. βarr2 vs G_z, βarr2 vs G_{oB} etc.). To eliminate observational bias linked to differences within biosensor assays (e.g. βarr2 vs G_i), we use the dopamine response at the WT receptor as internal standard for analyzing the ratios of areas under the curve (AUC). Obtained AUC ratios (i.e. the receptor's ability to couple differentially to effector proteins) is not affected by expression level of the receptor (i.e. receptor concentration) which can change upon mutation. AUC radar plots were generated from dose-response curves obtained from 3 independent experiments.

A common mechanism for monoaminergic GPCRs

Based on the obtained results, we propose that a ligand-mediated hydrogen bonding network between TM5 and TM6 contribute to βarr2 recruitment in the D2R. Previous studies highlight that other neurotransmitters can also form simultaneous TM5/TM6 interactions such as in the serotonin 2A (5HT2AR)[9] and the β-adrenergic 2A receptor (β2AR)[21]. This and the high conservation of a polar residue in position 6.55 (66%) among aminergic GPCRs suggests that the reported mechanism for dopamine is common for other neurotransmitters. In order to investigate this possibility, we studied the coupling response of serotonin and adrenaline in their parent receptors (Figure 4). We find that replacing the residue in position 6.55 by a non-polar one (N6.55A) reduces the capacity of the 5HT2AR and the β2AR to recruit βarr2 compared to G proteins upon neurotransmitter binding. This strongly supports the notion that position 6.55 is a hotspot for modulating the balance between βarr2 and G protein. We further studied this position, by focusing on a receptor lacking a polar residue in position 6.55, namely the serotonin 1A receptor (5HT1AR). According to our working model, the WT 5HT1AR (A6.55) should exhibit lower βarr2 recruitment efficacy compared to its variant with a polar residue in this position. Remarkably, BRET experiments show that a A6.55N variant of the 5HT1AR gains coupling of βarr2 over G_z, G_{oB} and G_{i2} as indicated by ratios > 1 (e.g. βarr2 vs G_{oB}, etc. Figure 4). This suggests that evolutionary variations in position 6.55 is a way of nature to fine-

tune βarr recruitment and in turn receptor internalization or βarr-mediated signaling for neurotransmitter receptors.

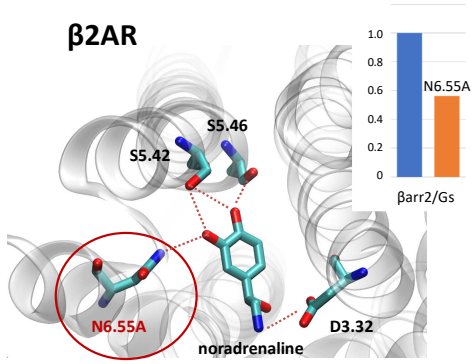

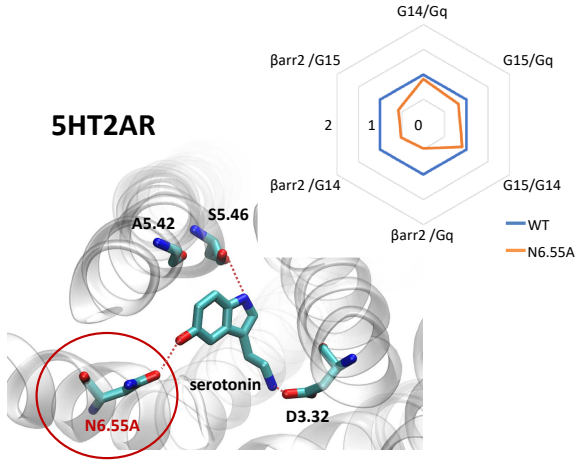

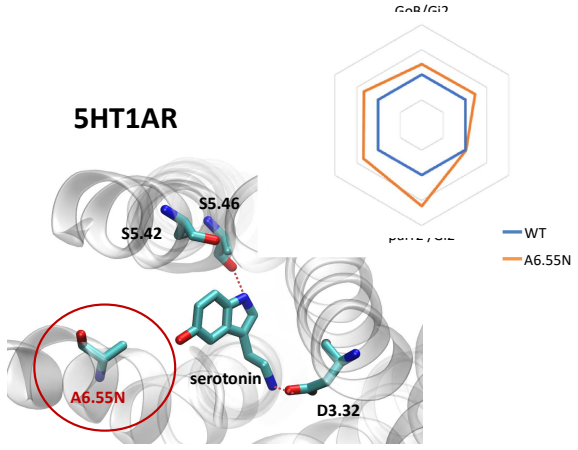

Figure 4 *Relevance of H6.55 for neurotransmission at the β2AR, 5HT2AR and 5HT1AR.*
Coupling response was approximated using the ratios of the AUC of corresponding response curves (Figure S6) for individual signaling effectors (e.g. βarr2 vs G_z, βarr2 vs G_{oB} etc.). To eliminate observational bias linked to differences within biosensor assays (e.g. βarr2 vs G_i), we use the response at the WT receptor as internal standard for analyzing the ratios of areas under the curve (AUC). Note that obtained AUC ratios (i.e. the receptor's ability to couple to different effector proteins) is not affected by expression levels of the receptor (i.e. receptor concentration) which can change upon mutation. All plots were generated from dose-response curves obtained from a minimum of 2 independent experiments.

Discussion

By means of classical molecular dynamics simulation, enhanced sampling techniques, live-cell biosensor assays and the use of structurally related signaling probes, we have dissected the balanced coupling profile (G_{i2}, G_z, G_{oB} and βarr2) of the neurotransmitter dopamine at the D2R. In order to understand the contribution of each aromatic OH-group to the coupling outcome, we studied p- and m-tyramine in a first step. We propose that exclusive TM5 interaction via the p-OH group of p-tyramine (Figure 1M) significantly alters the coupling profile compared to dopamine and yields a strong bias of G_{oB} over βarr2 (Figure 1D and R). A recent study by Sommer et al. identified the compound hordenine which differs from p-tyramine only by additional N,N-di-methyl groups[23]. Interestingly, authors report that hordenine induces G protein activation measured as cAMP inhibition whereas it antagonizes β-arrestin recruitment. We tested the ability of hordenine to recruit the different types of G_i proteins and βarr2 using our live-cell BRET-based biosensors. We find a preferential G_{oB} coupling profile similar to p-tyramine (Figure S7) concluding that mostly G_{oB} and less G_z or G_{i2} contribute to the observed cAMP inhibition. At the level of D2R binding, our data suggest that hordenine's preference for G_{oB} coupling is linked to exclusive TM5 interaction (Figure S7).

Based on the coupling outcome of dopamine, we further conclude that additional contacts with TM6 via its m-OH group are responsible for recovering in particular βarr2 coupling (Figure 1N-O). Curiously, a molecule, that possesses only the m-OH group (m-tyramine) elicits

a coupling response that is in between the one of dopamine and p-tyramine (Figure 1A-D, red line). This seems to be a result of its rotational freedom and the co-existence of two different binding modes (Figure 1P-Q). We prove this by using rigid dopamine analogues (5- and 7-OH-DPATs) that preferentially adopt one binding mode. Their coupling outcome is governed by their chirality which goes along with a recent study by Möller et al.[24]

Interestingly, none of the tested compounds induce preferential coupling to βarr2. McCorvy et al. suggest that βarr2 bias in the D2R can be induced by exclusive contacts to Ile184 in the extracellular loop 2 (ECL2).[25] Computing the frequency of ligand contacts with Ile184 indicate that our studied compounds (i.e. dopamine, m-/p-tyramine, DPATs and hordenine) are too small to establish significant contacts (Table S6, contact frequencies $\leq$15%). This would explain their preferential G protein or balanced coupling profile. Another study by Weichert et al. reports that βarr bias can be obtained by contacts in the extended binding pocket formed by TM2 and TM7[26] which again is hardly within reach of our tested small molecular probes. However, these examples highlight the existence of multiple sites that modulate βarr2 coupling in the D2R.

Altogether, our data suggests that the mechanism that underlies dopaminergic neurotransmission involves ligand-mediated polar network between TM5 and TM6 at the D2R. This translates into a balanced coupling response (G_{i2}, G_z, G_{oB} and βarr2). We were able to support this notion by a comprehensive mutational study of the key residue 6.55 in TM6. By introducing non-polar (alanine or phenylalanine) or polar residues (asparagine) into this position and thus hindering or facilitating a polar network that links TM5 and TM6, we are able to reduce or enhance βarr2 recruitment, respectively (Figure 3). This observation prompted us to investigate if the described structural features form part of a general mechanism for other systems. Importantly, we demonstrate that also serotonin- and adrenaline-mediated neurotransmission via the 5HT2AR and the β2AR is linked to a polar residue in position 6.55 (Figure 4). This finding is strongly supported by a study that was published during the preparation of this manuscript. Masureel et al. focused on the coupling/signaling response of salmeterol - a β2AR-targeted drug used for the treatment of asthma and chronic obstructive pulmonary disease[27]. The authors conclude that limited βarr recruitment

induced by salmeterol in the β2AR is linked to reduced contacts with N6.55 highlighting the significance of this position. This represents a case in which the site that are critical for the balanced neurotransmitter action as well as the biased drug action in the β2AR topologically overlap. Curiously, not all receptors have a polar residue in position 6.55 as seen for the serotonin receptor 5HT1AR (A6.55). It is possible that variation of this position is a way of how nature modulates βarr recruitment for different neurotransmitter receptor and in turn receptor internalization or βarr-mediated signaling. This is supported by our finding that introducing a polar residue into position 6.55 (A6.55N) yields an engineered 5HT1AR that upon neurotransmitter binding favors βarr2 over all tested G proteins.

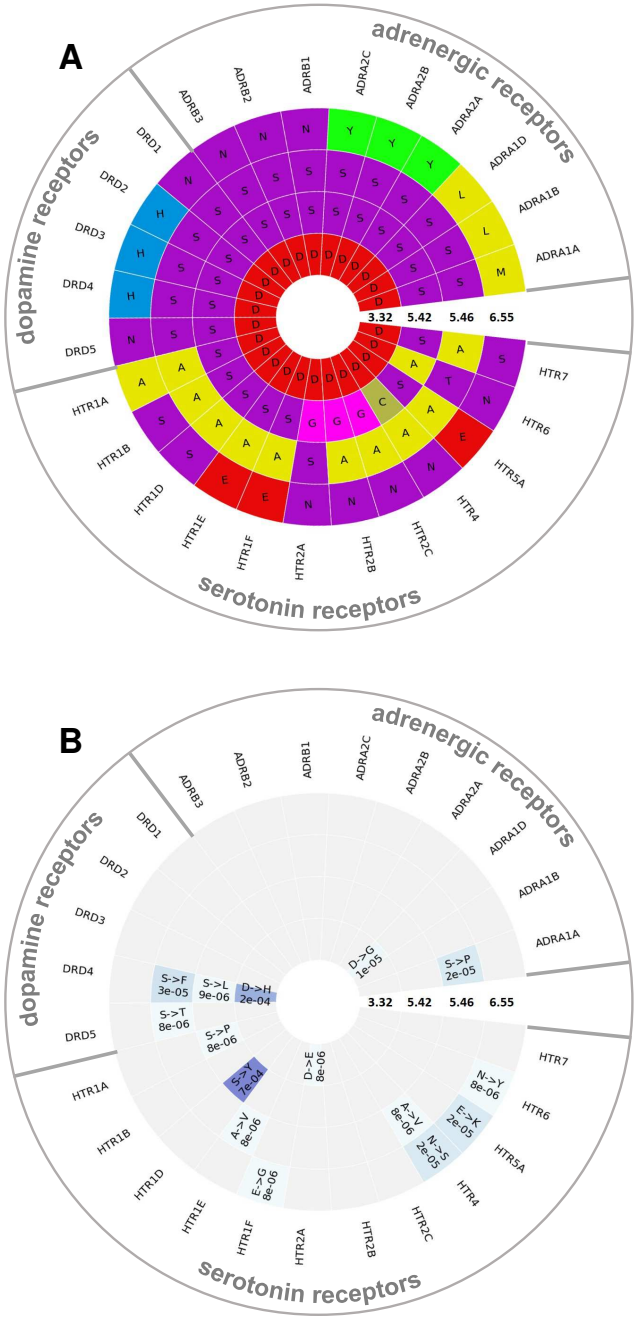

Figure 5 *Sequence conservation and natural genetic variance in key position for neurotransmitter binding across dopamine, serotonin and adrenergic receptors.*

*(**A**): Sequence alignment and conservation of key positions forming the salt bridge (3.32) and polar contacts in TM5 (5.42, 5.46) and TM6 (6.55). (**B**): Natural genetic variance indicating the type of substitution and frequency extracted from the GPCRdb database[22,28] and the Exome Aggregation Consortium.[29]*

A complete sequence analysis for all dopamine, serotonin and adrenaline receptors (26 GPCRs) provides a comprehensive overview of variations in neurotransmitter binding positions (3.32, 5.42, 5.46 and 6.55, Figure 5A). It appears that most variation is found in the serotonin receptor family compared to dopamine and adrenergic receptors. Across the studied set, position 3.32 and 5.42 are highly conserved whereas more differences are found in position S5.46 and 6.55. We envisage that such variation will modulate the coupling and signaling outcome for different subtype receptors within a family and beyond. For instance, we expect that differences in the polarity of position 6.55 impact in particular βarr coupling and in turn receptor internalization or βarr-mediated signaling. Thus, the group of α1 adrenergic receptors with a nonpolar residue (L,M6.55) is likely to have an innately reduced arrestin coupling compared to the β adrenergic receptors with a conserved polar residue in position 6.55 (N6.55). A similar tendency is expected for the 5HT1AR (A6.55) in comparison to the group of 5HT2, 5HT4, 5HT6 and 5HT7 (N6.55). This goes along with our finding that the 5HT1AR can be converted into a 5HT2-like receptor with enhanced βarr coupling properties by introducing a polar residue into position 6.55 (A6.55N, Figure 4). At times, substitution can be also polar-to-polar as seen in the dopaminergic receptor family (H6.55N). Such polar-to-polar substitutions should be able to mostly preserve the key interaction with the neurotransmitter and thus receptor coupling properties which is supported by experimental validation of the D2R H6.55N mutant (Figure 3).

All in all, selected validation experiments confirm that knowledge of the sequence in key positions for neurotransmitter binding can be used to predict the innate coupling specificity of distinct GPCRs. In this respect, our work suggests that natural genetic variations of these positions can also alter the functional outcome of a specific receptor. Analysis of healthy individuals (data extracted from the GPCRdb database[22,28] and the Exome Aggregation Consortium[29]) reveal primarily rare events (frequency < 1%) (Figure 5B) with the highest

occurrence in the serotonin receptor family when compared to dopamine and adrenergic receptors (Figure 5B). Despite potential impact on the signaling outcome, genetic variances within all three studied families seem to be well tolerated as they are observed in healthy individuals.

Conclusion

In the present work, we dissect the action of the neurotransmitter dopamine at the dopaminergic D2 receptor combining classical molecular dynamics simulation, enhanced sampling techniques, live-cell biosensor assays and mutational validation. By this means, we reveal how dopamine binding translates into a distinct coupling profile (G_{i2}, G_z, G_{oB} and βarr2) involving key contacts with TM5 (S5.42) and TM6 (H6.55). Most importantly, we report that this mechanism is common to other neurotransmitter receptors. In addition, we suggest that sequence variations across receptor subtypes or natural genetic variance in position 6.55 are a potential way to fine-tune β-arrestin recruitment and in turn receptor internalization or βarr-mediated signaling of neurotransmitter receptors. Ultimately, such structural insights have important implications for the rational development of new ligands with a tailored signaling profile.

Methods

Homology modelling of the active state of D2R

The canonical sequence of the D2 receptor was obtained from the Uniprot database (accession number: P14416). The sequence was aligned with that of the β2AR obtained from the template structure (PDB code: 3P0G) using Clustal Omega.[30] The alignment was manually refined to maintain the position of highly conserved residues. The first 36 residues of the D2R sequence were truncated as they formed a flexible N-terminal tail. The long intracellular loop 3 was shortened and the ends were fused. Based on the obtained alignment, we generated 500 models using homology model tool implemented in the available in the MOE package (http://www.chemcomp.com). The best model was selected based on the lowest DOPE (Discrete Optimized Protein Energy) score. The hydrogen network was optimized at pH 7 using Protonate3D[31] available in the MOE package (http://www.chemcomp.com).

Generation of protein-ligand complexes

The starting poses dopamine were obtained by docking with GOLD software.[32] The atoms of the protein were kept rigid, while the ligand was allowed flexibility. A positional restraint was included, to take into account only poses in which the ligand forms polar interactions with D3.32. Using this protocol 900 poses were generated per ligand. The poses were scored with goldscore, and rescored using the plp score. Afterwards the best poses for each ligand were picked taking into account the scoring, as well as visual inspection. Each ligand-protein complex was optimized during a MD run in conditions of constant pressure (see below for a description). Then, initial poses for m-tyramine and p-tyramine were obtained by removing the meta or para hydroxyl group of the dopamine pose obtained after the MD optimization.

Structural models for the 5HT1AR and 5HT2AR in complex with serotonin were obtained based on the work from Martí-Solano et al.[9] The complex for the β2AR with noradrenaline was modeled using the crystallized structure of the adrenaline-β2AR complex (PDB code: 4LDO). After converting adrenaline into noradrenaline (i.e. removing the N-methyl group), the structure was subjected to a short minimization using the MOE package (http://www.chemcomp.com).

Molecular dynamics simulations

To generate starting systems, ligands (in accordance with their poses obtained in the previous step) were placed in the active state model of the D2R. To ensure proper orientation of the receptor in the membrane, the complexes were aligned to the structure used as the template (PDB code: 3P0G) obtained from the OPM database.[33] Subsequently, we used the output aligned structures to generate systems for molecular dynamics. The systems were generated using CHARMM-GUI.[34] The receptor was embedded in a ~ 80 x 80Å POPC bilayer. The resulting complex was solvated with ~ 8200 TIP3 molecules. The ionic strength of the solution was kept at a 0.15 M with of NaCl ions. Additional chloride ions were added in order to keep the charge of the system neutral. Disulfide bonds were introduced in accordance with data obtained from the Uniprot database. Parameters for the simulation were obtained from the CHARMM36 forcefield.[35] Parameters for the ligand were assigned from the CGenFF forcefield automatically by the ParamChem tool

implemented in CHARMM-GUI.[36,37] The systems were first equilibrated in conditions of constant pressure (NPT, 1.01325 bar) for 100 ns. Over the first half of the simulation we applied constraints to the backbone atoms. The constraints were gradually released over the first 50ns of the simulation. After the NPT step, we have carried out simulations in conditions of constant volume (NVT) of the system for 600 ns in 4 replicates. The simulations were run in ACEMD.[38] We used a time-step of 4 fs. Such a large time-step was possible due to the hydrogen mass repartitioning scheme being employed in Acemd.[39] A non-bonded interaction cutoff was set at 9 Å. A smooth switching function for the cut-off was applied, starting at 7.5 Å. Long-distance electrostatic forces were calculated using the Particle Mesh Ewald algorithm. The algorithm had grid spacing of 1 Å. The bond lengths of hydrogen atoms were kept constrained using the RATTLE algorithm. Simulations were carried out at a temperature of 300K in periodic boundary conditions.

Metadynamics

Metadynamics is a biased dynamics technique widely used to improve sampling for free energy calculations over a set of multidimensional reaction coordinates which would not be sampled exhaustively with normal unbiased simulations.[40] It is implemented in the molecular dynamics code ACEMD using the PLUMED plugin interface.[41] Here, we use this approach to construct the complete energetic binding landscape of dopamine and its derivatives. For this, we used as collective variables the distance of oxygen atoms of m- and/or p-OH groups of the ligand to the OG atom of S5.42 (CV1) and/or S5.46 (CV2) in TM5 (Figure S2). The metadynamics parameters were set to a Gaussian hill height of 0.1 kcal mol-1 with a spread of 0.1 Å for the CV1 and/or CV2. The deposition rate was one hill every 4 ps and a well-tempered bias factor of 10. To ensure exhausted sampling within the orthosteric binding site, we set a restraining potential with an energy constant Kappa of 100 that starts acting when the distance of the CV1 or CV2 exceeds 12 Å. In addition, we used the multiple walker approach,[42] in which 6 walkers simultaneously explore the same free-energy landscape and interact by contributing to the same history-dependent bias potential every 20 ps. Walkers for each ligand were obtained from unbiased NVT simulations (protocol described in previous step). Each system was simulated for an accumulated time of at least 1.1 μs or until the free-energy landscape converged. General

simulation parameters were kept as described for the production run in the previous section. Ultimately, we plotted the energies as a function of the distance between the ligand's oxygen group and S5.42 or S5.46 (Figure 1 and 2). In order to ensure the convergence of our metadynamics simulation, we monitored the changes of the free energy profile along the simulation time. For this, we computed the free energy every 20000 deposited Gaussians yielding 15 to 20 graphs per simulation setup.

Experimental validation using a cell-based assay

Bioluminescence resonance energy transfer (BRET)-based biosensor assays (bioSensAll^{TM}) were conducted at Domain Therapeutics NA Inc. (Montreal, QC, Canada). Assays were performed in HEK-293T cells, which were cultured in Dulbecco's Modified Eagle Medium (DMEM) (Wisent # 319-015-CL) supplemented with 1% penicillin-streptomycin (Wisent; cat# 450-201-EL) and 10% fetal bovine serum (Wisent # 090150) and maintained at 37 °C with 5% CO2. All biosensor-coding plasmids and related information are the property of Domain Therapeutics NA Inc: GAPL-Gi2 (cat# DTNA A29), GAPL-, GAPL-GoB (cat# DTNA A32), GAPL-Gz (cat# DTNA A33) and βarr2-PM + GRK2 WT (cat# DTNA A46). Information pertaining to the βarr2-PM biosensor has been previously published.[43] Experiments with the D2R were performed with the long isoform (canonical sequence, post-synaptic localization; Uniprot P14416-1). All receptor point mutations were produced by TOP Gene Technologies Inc. (Montreal, QC, Canada). Transfections were performed using 25-kDa linear PEI (Polysciences, Warrington, PA) at a 3:1 µl of PEI/µg of DNA ratio. Briefly, DNA and PEI were diluted separately in 150 mM NaCl, mixed and then incubated for at least 20 minutes at room temperature (note: total amount of DNA transfected was adjusted to a final quantity of 2 µg with salmon sperm DNA (Invitrogen)). During the 20 minute incubation, HEK-293T cells were detached, counted and re-suspended into cell culture medium to a final density of 350 000 cells/mL. At the end of the 20 minute incubation, DNA/PEI complexes were added to cells followed by a gentle mixing. Cells were subsequently distributed in cell culture-treated 96-well plates (White Opaque 96-well Microplates, Greiner, cat# 655) at a density of 35 000 cells per well (i.e., 100 µL of cell suspension per well) and incubated at 37°C for 48h. At 48 hours post-transfection, the transfection medium was removed and cells were washed once with 100 µl of Tyrode-Hepes

buffer (Sigma, cat# T2145 + H9136) per well. Wash buffer was then replaced by 100 µl of fresh Tyrode-Hepes buffer per well and plates were incubated for 60 min at room temperature. At the end of this equilibration period, 10 µl of 20µM e-Coelenterazine Prolume Purple (Methoxy e-CTZ; Nanolight, # 369) was added to each well followed immediately by the addition of increasing test compound concentrations. Cells were then incubated at room temperature for 10 minutes and BRET readings subsequently collected with a 0.4sec integration time on a Synergy NEO plate reader (BioTek Instruments, Inc., USA; filters: 400nm/70nm, 515nm/20nm). The BRET signal was calculated as the ratio of GFP10 emission to RLucII emission. All resulting dose response curves are represented as baseline-corrected *u*BRET (i.e., baseline *u*BRET values subtracted from curves).

Purchased compounds

(R)-7-OH-DPAT: Cedarlane (Axon Medchem # 1013), (S)-7-OH-DPAT: Cedarlane (Axon Medchem # 1014), (R)-5-OH-DPAT: Cedarlane (Axon Medchem # 1007), (S)-5-OH-DPAT: Cedarlane (Axon Medchem # 1008), hordenine: Sigma #04476, m-tyramine hydrochloride: Sigma # D017, Lot: 063K4620, p-tyramine hydrochloride: Sigma # T90344, noradrenaline hydrochloride: Sigma # 74480, serotonin hydrochloride: Sigma #H9523, dopamine hydrochloride: Sigma # H8502.

Operational model of bias

The operational model of agonism was used to estimate ligand bias when applicable according to recently published protocols.[18,19] All data was analyzed using the nonlinear curve fitting functions in GraphPad Prism (v6.0; GraphPad Software, La Jolla, CA). Ligand bias was quantified by analyzing the dose-response curves using the operational model of agonism according to the equation

$$E = Basal + \frac{(E_m - Basal)}{1 + \left(\frac{\left(\frac{[A]}{10^{logK_A}} + 1 \right)}{10^{logR}\ x\ [A]} \right)^n}$$

where:

E = effect of the ligand;

$[A]$ = concentration of agonist;

Em = maximal possible response of the system;
Basal = basal level of response in the absence of agonist;
logKA = logarithm of the functional equilibrium dissociation constant of the agonist;
n = slope of the transducer function that links occupancy to response;
logR = logarithm of the transduction ratio, τ/KA, where τ is an index of the coupling efficiency (or efficacy) of the agonist.

The following parameters were used for fitting of all families of agonist curves at each pathway to the model: *Basal, Em*, and *n* were shared between all agonists; for full agonists, *logKA* was constrained to a value of zero; for partial agonists, *logKA* was directly estimated by the curve fitting procedure. The *logR* [i.e., *log*(τ/KA)] parameter was estimated as a unique measure of activity for each agonist.
The logarithmic form of the transduction ratios (τ/KA) were then obtained from fitted dose-response curves for the recruitment of G_{oB} and β-arrestin-2 (determined BRET-based assay). To account for cell-system-dependent factors between different assay systems, the transduction coefficients (τ/KA) were normalized to the response of the reference agonist dopamine:

$$\Delta log\left(\frac{\tau}{KA}\right) = log\left(\frac{\tau}{KA}\right)_{test\ ligand} - log\left(\frac{\tau}{KA}\right)_{reference\ ligand}$$

Coupling bias was obtained by calculating the difference between two investigated pathways for the same ligand:

$$\Delta\Delta log\left(\frac{\tau}{KA}\right)_{GoB\ vs\ \beta arr2} = \Delta log\left(\frac{\tau}{KA}\right)_{GoB} - \Delta log\left(\frac{\tau}{KA}\right)_{\beta arr2}$$

$$bias\ factor = 10^{\Delta\Delta log\left(\frac{\tau}{KA}\right)_{GoB\ vs\ \beta arr2}}$$

Acknowledgements
The authors would like to thank Dorothee Möller, Peter Gmeiner and Michel Bouvier for discussion and helpful comments on GPCR signaling bias.

Author Contributions
TMS, JS performed computational experiments which guided wet lab experiments carried out by AM. TMS, AM, BB and JS analysed and interpreted obtained results. MTF carried out the sequence analysis of receptors and their natural genetic variants. TMS, MTF and JS prepared figures for publication. TMS and JS wrote the manuscript

with input from AM and BB. JS supervised and coordinated the project.

Competing interests
The authors declare no conflict of interest.

References
1. Elias, L. J. & Saucier, D. M. Neuropsychology : clinical and experimental foundations. (Pearson/Allyn & Bacon, 2006).
2. Venter, J. C. et al. The sequence of the human genome. Science 291, 1304–1351 (2001).
3. Beaulieu, J. M., Espinoza, S. & Gainetdinov, R. R. Dopamine receptors - IUPHAR review 13. Br. J. Pharmacol. 172, 1–23 (2015).
4. Violin, J. D. et al. Selectively Engaging B-Arrestins at the Angiotensin II Type 1 Receptor Reduces Blood Pressure and Increases Cardiac Performance. Pharmacol. Ther. 335, 572–579 (2010).
5. White, K. L. et al. The G protein-biased κ-opioid receptor agonist RB-64 is analgesic with a unique spectrum of activities in vivo. J. Pharmacol. Exp. Ther. 352, 98–109 (2015).
6. Masri, B. et al. Antagonism of dopamine D2 receptor/beta-arrestin 2 interaction is a common property of clinically effective antipsychotics. Proc. Natl. Acad. Sci. U. S. A. 105, 13656–13661 (2008).
7. Männel, B. et al. Hydroxy-Substituted Heteroarylpiperazines: Novel Scaffolds for β-Arrestin-Biased D2R Agonists. J. Med. Chem. 60, 4693–4713 (2017).
8. Möller, D. et al. Discovery of G Protein-Biased Dopaminergics with a Pyrazolo[1,5-a]pyridine Substructure. J. Med. Chem. 60, 2908–2929 (2017).
9. Martí-Solano, M. et al. Detection of new biased agonists for the serotonin 5-HT2A receptor: modeling and experimental validation. Mol. Pharmacol. 87, 740–746 (2015).
10. Woodward, R., Coley, C., Daniell, S., Naylor, L. H. & Strange, P. G. Investigation of the role of conserved serine residues in the long form of the rat D2 dopamine receptor using site-directed mutagenesis. J. Neurochem. 66, 394–402 (1996).
11. Fowler, J. C., Bhattacharya, S., Urban, J. D., Vaidehi, N. & Mailman, R. B. Receptor Conformations Involved in Dopamine D2L Receptor Functional Selectivity Induced by Selected

Transmembrane-5 Serine Mutations. Mol. Pharmacol. 81, 820–831 (2012).
12. Wiens, B. L., Nelson, C. S. & Neve, K. A. Contribution of Serine Residues to Constitutive and Agonist- Induced Signaling via the D 2S Dopamine Receptor : Evidence for Multiple , Agonist-Specific Active Conformations. Mol. Pharmacol. 444, 435–444 (1998).
13. Cox, B. A., Henningsen, R. A., Spanoyannis, T., Neve, T. L. & Neve, K. A. Contributions of Conserved Serine Residues to the Interactions of Ligands with Dopamine D , Receptors. J. Neurochem. 59, 627–635 (1992).
14. Saleh, N., Ibrahim, P. & Clark, T. Differences between G-Protein-Stabilized Agonist–GPCR Complexes and their Nanobody-Stabilized Equivalents. Angew. Chemie - Int. Ed. 56, 9008–9012 (2017).
15. Marino, K. a., Sutto, L. & Gervasio, F. L. The effect of a widespread cancer-causing mutation on the inactive to active dynamics of the B-Raf kinase. J. Am. Chem. Soc. 137, 5280–5283 (2015).
16. Coley, C., Woodward, R., Johansson, A. M., Strange, P. G. & Naylor, L. H. Effect of Multiple Serine / Alanine Mutations in the Transmembrane Spanning Region V of the D 2 Dopamine Receptor on Ligand Binding. J. Neurochem. 74, 358–366 (2000).
17. Kling, R. C., Tschammer, N., Lanig, H., Clark, T. & Gmeiner, P. Active-state model of a dopamine D2 receptor - Gai complex stabilized by aripiprazole-type partial agonists. PLoS One 9, 1–10 (2014).
18. Kenakin, T. & Christopoulos, A. Signalling bias in new drug discovery: detection, quantification and therapeutic impact. Nat. Rev. Drug Discov. 12, 205–216 (2013).
19. van der Westhuizen, E. T., Breton, B., Christopoulos, A. & Bouvier, M. Quantification of Ligand Bias for Clinically Relevant 2-Adrenergic Receptor Ligands: Implications for Drug Taxonomy. Mol. Pharmacol. 85, 492–509 (2014).
20. Cannon, J. G. Structure-activity relationships of dopamine agonists. Annu. Rev. Pharmacol. Toxicol. 23, 103–129 (1983).
21. Ring, A. M. et al. Adrenaline-activated structure of β2-adrenoceptor stabilized by an engineered nanobody. Nature 502, 575–579 (2013).

22. Pándy-Szekeres, G. et al. GPCRdb in 2018: Adding GPCR structure models and ligands. Nucleic Acids Res. 46, D440–D446 (2018).
23. Sommer, T. et al. Identification of the beer component hordenine as food-derived dopamine D2 receptor agonist by virtual screening a 3D compound database. Sci. Rep. 7, 1–12 (2017).
24. Möller, D. et al. Discovery of G Protein-Biased Dopaminergics with a Pyrazolo [1,5-a] pyridine Substructure Discovery of Substructure. J. Med. Chem. 60, 2908–2929 (2017).
25. McCorvy, J. D. et al. Structure-inspired design of β-arrestin-biased ligands for aminergic GPCRs. Nat. Chem. Biol. 14, 126–134 (2017).
26. Weichert, D. et al. Molecular Determinants of Biased Agonism at the Dopamine D 2 Receptor. J. Med. Chem. 58, 2703–2717 (2015).
27. Masureel, M. et al. Structural insights into binding specificity, efficacy and bias of a β2AR partial agonist. Nat. Chem. Biol. 14, 1059–1066 (2018).
28. Hauser, A. S. et al. Pharmacogenomics of GPCR drug targets. Cell 172, 1–14 (2018).
29. Lek, M. et al. Analysis of protein-coding genetic variation in 60,706 humans. Nature 536, 285–291 (2016).
30. Sievers, F. et al. Fast, scalable generation of high-quality protein multiple sequence alignments using Clustal Omega. Mol. Syst. Biol. 7, 539–539 (2014).
31. Labute, P. Protonate3D: Assignment of ionization states and hydrogen coordinates to macromolecular structures. Proteins Struct. Funct. Bioinforma. 75, 187–205 (2009).
32. Verdonk, M. L., Cole, J. C., Hartshorn, M. J., Murray, C. W. & Taylor, R. D. Improved protein-ligand docking using GOLD. Proteins Struct. Funct. Genet. 52, 609–623 (2003).
33. Lomize, M. a., Lomize, A. L., Pogozheva, I. D. & Mosberg, H. I. OPM: Orientations of proteins in membranes database. Bioinformatics 22, 623–625 (2006).
34. Jo, S., Lim, J. B., Klauda, J. B. & Im, W. CHARMM-GUI Membrane Builder for mixed bilayers and its application to yeast membranes. Biophys. J. 97, 50–58 (2009).
35. Klauda, J. B. et al. Update of the CHARMM All-Atom Additive Force Field for Lipids: Validation on Six Lipid Types. J. Phys. Chem. B 114, 7830–7843 (2010).

36. Vanommeslaeghe, K. et al. CHARMM general force field: A force field for drug-like molecules compatible with the CHARMM all-atom additive biological force fields. J. Comput. Chem. 31, 671–690 (2010).
37. Yu, W., He, X., Vanommeslaeghe, K. & MacKerell, A. D. Extension of the CHARMM general force field to sulfonyl-containing compounds and its utility in biomolecular simulations. J. Comput. Chem. 33, 2451–2468 (2012).
38. Harvey, M. J., Giupponi, G. & De Fabritiis, G. ACEMD: Accelerating biomolecular dynamics in the microsecond time scale. J. Chem. Theory Comput. 5, 1632–1639 (2009).
39. Feenstra, K. A., Hess, B. & Berendsen, H. J. C. Improving efficiency of large time-scale molecular dynamics simulations of hydrogen-rich systems. J. Comput. Chem. 20, 786–798 (1999).
40. Laio, A. & Gervasio, F. L. Metadynamics: a method to simulate rare events and reconstruct the free energy in biophysics, chemistry and material science. Reports Prog. Phys. 71, 126601 (2008).
41. Bonomi, M. et al. PLUMED: A portable plugin for free-energy calculations with molecular dynamics. Comput. Phys. Commun. 180, 1961–1972 (2009).
42. Raiteri, P., Laio, A., Gervasio, F. L., Micheletti, C. & Parrinello, M. Efficient reconstruction of complex free energy landscapes by multiple walkers metadynamics. J. Phys. Chem. B 110, 3533–3539 (2006).
43. Namkung, Y. et al. Monitoring G protein-coupled receptor and β-arrestin trafficking in live cells using enhanced bystander BRET. Nat. Commun. 7, 12178 (2016)

Supplementary information

Summary of molecular dynamics simulations

Table S1. *Molecular dynamics simulation: classical unbiased simulation and metadynamics enhanced sampling.*

Compound	comment	Simulation time [μs]
dopamine	unbiased simulation protonation state 1: HSD6.55 protonation state 2: HSE6.55	 4 x 0.6 4 x 0.6
p-tyramine	unbiased simulation	4 x 0.6
m-tyramine	unbiased simulation	4 x 0.6
(R)-7-OH-DPAT	unbiased simulation	4 x 0.6
(S)-7-OH-DPAT	unbiased simulation	4 x 0.6
(R)-5-OH-DPAT	unbiased simulation	4 x 0.6
(S)-5-OH-DPAT	unbiased simulation	4 x 0.6
dopamine	metadynamics bias on m-OH	3.04
dopamine	metadynamics bias on p-OH	1.45
p-tyramine	metadynamics bias on p-OH	2.40
m-tyramine	metadynamics bias on m-OH	1.25
(R)-7-OH-DPAT	metadynamics bias on 7-OH	1.50
(S)-7-OH-DPAT	metadynamics bias on 7-OH	1.35
(R)-5-OH-DPAT	metadynamics bias on 5-OH	1.30
(S)-5-OH-DPAT	metadynamics bias on 5-OH	3.20
hordenine	metadynamics bias on p-OH	3.58
	Total simulation time	**38.27**

General binding mode of dopamine by unbiased molecular dynamics simulation

A first approximation of the dopamine binding mode was obtained by unbiased molecular dynamics simulation (Figure S1). The initial pose of dopamine, was obtained using the structure of adrenaline bound to the active β2-adrenergic receptor in complex with adrenaline (PDB code: 4LDO). The binding of dopamine is mediated via a salt bridge formed between the protonated nitrogen of dopamine and the highly conserved D3.32. In addition, meta and para hydroxyl groups establish polar contacts with TM5 and TM6. In particular, polar interactions with TM5 are in agreement with site directed mutagenesis[1–5] and computational[6] studies. Note that interaction with TM6 are mediated by a water molecule at times.

Previous site directed mutagenesis studies[7] propose that H6.55 is important in binding several D2R ligands. At the simulated pH 7.0, H6.55 can exist in two transient protonation states. Individual protonation states are driven by its environment such as a completely solvated pocket or a pocket occupied by diverse ligands. We have carried out parallel simulations of the dopamine-D2R complex, to compare how the protonation state impacts dopamine binding. Thereby, HSD corresponds to the histidine with protonation on δ1 whereas HSE corresponds to the histidine with protonation on ε2. The results show that in the HSD state this residue establishes more frequently polar interactions with dopamine. Thus H6.55 was assigned the HSD protonation state in all of the subsequent simulations.

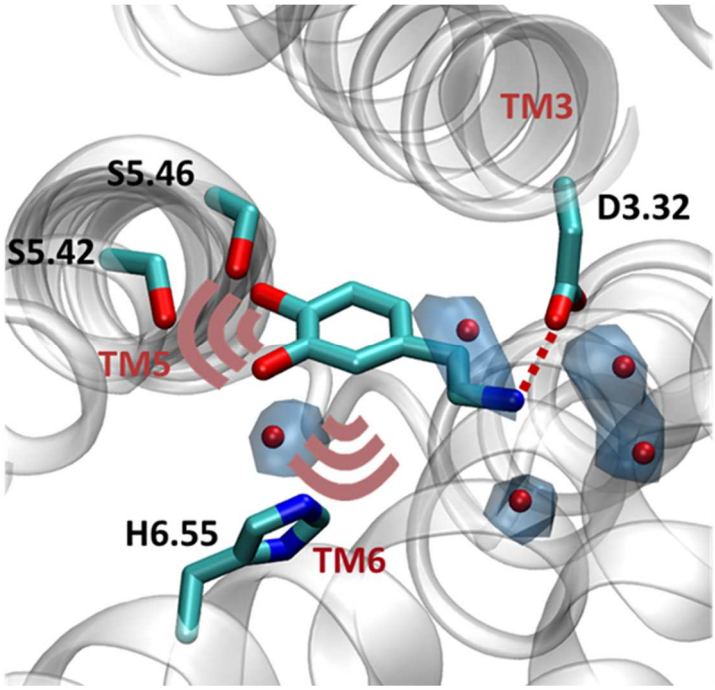

Figure S1 *General binding mode of dopamine.*
Green dashed line: hydrophobic interactions, red dashed lines: salt bridge, red radar: polar contacts, blue surface: occupancy map of water is calculated over classical unbiased simulation using the volmap tool implemented in VMD software package.[8]

Site directed mutagenesis data

During the last decades, several mutagenesis studies have explored the impact of polar residues (S5.42, S5.43 and S5.46) in TM5 for binding of dopamine analogues. While they agree in TM5 as important anchor point for binding of dopamine analogues, deviating results are obtained for individual residues. Here we provide a selection of references in Table S2. It is worth noting that mutation-induced alteration of ligand binding (Table S2A) does not always correlate to an altered ligand efficacy even in the same experimental setup (summarized in Table S2B). For instance, a S5.46A mutation reduces only slightly DA binding while almost abolishing ligand efficacy.[2] One possible explanation is that the S5.46A mutation affects signaling in a manner independent of ligand-receptor contacts (i.e. by disturbing a conserved ionic lock within the receptor). In addition, the slight effect on the binding affinity can be induced by

water-mediated indirect interaction or by a general perturbation of the hydrogen bonding network around the ligand.

Table S2A *Impact of mutations of serine residues in TM5 on binding of dopamine and its analogues at the D2 receptor.*

Single mutants	Isoform	Assay type	S5.42A	S5.46A	reference
Dopamine	long	K_i versus [^{3}H]spiperone	77↓	2↓	[171]
Dopamine	long	$K_{0,5}$ versus [^{3}H]N-methylspiperone	177↓	8↓	[172]
Dopamine (low affinity state)	short	K_L versus [^{3}H]spiperone	250↓	4↓	[173]
Dopamine (high affinity state)	short	K_H versus [^{3}H]spiperone	400↓	4↓	[173]
Dopamine	short	KI versus ['251]epidepride	48↓	2.6↓	[174]
p-tyramine	short	KI versus ['251]epidepride	2↓	insignificant	[174]
m-tyramine	short	KI versus ['251]epidepride	insignificant	insignificant	[174]

Table S2B *Impact of mutations of serine residues in TM5 on the signaling response elicited by dopamine and its analogues at the D2 receptor.*

Single mutants	Assay type	WT	S5.42A	S5.46A	ref
Dopamine	Inhibition of isoproterenol-stimulated cAMP accumulation [EC50]	1	220↓	18↓	[174]
Dopamine	Inhibition of isoproterenol-stimulated cAMP accumulation [EC50]	1	667↓	1,6↓	[173]
Dopamine	Inhibition of forskolin-stimulated cAMP accumulation [EC50]	1	no observable inhibition	no observable inhibition	[172]
Dopamine	Potency of probe ligands in affecting GTP γ S binding [EC50]	1	6,29↓	no observable binding	[172]
Dopamine	Inhibition of isoproterenol-stimulated cAMP accumulation [Emax]	92%	81%	90%	[174]
Dopamine	Inhibition of isoproterenol-stimulated cAMP accumulation [Emax]	81%	78%	94%	[173]

Dopamine	Inhibition of forskolin-stimulated cAMP accumulation [percent of the inhibition elicited by quinpirole in the WT receptor]	100%	5%	20%	[172]
Dopamine	Ligand-stimulated binding of [35S]GTPgS [percent of the response in the WT receptor]	100%	97%	80%	[173]
p-tyramine	Inhibition of isoproterenol-stimulated cAMP accumulation [EC50]	1	no significant change in respect to WT	no significant change in respect to WT	[174]
p-tyramine	Inhibition of isoproterenol-stimulated cAMP accumulation [Emax]	60%	no significant change in respect to WT	no significant change in respect to WT	[174]
m-tyramine	Inhibition of isoproterenol-stimulated cAMP accumulation [EC50]	1	no significant change in respect to WT	no significant change in respect to WT	[174]
m-tyramine	Inhibition of isoproterenol-stimulated cAMP accumulation [Emax]	70%	no significant change in respect to WT	no significant change in respect to WT	[174]

Metadynamics and applied bias

To exhaustively sample all potential binding modes, we biased contacts of m- and/or p-OH groups to polar residues in TM5 (S5.42 and S5.46) with a distance restraint of 12 Å. In addition, we applied a constraint to maintain the protonated nitrogen within a distance of 5 Å of the carboxylic group the D3.32. In initial experiments, we also biased the distance of aromatic substituents to S5.43. However, we did not obtain any binding peaks, therefore neglecting this interaction for following experiments.

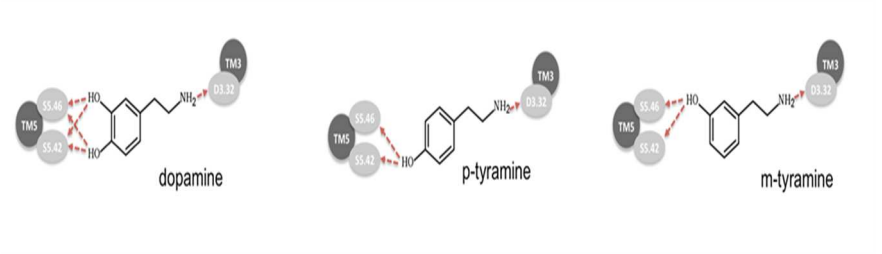

Figure S2 *Metadynamics and applied bias.*

List of pEC50 and Emax

Table S3A *Ligand potencies (pEC50) and corresponding standard errors (SE) for different coupling partners.*

	GoB		Gz		Gi2		βarr2	
compound	pEC50	SE	pEC50	SE	pEC50	SE	pEC50	SE
dopamine	9.35	0.04	8.51	0.04	8.30	0.05	7.33	0.07
m-tyramine	7.29	0.12	6.31	0.05	6.22	0.02	5.46	0.20
p-tyramine	5.00	0.03	4.20	0.10	4.23	0.14	N/D	N/D
hordenine	5.08	0.02	4.67	0.34	4.50	0.20	N/D	N/D
(R)-5-OH-DPAT	8.64	0.03	7.84	0.06	7.73	0.07	6.92	0.22
(S)-5-OH-DPAT	10.63	0.06	9.62	0.07	9.51	0.05	8.57	0.08
(R)-7-OH-DPAT	9.97	0.07	9.15	0.07	8.74	0.06	8.06	0.07
(S)-7-OH-DPAT	8.26	0.05	7.08	0.07	6.90	0.04	5.79	0.20

Table S3B *Ligand efficacies (Emax) and corresponding standard errors (SE) for different coupling partners.*

	GoB		Gz		Gi2		βarr2	
compound	Emax	SE	Emax	SE	Emax	SE	Emax	SE
dopamine	100.00	0.83	100.00	0.93	100.00	1.27	100.00	1.94
m-tyramine	98.79	3.22	92.11	1.83	83.27	0.80	47.98	4.18
p-tyramine	90.98	1.71	61.43	5.10	47.00	5.61	N/D	N/D
hordenine	79.74	1.11	26.82	4.86	18.33	2.59	N/D	N/D
(R)-5-OH-DPAT	104.30	0.82	86.60	2.87	72.27	1.46	41.63	2.69
(S)-5-OH-DPAT	108.40	1.12	100.80	1.32	99.38	1.04	96.31	1.71
(R)-7-OH-DPAT	107.50	1.39	97.44	1.30	97.36	1.40	85.38	1.60
(S)-7-OH-DPAT	106.30	1.40	97.05	2.21	94.56	1.43	77.27	6.43

Operational model of bias

Table S4 *Quantification of ligand bias at D2R using the operational model. The nature of the βarr2 dose response curves for p-tyramine and hordenine do not permit for reliable calculation of bias using the operation model which is indicated by ND in the table.*

	GoB		βarr2		GoB/ βarr2	bias factor
compound	log(τ/KA)	Δlog(τ/KA)	log(τ/KA)	Δlog(τ/KA)	ΔΔlog(τ/KA)	$10^{\Delta\Delta\log(\tau/KA)}$
dopamine	9.25	0.00	7.34	0.00	0.00	1.00
m-tyramine	7.34	-1.91	3.77	-3.57	1.66	45.39
p-tyramine	4.88	-4.37	ND	ND	ND	ND
hordenine	4.77	-4.48	ND	ND	ND	ND
(R)-5-OH-DPAT	8.61	-0.64	4.30	-3.08	2.44	274.16
(S)-5-OH-DPAT	10.61	1.36	8.65	1.31	0.05	1.12
(R)-7-OH-DPAT	9.94	0.69	7.82	0.48	0.21	1.61
(S)-7-OH-DPAT	8.25	-1.01	5.24	-2.10	1.09	12.27

Conformational variability of ligand binding

Typically, GPCR-ligand complexes obtained by X-ray crystallography reveal only one binding mode. In our study, enhanced molecular dynamics simulation shows that dopamine and analogues often adopt different binding modes within the orthosteric

binging pocket. In particular, the energetic plot for m-tyramine (Figure 1L in main manuscript) predicts two distinct binding modes which involves an aromatic ring rotation. The energetic barrier between both binding modes is less than a 1.5 kcal/mol. This makes it possible to observe both modes in unbiased simulations (Figure S3A). Such diversity in binding modes is not surprising and captured in several X-ray structures (Table S5). An example similar to m-tyramine is shown for the ovine cyclooxygenase-1 in complex with meloxicam (PDB code: 4O1Z).

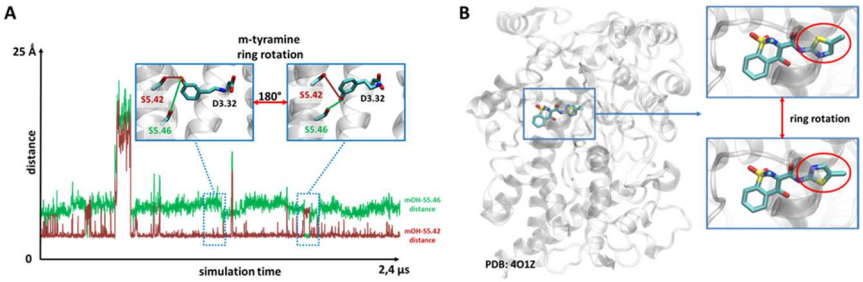

Figure S3. Conformational variability of ligand binding. (A) aromatic ring rotation in m-tyramine and (B) example of a crystallized ring rotation showing cyclooxygenase-1 in complex with meloxicam (PDB code: 4O1Z)

Table S5 *Ligand flips observed in X-ray crystal structures**

PDB ID	chain	residue ID	Resolution
1EXX	A	450	1.67
1H1R	A	1298	2.00
1XDD	A	401	2.20
2C5N	A	1297	2.10
2C5O	A	1297	2.10
2F71	A	608	1.55
2R3I	A	501	1.28
2R3P	A	501	1.66
2VIP	A	1247	1.72
2VWX	A	1889	1.65
2VWY	A	1889	1.65
2VWZ	A	1889	1.65
2VX1	A	1889	1.65

2X9F	A	1889	1.75
2XNB	A	1299	1.85
3EJJ	A	365	1.80
3O0I	A	237	1.47
3P4V	A	300	2.00
3S9S	A	1	2.55
3SI4	H	1	1.27
4ANW	A	1189	2.31
4EK6	A	301	1.52
4EK8	A	301	1.70
4FTT	A	301	2.30
4IWV	A	503	2.10
4JS3	A	403	2.00
4L2L	A	702	1.65
4O1Z	A	807	2.40

[*]This list has been kindly provided by Gydo van Zundert, Bijvoet Center for Biomolecular Research, Utrecht University, the Netherlands

Chirality-driven binding mode of (R)- and (S)-DPATs

A deeper structural analysis helps clarify why the S-enantiomer binds in an inverted position that allows only for TM5 contacts compared to the corresponding R-enantiomer of the 7-OH-DPAT (Figure S4A-B). A common feature of ligands in aminergic GPCRs is that the protonated nitrogen faces D3.32. In this position the two N-propyl substituents are directed to TM7. We find that a steric requirement for DPAT binding is that the chiral center (red asterisk, Figure S4) of the DPAT scaffold points the smaller substituent, namely the hydrogen (highlighted in red in Figure S4) to the same direction as the bulky N-propyl substituents. This structural arrangement forces the aromatic OH group of (S)-7-OH-DPAT to extend to the bottom of the binding pocket allowing only for TM5 interaction (Figure S4A, right). Our data shows that forming exclusively TM5 interactions is linked to G protein bias. Due to the same steric requirements, the 7-OH group of the R-enantiomer is restricted to point towards the top of the binding pocket. In turn, this binding mode promotes TM5/TM6 contacts (Figure S4B, right) that favors βarr2 recruitment and balanced signaling. The same observation is true for the 5-OH-DPATs. Here, the R-enantiomer points the OH-group down whereas

the S-enantiomers orientates it to the top of the binding pocket due to described steric requirements.

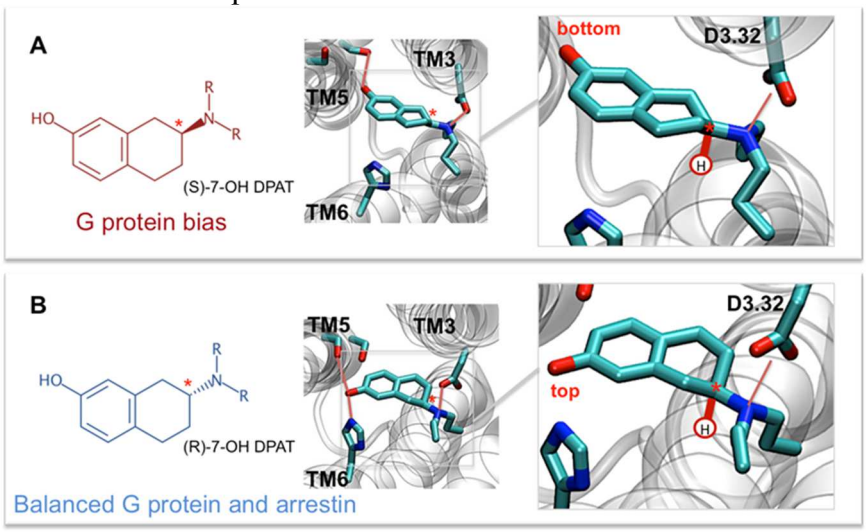

Figure S4 *Chirality induces inverted binding modes for 7-OH-DPATs.*

Recruitment of G proteins (G_{i2}, G_z, G_{oB}) and β-arrestin 2 (βarr2) using the bioSensAll™ assay for D2R mutants

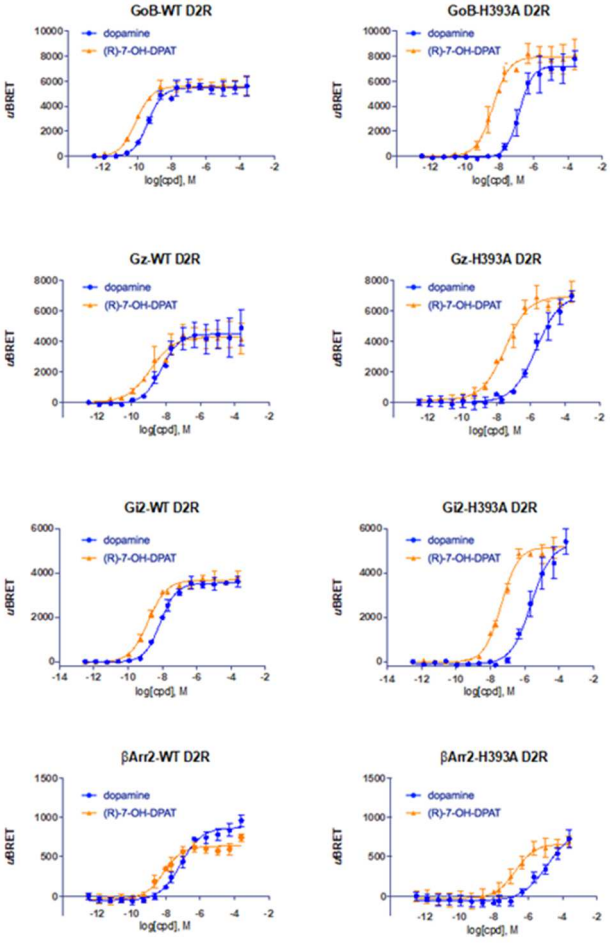

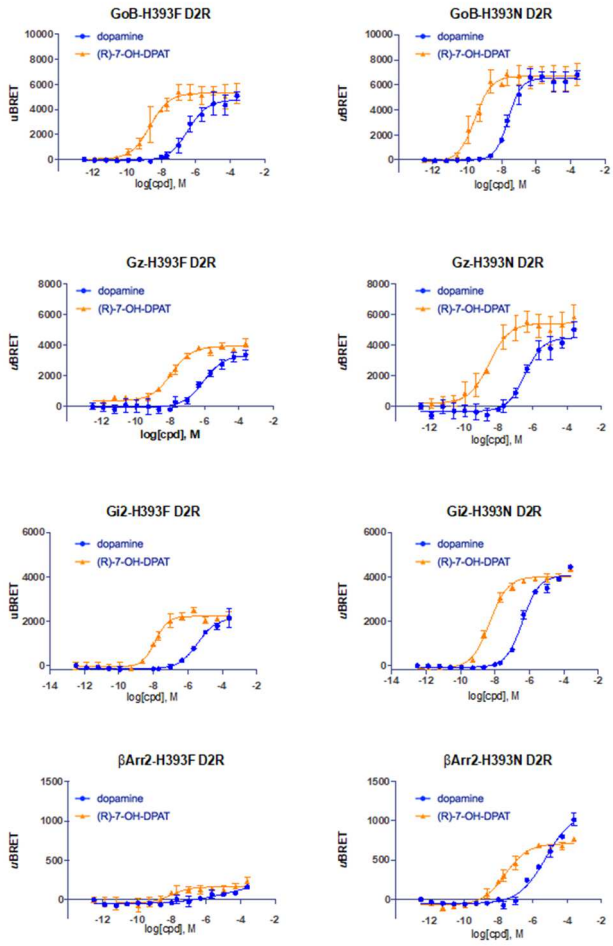

Figure S5 *Response curves to G protein (G_{i2}, G_z, G_{oB}) and β-arrestin 2 (βarr2) for the D2R mutants (H6.55A, H6.55F, H6.55N). The functional outcome for dopamine, p-tyramine, m-tyramine, (R)- and (S)-enantiomers of 5-OH-DPATs and 7-OH-DPATs are measured as the ability of the D2 receptor and their mutants (H6.55A, H6.55F, H6.55N) to recruit G proteins (G_{i2}, G_z, G_{oB}) and β-arrestin 2 (βarr2) using the bioSensAll™ assay. Plots were generated from dose-response curves obtained from at least 2 independent experiments.*

Ligand interaction with the extracellular loop 2 (ECL2)

Table S6 *D2R MD simulations predict no EL2 engagement for our set of compounds. Contacts have been computed over preferred binding modes extracted from metadynamics and are defined as distance < 4Å between ligand and Ile184. Preferred binding modes have been extracted according to detected energetic wells in Figure 1 and 2.*

Compound	Frequency of Ile184 contacts [%]
Dopamine	15
p-tyramine	9
m-tyramine	0
(R)-7-OH-DPAT	0
(S)-7-OH-DPAT	1

Recruitment of G proteins and β-arrestin 2 (βarr2) using the bioSensAll™ assay for 5HT1AR, 5HT2AR and β2AR mutants

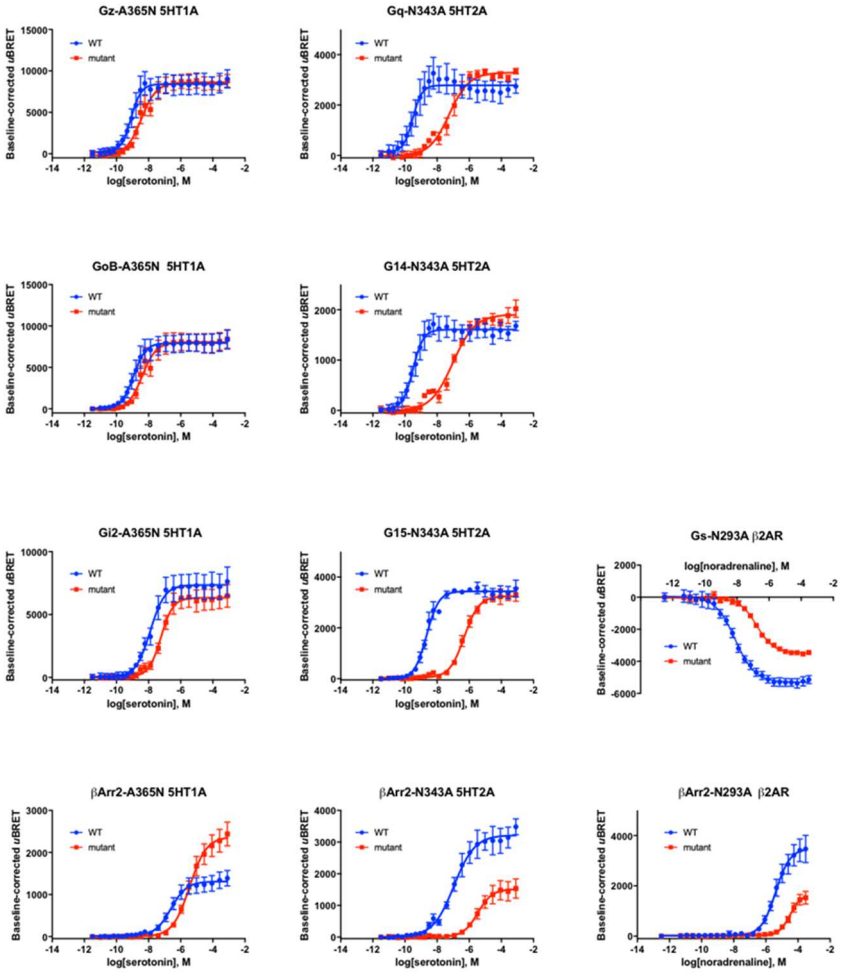

Figure S6 *Response curves to G protein (G_{i2}, G_z, G_{oB}, G_q, G_{14}, G_{15}, Gs) and β-arrestin 2 (βarr2) for the 5-HT1AR, 5HT2AR and β2AR mutants (H6.55A, H6.55F, H6.55N).*
The coupling outcome for the natural agonists serotonin or noradrenaline for WT and mutants are measured using the bioSensAll™ assay. Plots were generated from dose-response curves obtained from 2 independent experiments.

Binding signature of hordenine and its coupling outcome

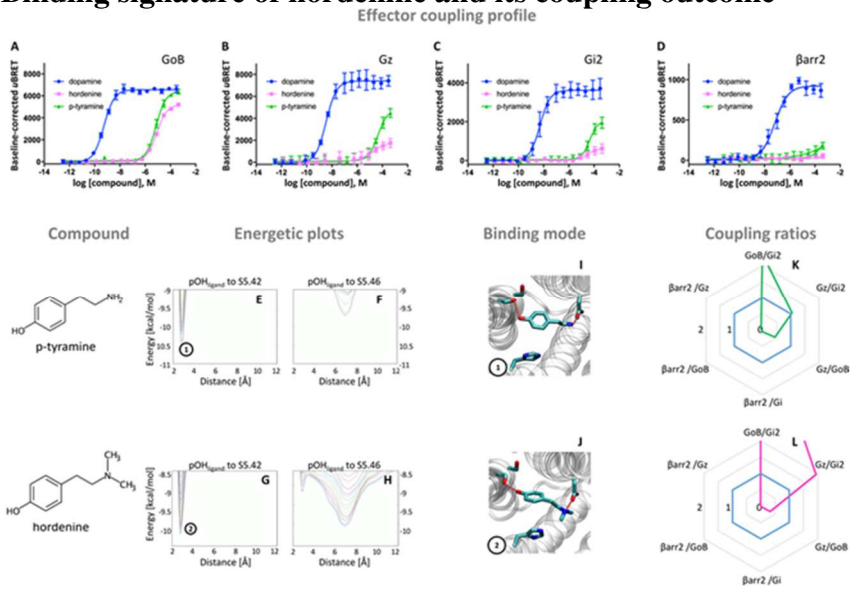

Figure S7. *Coupling profile and binding profile of hordenine versus p-tyramine.*

The corresponding chemical structures are depicted on the left. ***A-D****: Coupling curves for G protein (G_{i2}, G_z, G_{oB}) and β-arrestin 2 (βarr2) at the D2R in response to dopamine (blue), p-tyramine (green) and hordenine (pink) have been monitored using bioSensAll™ technology. For corresponding pEC50 and Emax values see Table S3.* ***E-H****: Energetic plots of ligand binding obtained by metadynamics using as metrics the distance of the p-OH groups to S5.42 and S5.46. An energetic well at ~2.8 Å indicates a favorable distance for binding contacts with the corresponding residue. To ensure convergence of binding energetics, we monitored free energy profiles along simulation by plotting the profile every 20000 deposited Gaussians (graphs shown in different colors).* ***I-J****: Representative structures of the binding mode corresponding to the energetic wells identified in the energetic plots.* ***K-L****: Coupling ratios were approximated using the curve (AUC) and its ratio for individual signaling effectors (e.g. βarr2 vs G_z, βarr2 vs G_{oB} etc.). Note, to eliminate observational bias linked to differences within different recruitment assays (e.g. βarr2 vs G_i), we use dopamine as internal standard for analyzing the areas under the curve (AUC). A balanced coupling profile of DA (reference ligand) is denoted by a coupling ratio of 1 for all pathway combinations and highlighted in all plots as blue line. Preferential or disfavoured coupling are indicated by*

ratios > 1 or < 1, respectively. Dose-response curves were generated using data obtained from 2 independent experiments.

Experimental Procedures - Radar graph generation

Radar graphs were produced using the area under the dose response curves (AUC; calculated using GraphPad Prism 6 software). For every compound tested, the calculated pathway-specific AUCs were divided by one another (e.g., AUC G_{oB}/AUC G_{i2}, AUC βarr2/AUC G_{oB}, etc.) resulting in "relative AUCs". To eliminate the influence of system (i.e. different coupling sensitivity of partners), we use dopamine as internal standard to obtain standardized coupling ratios for all compounds (Table S7). Relative AUCs for dopamine were used as reference values to which corresponding relative AUCs for other compounds were normalized (e.g., [AUC βarr2/AUC G_{oB}] (R)-5-OH-DPAT / [AUC βarr2/AUC G_{oB}] Dopamine). These normalized values, referred to as "normalized relative AUCs", were plotted as radar graphs. Normalization of AUCs for mutant receptor radar graph generation was conducted using an identical approach. However, relative AUCs for the mutant receptors were always normalized to the corresponding relative AUCs for the WT receptor. For hD2R mutants (for which multiple ligands were tested), the relative AUCs for dopamine for the WT receptor were used as reference values to which all other corresponding relative AUCs were normalized.

Pathway-specific AUCs

AUC per pathway

	Gi2	**GoB**	**Gz**	**βarr2+ GRK2**
dopamine	14068	24603	23675	1494
m-tyramine	6799	17205	12475	338
p-tyramine	1497	6180	2639	9
hordenine	874	9033	2858	1
(R)-5-OH-DPAT	7979	20850	15346	467
(S)-5-OH-DPAT	16099	30297	27013	1805
(R)-7-OH-DPAT	13994	27420	24451	1434
(S)-7-OH-DPAT	8516	19773	15659	623

Relative AUCs

$$\text{relative AUC} = \frac{\text{AUC}_{\text{pathway1}}}{\text{AUC}_{\text{pathway2}}}$$

	GoB /Gi2	Gz /Gi2	Gz /GoB	βarr2 /Gi2	βarr2 /GoB	βarr2 /Gz
dopamine	1.75	1.68	0.96	0.11	0.06	0.06
m-tyramine	2.53	1.83	0.73	0.05	0.02	0.03
p-tyramine	4.13	1.76	0.43	0.01	0.00	0.00
hordenine	10.34	3.27	0.32	0.00	0.00	0.00
(R)-5-OH-DPAT	2.61	1.92	0.74	0.06	0.02	0.03
(S)-5-OH-DPAT	1.88	1.68	0.89	0.11	0.06	0.07
(R)-7-OH-DPAT	1.96	1.75	0.89	0.10	0.05	0.06
(S)-7-OH-DPAT	2.32	1.84	0.79	0.07	0.03	0.04

Normalized Relative AUCs

$$\text{normalized relative AUC} = \frac{\text{relative AUC}_{\text{compound x}}}{\text{relative AUC}_{\text{dopamine}}}$$

	GoB /Gi2	Gz /Gi2	Gz /GoB	βarr2 /Gi2	βarr2 /GoB	βarr2 /Gz
dopamine	1	1	1	1	1	1
m-tyramine	1.45	1.09	0.75	0.47	0.32	0.43
p-tyramine	2.36	1.05	0.44	0.06	0.02	0.05
hordenine	5.91	1.94	0.33	0.01	0.00	0.01
(R)-5-OH-DPAT	1.49	1.14	0.76	0.55	0.37	0.48
(S)-5-OH-DPAT	1.08	1.00	0.93	1.06	0.98	1.06
(R)-7-OH-DPAT	1.12	1.04	0.93	0.96	0.86	0.93
(S)-7-OH-DPAT	1.33	1.09	0.82	0.69	0.52	0.63

References

[1] R. Woodward, C. Coley, S. Daniell, L. H. Naylor, P. G. Strange, J. Neurochem. 1996, 66, 394–402.

[2] J. C. Fowler, S. Bhattacharya, J. D. Urban, N. Vaidehi, R. B. Mailman, Mol. Pharmacol. 2012, 81, 820–831.

[3] C. Coley, R. Woodward, A. M. Johansson, P. G. Strange, L. H. Naylor, J. Neurochem. 2000, 74, 358–366.

[4] B. L. Wiens, C. S. Nelson, K. A. Neve, Mol. Pharmacol. 1998, 444, 435–444.

[5] B. A. Cox, R. A. Henningsen, T. Spanoyannis, T. L. Neve, K. A. Neve, J. Neurochem. 1992, 59, 627–635.

[6] R. C. Kling, N. Tschammer, H. Lanig, T. Clark, P. Gmeiner, PLoS One 2014, 9, 1–10.

[7] N. Tschammer, S. Bollinger, T. Kenakin, P. Gmeiner, T. Park, N. C. T. K, Mol. Pharmacol. 2011, 79, 575–585.
[8] W. Humphrey, A. Dalke, K. Schulten, J. Molec. Graph. 1996, 14, 33–38.
[9] T. Kenakin, A. Christopoulos, Nat. Rev. Drug Discov. 2013, 12, 205–16.
[10] E. T. van der Westhuizen, B. Breton, A. Christopoulos, M. Bouvier, Mol. Pharmacol. 2014, 85, 492–509.
[11] F. Sievers, a. Wilm, D. Dineen, T. J. Gibson, K. Karplus, W. Li, R. Lopez, H. McWilliam, M. Remmert, J. Soding, et al., Mol. Syst. Biol. 2014, 7, 539–539.
[12] P. Labute, Proteins Struct. Funct. Bioinforma. 2009, 75, 187–205.
[13] M. L. Verdonk, J. C. Cole, M. J. Hartshorn, C. W. Murray, R. D. Taylor, Proteins Struct. Funct. Genet. 2003, 52, 609–623.
[14] M. Martí-Solano, A. Iglesias, G. De Fabritiis, F. Sanz, J. Brea, M. I. I. Loza, M. Pastor, J. Selent, Mol. Pharmacol. 2015, 87, 740–6.
[15] M. a. Lomize, A. L. Lomize, I. D. Pogozheva, H. I. Mosberg, Bioinformatics 2006, 22, 623–625.
[16] S. Jo, J. B. Lim, J. B. Klauda, W. Im, Biophys. J. 2009, 97, 50–58.
[17] J. B. Klauda, R. M. Venable, J. A. Freites, J. W. O'Connor, D. J. Tobias, C. Mondragon-Ramirez, I. Vorobyov, A. D. MacKerell, R. W. Pastor, J. Phys. Chem. B 2010, 114, 7830–7843.
[18] K. Vanommeslaeghe, E. Hatcher, C. Acharya, S. Kundu, S. Zhong, J. Shim, E. Darian, O. Guvench, P. Lopes, I. Vorobyov, et al., J. Comput. Chem. 2010, 31, 671–690.
[19] W. Yu, X. He, K. Vanommeslaeghe, A. D. MacKerell, J. Comput. Chem. 2012, 33, 2451–2468.
[20] M. J. Harvey, G. Giupponi, G. De Fabritiis, J. Chem. Theory Comput. 2009, 5, 1632–1639.
[21] K. A. Feenstra, B. Hess, H. J. C. Berendsen, J. Comput. Chem. 1999, 20, 786–798.
[22] A. Laio, F. L. Gervasio, Reports Prog. Phys. 2008, 71, 126601.
[23] M. Bonomi, D. Branduardi, G. Bussi, C. Camilloni, D. Provasi, P. Raiteri, D. Donadio, F. Marinelli, F. Pietrucci, R. A. Broglia, et al., Comput. Phys. Commun. 2009, 180, 1961–1972.
[24] P. Raiteri, A. Laio, F. L. Gervasio, C. Micheletti, M. Parrinello, J. Phys. Chem. B 2006, 110, 3533–3539.

[25] Y. Namkung, C. Le Gouill, V. Lukashova, H. Kobayashi, M. Hogue, E. Khoury, M. Song, M. Bouvier, S. A. Laporte, Nat. Commun. 2016, 7, 12178.

3.2 Network rearrangements in the initial phase of β-arrestin signaling in the δ-opioid receptor

In this chapter, we present our work in form of a journal article

Summary:
In this paper we study how alterations within the allosteric network of the δ-opioid receptor contribute towards a specific signaling response. For this, we analyze how a mutation within this receptor, transforms the antagonist naltrindole into a potent βarr biased agonist.

By using multiple short MD runs, we are able to investigate how the studied mutation disturbs contacts between two receptor segments, resulting in increased fluctuations of TM7. Markov-state model analysis reveals, that this alters the behavior of a conserved microswitch in the intracellular part of TM7. Based on this data we propose a model of biased signaling for this ligand-receptor complex which is supported by further mutagenesis as well as NMR data.

The results of our study help us better understand allosteric communication within GPCRs and how it contributes towards a specific signaling outcome.

The PhD candidate was responsible for analyzing the unbiased simulations, studying local structural disturbances, microswitch behavior and the water network. He formulated the proposed signaling hypothesis, and was responsible for writing the manuscript. IRE was responsible for the markov state model analysis.

Network rearrangements in the initial phase of β-arrestin signaling in the δ-opioid receptor

Tomasz Maciej Stepniewski[1#], Ismael Rodríguez-Espigares[1#], Maria Martí-Solano[1], Anna Troya Bruguer[1], Mariona Torrens-Fontanals[1], Gianni De Fabritiis[1], Slawomir Filipek[2] and Jana Selent[1]*
[#]Both authors contributed equally to this work

[1]*Research Programme on Biomedical Informatics (GRIB), Hospital del Mar Medical Research Institute (IMIM) - Pompeu Fabra University (UPF), Dr. Aiguader 88, E-08003, Barcelona, Spain*
[2] *Faculty of Chemistry, Biological and Chemical Research Centre, University of Warsaw, Warsaw, Poland*

*Corresponding author:
e-mail: jana.selent@upf.edu

Abstract
Signaling bias is an established concept for obtaining more efficient drugs, however it remains poorly understood. Herein, we use all-atom molecular dynamics simulations with hundreds of replicas to show that rearrangements of interaction networks related to β-arrestin signaling in the δ-opioid receptor. We find that the initial rearrangements involve a destabilization of transmembrane helix (TM) 2 and 7 contacts caused by alterations of the intramolecular water network and interhelical interactions. Together, this translates into higher TM7 fluctuations in proximity to the binding site of intracellular signaling proteins, a behavior that has been associated to β-arrestin biased signaling by biophysical experiments.

Introduction

G-protein coupled receptors (GPCRs) are flexible transmembrane proteins that exist in an equilibrium of conformations ranging from inactive, intermediate to fully active. Some GPCR ligands, known as biased agonists, can stabilize receptor conformations that preferentially couple to specific intracellular signaling proteins.

Given their pathway selectivity, biased agonists could act as more efficacious and safer drugs.[1] However, to rationally design them, we first need to understand the molecular determinants of GPCR signaling bias.

In the present study, we address this question by studying β-arrestin (β-arr) bias at the delta opioid receptor (δOR), a member of class A GPCRs, using molecular dynamics simulations. We take advantage of the D2.50A receptor mutant in which the antagonist naltrindole converts into a potent β-arr biased agonist.[2] The mutated site is a well-known allosteric sodium binding site in class A GPCRs.[3,4] Thus inducing sodium decoupling seems to structurally mimic the effect of β-arr biased agonists in the δOR.[2]

Previous computational studies identified the formation of a water channel as an important event in GPCR activation.[5] To assess its importance in β-arr signaling events, we studied the β-arr biased D2.50A mutant and the inactive wild-type (WT) δOR in complex with naltrindole in all-atom molecular dynamics simulations performing three replicates of 1.5 μs per investigated system. Despite not observing a continuous water channel in neither of the simulations, we can appreciate differences in local water occupancies (Figure S1B and C, highlighted by arrows).

To further increase the statistical robustness of our analysis, we carried out 100 replicates of 128 ns for each system (Table S1). This short time interval is suitable due to the high diffusion coefficient of water molecules (Figure S2). Our results suggest that the D2.50A mutation alters the water network of the connector region which is located between the orthosteric ligand binding site and the intracellular site where signaling proteins couple. In the WT δOR, we find pronounced water occupancies in positions 1 to 3 and 5, 6 (Figure 1A). These positions correlate well with locations of waters in the δOR crystal structure (Figure S3A), supporting the reliability

of our model. In contrast, in the β-arr biased δOR, we find an overall destabilization of the water network, in particular in positions 2, 3 and 5 (Figure 1B). Destabilization of these waters indicates higher solvent fluctuation in these positions (Figure S4B). In the inactive WT structure, water molecule 2 forms a hydrogen bond with N3.55, S7.46 and water molecule 3, whereas water molecule 3 is further coordinated via W6.48, N7.45 and the sodium ion (Figure 1A). Despite the overall decrease of water network stability in the β-arr biased δOR, we find one additional water molecule of high occupancy in position 4, which replaces the sodium ion found in the WT δOR.

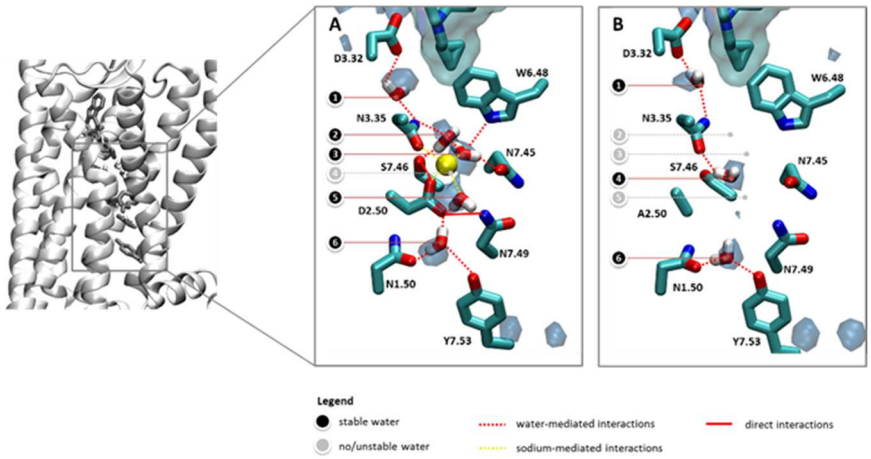

Figure 1 *Water occupancy map of the connector region for the WT (**A**) and β-arr biased δOR (**B**) plotted at 40% water occupancy. The connector region links the orthosteric binding site (D3.32) to receptor regions close to the intracellular coupling site of signaling proteins (Y7.53). Direct polar interactions between residues are displayed as solid lines whereas indirect (water or sodium-mediated) polar interactions are displayed as dashed lines. A summary of absolute values of water occupancies can be found in Figure S4A.*

Our data clearly suggest that the D2.50A mutation results in a significant alteration of the water network. However, it is not clear how changes contribute to β-arr bias. It is tempting to speculate that distinct changes in the conserved water network transmit a structural message through the receptor. To address this, we studied the interhelical hydrogen bonding network of the WT and the β-arr biased δOR. Flare plots[6] emphasize differences between receptors

related to conserved activation motifs (Figure 2AB). Furthermore, Figure 2C shows how changes in this network contribute to altered dynamic properties of the δOR in terms of Cα root mean square fluctuation (RMSF). This analysis reveals higher fluctuation in the β-arr biased δOR compared to the inactive δOR. Surprisingly, the most pronounced difference is not found at the mutated D2.50A site in TM2 but in the middle-lower part of TM7 (in red, Figure 2C). This area contains three highly conserved residues - N7.45, S7.46 and N7.49 (Figure S3), with N7.49 being part of the conserved NPXXY motif. All three residues are in proximity to the mutated 2.50 residue and involved in direct or indirect interaction with the sodium ion.[2] Studying the distances between Cα atoms of N7.45, N7.49 and the Cα atom of residue 2.50 (Figure 2B, distance 3 and 4) shows that these distances fluctuate significantly more in the D2.50A δOR compared to the WT δOR (Figure 2C). Higher fluctuations of N7.45 and N7.49 (Figure 1) are likely the result of a disruption of sodium and water-mediated interactions (molecules 2, 3 and 5). In addition, there is a loss of direct interaction between N7.45, S7.46 and D2.50. In light of these observations, we next analyzed how far this disturbance extends within the δOR during the initial phase of β-arr signaling. Analysis of our 100 short replicates indicates that there is substantial propagation at a nanosecond scale to extra- and intracellular sides. Towards the extracellular side, we observe a higher fluctuation of the so called “rotamer toggle switch” W6.48 (Figure 2E, torsion angle 2) in the β-arr biased δOR as well as a higher opening frequency of the D3.32-Y7.43 bridge (55%) compared to the inactive state (33%) (Figure 2C, distance 5). Higher mobility of W6.48 seems to be a result of the destabilization of water molecule 3, which in the WT receptor is stabilized by the sodium ion. This goes along with recent computational studies.[7] Moreover, movement of W6.48 has been previously related to GPCR activation.[8] In this respect, our study suggests that higher W6.48 fluctuation is also an initial step of β-arr bias. In fact, mutagenesis of W6.48 into L, F, A or D in the δOR results in loss of ligand-specific activity for the β-arr pathway, while G-protein signaling is maintained.[9] Tyrosine 7.43 is another highly conserved residue, which forms an ionic lock with D3.32 in the δOR.[2] This lock remains more frequently open in the β-arr biased δOR (Figure 2C, top). Previous work on the μ and κOR highlights the importance of this lock in opioid receptor functionality.[10] In our simulations, more frequent opening of this lock is the result of a destabilized

network between the conserved residues D3.32, N3.35, W6.48, S7.46 and water molecules 1, 2 and 3 (Figure 1A and B).

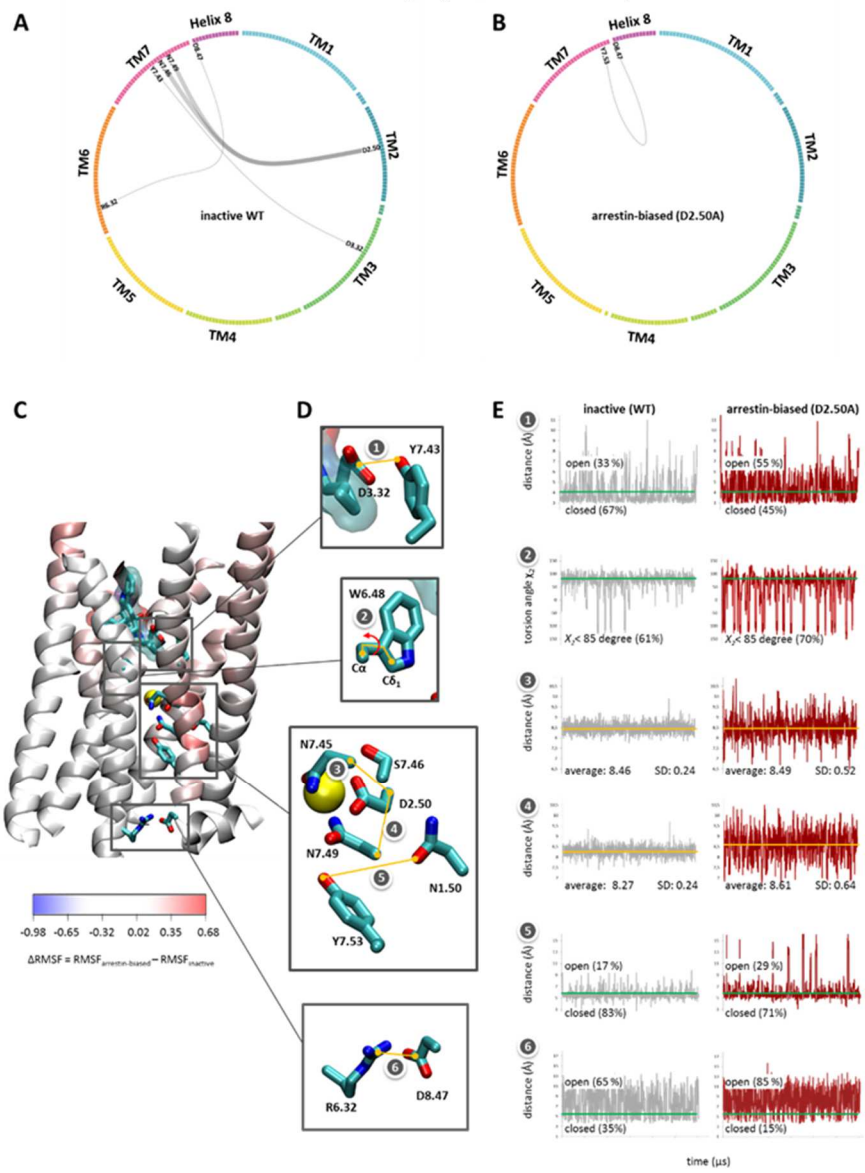

Figure 2 *Dynamics for β-arr biased and inactive δOR. Intrahelical hydrogen bonding network for the inactive WT (**A**) and the β-arr biased (**B**) δOR. Line thickness relates to how strongly an interaction is preserved over the simulation time in comparison to its preservation in the other receptor. Complete network plots are found in Figure S5. (**C**) Difference of Cα root mean square fluctuation (ΔRMSF = RMSFβ-arr biased – RMSFinactive) between receptors.*

*Positive values (red color) indicate regions of higher fluctuation in the β-arr biased receptor. (**D**) Structural depiction of selected relevant residues that link the orthosteric site towards the intracellular δOR end. (**E**) Distances and torsion angles of selected residues over the studied simulation time (6.4 μs) plotted using a 4 ns window (1600 data points).*

A similar tendency of signal propagation is observed towards the intracellular side. N1.50 and Y7.53 form a conserved lock mediated via a water molecule at the intracellular end of the δOR (Figure S6). The studied lock is part of the NPXXY7.53 motif and forms an important gateway for water molecules entering the receptor from the intracellular side.[5] In our simulations, we find that this lock, which is maintained in a closed state via water molecule 6 (Figure 1A and B), fluctuates more in the β-arr biased δOR, visiting the open state during 29% of the simulation time compared to 17% in the inactive δOR simulations (Figure 2C, plot 5). A similar trend is observed for the polar lock between TM6 (R6.32) and helix 8 (D8.47) (Figure 2C, plot 6).

All in all, our data indicate that initial destabilization of the connector region (D2.50A mutation) causes higher fluctuations in the middle-lower part of TM7 towards the intracellular side. Importantly, higher TM7 fluctuation has been related to β-arr bias by biophysical studies using 19F-NMR experiments.[11] In their study, authors report that β-arr biased ligands predominantly impact the conformational state of TM7 whereas changes in TM6 state are related to G protein signaling. In line with this finding, we propose that the initial phase of β-arr bias involves higher fluctuation of TM7 in a nanosecond timescale. In turn, this could facilitate further global conformational changes of the δOR that occur in milliseconds. Subsequently, this leads to β-arr coupling, which has been described to happen after seconds.[12]

To study in more detail TM7 fluctuations observed in the β-arr biased mutant, we used a Markov State Model (MSM) analysis. This analysis revealed different populations of δOR macrostates (Figure S7). In particular, we find two macrostates, which are exclusively found for the β-arr biased δOR and involve a partial anti-clockwise rotation of Y7.53 (Figure S8, state 4 and 5). This rotation is sampled for 1.2 μs within a total of 12.8 μs and is similar to the observed

rotation in the arrestin-coupled rhodopsin structure (Figure S8C). Y7.53 rotation impacts also the formation of new intrahelical bonds between TM7 and helix 8 as captured in Figure 2B. In addition, the adjacent residue towards the intracellular side (7.54) significantly changes its environment. This finding goes along with previously mentioned 19F-NMR[11] experiments, which report pronounced shifts of the NMR signal in position 7.54 upon binding of β-arr biased agonists. Note that the observed Y7.53 rotation (state 4 and 5) occurs sporadically during receptor fluctuation and indicates altered δOR dynamics, which might result in the larger conformational changes leading to β-arr coupling.

Mechanistically (Figure 3A), higher TM7 fluctuation in the δOR can be related to the loss of three important interactions between TM2 and TM7 comprising sodium and water-mediated indirect (dashed line) and direct (solid line) interactions, which stabilize the antagonist-bound δOR. This finding is supported by the observation that mutations of residues contributing to TM2-TM7 linkage (e.g. N7.45 and N7.49) also promote β-arr bias in the δOR[2]. Surprisingly, the magnitude of β-arr bias in these mutations is less potent than upon mutation in TM2 (i.e. D2.50) (Table S2). In this respect, our data provides a plausible explanation for the different impact of different mutations on β-arr bias (Figure 3). In the fully inactive δOR, TM7 is stabilized by three interactions between D2.50 and N7.45, S7.46 and N7.49 (Figure 3A). These three interactions are lost upon D2.50A mutation which strongly weakens TM2-TM7 interaction and consequently increases TM7 fluctuation leading to full β-arr bias. In contrast, mutation of N7.45 or N7.49 would only abolish one interaction. This would cause a partial increase of TM7 fluctuation with less capacity for β-arr coupling, (i.e. partial β-arr) which is in line with experimental data (Table S2).

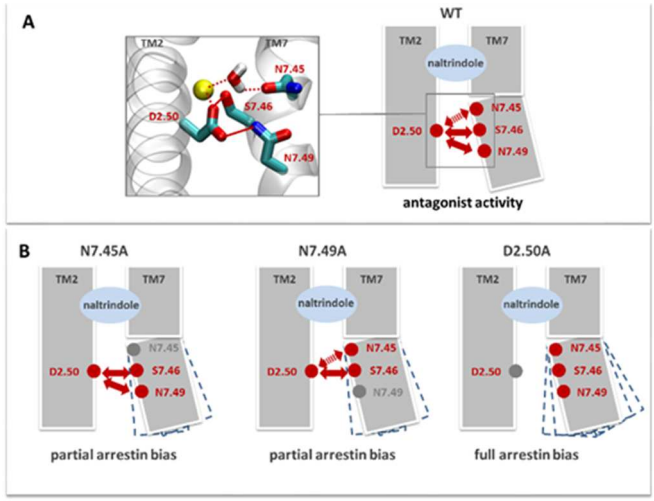

Figure 3 *Potency of β-arrestin bias correlates with the destabilization of TM2-TM7 contacts.*
*Direct interactions are shown in solid lines and water-mediated interactions in dashed lines. (**A**) TM2-TM7 interhelical contacts within the WT receptor. (**B**) TM2-TM7 interhelical contacts within various mutants demonstrating arrestin bias*

The functional relevance for signaling of the connector region around the sodium-binding residue D2.50 appears to be partially conserved among class A GPCRs. An interesting case is the neurokinin 1 receptor.[13] Despite being sodium-insensitive (i.e. no sodium binding at position 2.50), a E2.50A mutation transforms the natural agonist SP, into a β-arr biased agonist. Residue E2.50 stabilizes TM2-TM7 interactions by direct contacts with S7.45 and N7.49. Moreover, mutating either residue N7.49 or S7.45 into alanine leads to a loss of Gs signaling while maintaining β-arr signaling. These results point to modulation of TM2-TM7 interaction as a common mechanism to elicit β-arr signaling bias in GPCRs.

In summary, a key finding of our study is the existence of a series of rapid network rearrangements at the initial phase of β-arr signaling which can be captured at a timescale of nanoseconds. Analysis of these rearrangements provides a molecular mechanism on how β-arr signaling result from signal propagation through the δOR leading to higher TM7 fluctuation at the intracellular side – an event which has been previously associated to arrestin signaling.[11] Importantly, we observe that this fluctuation contributes to the conformation state of

Y7.53, an important GPCR microswitch. This finding is confirmed by MSM analysis.
In hundreds of replicates, we show that an important trigger for β-arr bias is the disruption of direct and indirect interactions between TM2 and TM7 in the connector region, which otherwise stabilize TM7 in the inactive δOR. This initial events of β-arr bias can be probed on the relatively short timescale of nanoseconds. In this regard, our study indicates that the impact of a signaling stimulus such as ligand binding can be approximated by simulating network rearrangements and structural fluctuations in the initial phases of receptor activation. Ultimately, this finding opens new avenues to study receptor signaling by multiple short simulations instead of monitoring the entire activation process, an approach that is still out of reach of conventional simulation methods.

Experimental Details are found in the Supplemental Material.

References

[1] M. Martí-Solano, D. Schmidt, P. Kolb, J. Selent, Drug Discov. Today 2016, 21, 625–31.
[2] G. Fenalti, P. M. Giguere, V. Katritch, X.-P. Huang, A. a Thompson, V. Cherezov, B. L. Roth, R. C. Stevens, Nature 2014, 506, 191–196.
[3] V. Katritch, G. Fenalti, E. E. Abola, B. L. Roth, V. Cherezov, R. C. Stevens, Trends Biochem. Sci. 2014, 39, 233–244.
[4] J. Selent, F. Sanz, M. Pastor, G. De Fabritiis, PLoS Comput. Biol. 2010, 6, 1–6.
[5] S. Yuan, S. Filipek, K. Palczewski, H. Vogel, Nat. Commun. 2014, 5, 4733.
[6] F. Rasmuss, A. J. Venkatakrishnan, preprint 2017.
[7] X. Sun, G. Laroche, X. Wang, H. Ågren, G. Bowman, P. M. Giguère, Y. Tu, Chem. - A Eur. J. 2017, 4615–4624.
[8] X. Deupi, J. Standfuss, Curr. Opin. Struct. Biol. 2011, 21, 541–551.
[9] X. Sun, G. Laroche, X. Wang, H. Ågren, G. Bowman, P. M. Giguère, Y. Tu, Chem. - A Eur. J. 2017, 4615–4624.
[10] S. Yuan, K. Palczewski, Q. Peng, M. Kolinski, H. Vogel, S. Filipek, Angew. Chemie - Int. Ed. 2015, 54, 7560–7563.
[11] J. J. Liu, R. Horst, V. Katritch, R. C. Stevens, K. Wuethrich, Science (80-.). 2012, 335, 1106–1110.

[12] S. Nuber, U. Zabel, K. Lorenz, A. Nuber, G. Milligan, A. B. Tobin, M. J. Lohse, C. Hoffmann, P. Group, T. Unit, et al., 2016, 531, 661–664.
[13] L. Valentin-Hansen, T. M. Frimurer, J. Mokrosinski, N. D. Holliday, T. W. Schwartz, J. Biol. Chem. 2015, 290, 24495–24508.

Acknowledgements
We are grateful to the people who volunteered their computer time to GPUGRID.net for this research.

Supplementary information

Overview of all-atom molecular dynamics simulations

Table S1. *Amassed simulation time for studied systems*

system	Time [μs]	replicates
Wt δOR	1,5	3
D2.50A δOR	1,5	3
Wt δOR	0,128	100
D2.50A δOR	0,128	100
Total time	34,6	

Long-time simulations

Despite water influx, we do not observe the formation of a stable continuous water channel connecting the extra- with the intracellular side for none of the receptors (Figure S1B and C). This is not surprising as our simulation were carried out in the presence of an antagonist (Figure S1B) or in the presence of a biased agonist but in the absence of an intracellular signaling protein (Figure S1C). An intracellular agent is needed to facilitate the opening of the intracellular receptor regions and thus the formation of a continuous water channel.[1] Instead, we can appreciate differences in the structure of the partially formed water channel when comparing the inactive wild-type delta opioid receptor (WTδOR) with the β-arrestin (β-arr) biased mutant (Figure S1B and C, highlighted by arrows).

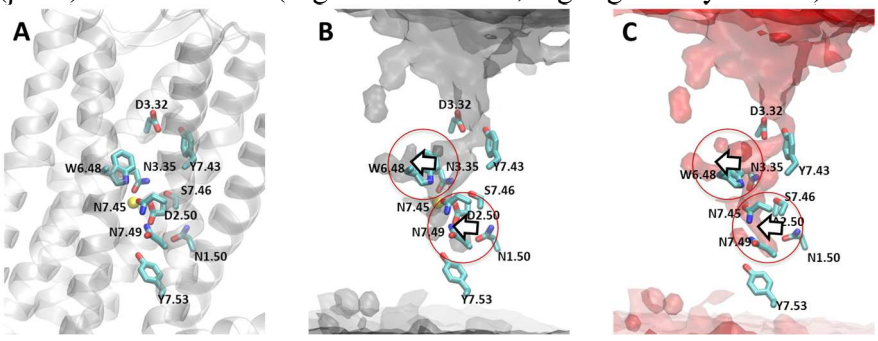

Figure S1 *Water occupancy in the inactive WT and β-arr biased D2.50A mutant receptors.*

*The δOR WT with relevant residues (displayed as licorice) and a sodium ion (yellow sphere) (**A**). (**B**) and (**C**) show water occupancy maps for the WT and D2.50A δOR, respectively. The maps are computed over 4.5 μs (3 replicates x 1.5 μs) per system. Differences in water occupancy between inactive and biased δOR are highlighted by arrows. Water occupancy is plotted at a value of 0.2 (i.e. water is present in at least 20% of the simulation).*

Water diffusion and equilibration

In our studies we have utilized the TIP3P water model.[2] This model has been shown to reproduce well solvent properties.[3] One of the parameters that characterizes water is the self-diffusion coefficient. This parameter takes into account the mean square displacement (MSD) of molecules that occurs at a certain time-step. Experimental studies have shown that this parameter equals 2.299 at 298.15K and 2.597 at 303.15K.[4] We have studied the progression of the water self-diffusion coefficient in one of our replicates. The parameter has been computed with Newton's equation:

$$D(\tau)=MSD(\tau)/6\tau$$

in which D is the self-diffusion coefficient and τ is the timestep between two distinct states of the system.

In our system, we computed MSD of water oxygens once every 2.5 ns. By studying the progression of this parameter (see below), we can observe that waters converge to a stable rate of diffusion after around 25 ns, with a self-diffusion parameter of around 2.7 m2*10-9/s which is slightly higher than the value observed in nature. This is consistent with previous studies that show slight increase in mobility of the TIP3P waters.[5] The below graph (Figure S2) clearly shows that at the beginning of the replicate there is a equilibration phase, during which the waters in the system converge, towards a dynamic equilibrium. The slightly increased mobility of the waters in the system on one hand shows us that our computational models still has limitations. On the other hand, more mobile waters ensure a faster and more efficient sampling of different positions of this molecules.

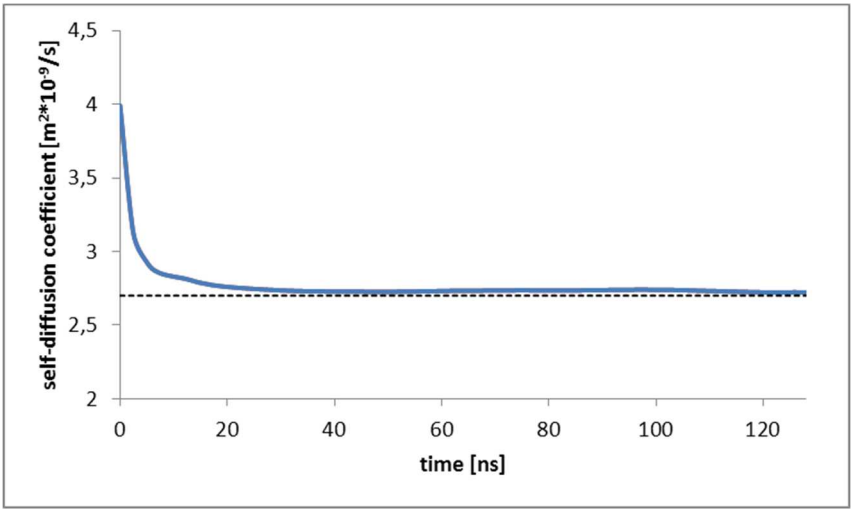

Figure S2 *Progression of the water self-diffusion parameter studied overn 2.5 ns intervals in a single replicate, of the simulated WTδOR*

Highly conserved residues in the connector region of the δOR

To compare the water network observed in our simulations with the one observed in the δOR crystal structures (PDB code: 4N6H) we have superimposed the WTδOR simulations coordinates used for the water network analysis with the crystal structure, using the protein backbone as reference. We superimposed the water occupancy map generated for the protein (Figure S3A, shown in blue) with water molecules present in the crystal structure (Figure S3A, shown as red spheres). The comparison highlights that our simulations reproduce the water network observed in the crystal structure. In Figure S3B we show the conservation of residues involved in maintaining this network.

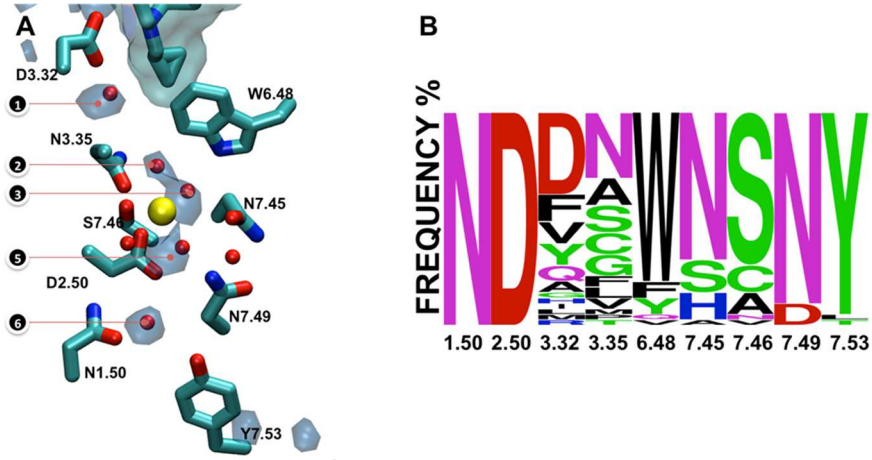

Figure S3 *Highly conserved residues in the connector region of the δOR.*
*Water occupancy map in the connector region of the WT δOR was generated for coordinates obtained fom the short-replicate simulations at an occupancy threshold of 40%. The studied system was aligned to the δOR crystal structure (PDB code: 4N6H) (**A**). Waters present in the crystal structure are displayed as red spheres. Evolutionary conservation of residues in the connector region computed among class A GPCRs with available crystal structures (**B**).*

Water occupancies and fluctuation

Occupancies values for WT (grey) and arrestin-biased receptor are summarized in Figure S4A. It can be seen that occupancies of water numbers 1,2,3,5 and 6 are lower in the arrestin-biased receptor compared to the WT δOR. Lower occupancy suggests higher fluctuation in the connector region. In fact, plotting the transition of waters through defined slices in 100 ns (i.e. water fluctuation) supports this statement (Figures S4B, right top). In particular in slices 5 to 8, we observe higher water fluctuations whereas slices 1 to 4 and 9 to 10 are not significant different between arrestin-biased and WT receptor.

Surprisingly, we observe that occupancy of water molecule 6 which mediates the interaction between N1.50-Y7.53 lock is similar comparing the WT and β-arr biased δOR (Figure 1B and Figure S4A) despite the lock being more open in the β-arr biased δOR (Figure 2E, point 5). However, measuring the fluctuation rate of waters in the

different compartments shows that highest rates are found at the surroundings of the N1.50-Y7.53 lock (Figure S4B, slices 7 and 8). This high fluctuation might contribute to a partial disruption of the N1.50-Y7.53 lock and on a larger scale to the initiation of global TM7 conformational changes.

In addition, we find that slices with pronounced differences in fluctuation (Figure S4B, right top: slices 5 to 9) have a lower average number of waters (Figure S4B, right bottom: slices 5 to 9) whereas slices with no significant differences in fluctuation (Figure S4B, right top: slices 1 to 4 and 9 to 11) have high numbers of waters (Figure S4B, right bottom: slices 1 to 4 and 9 to 11).

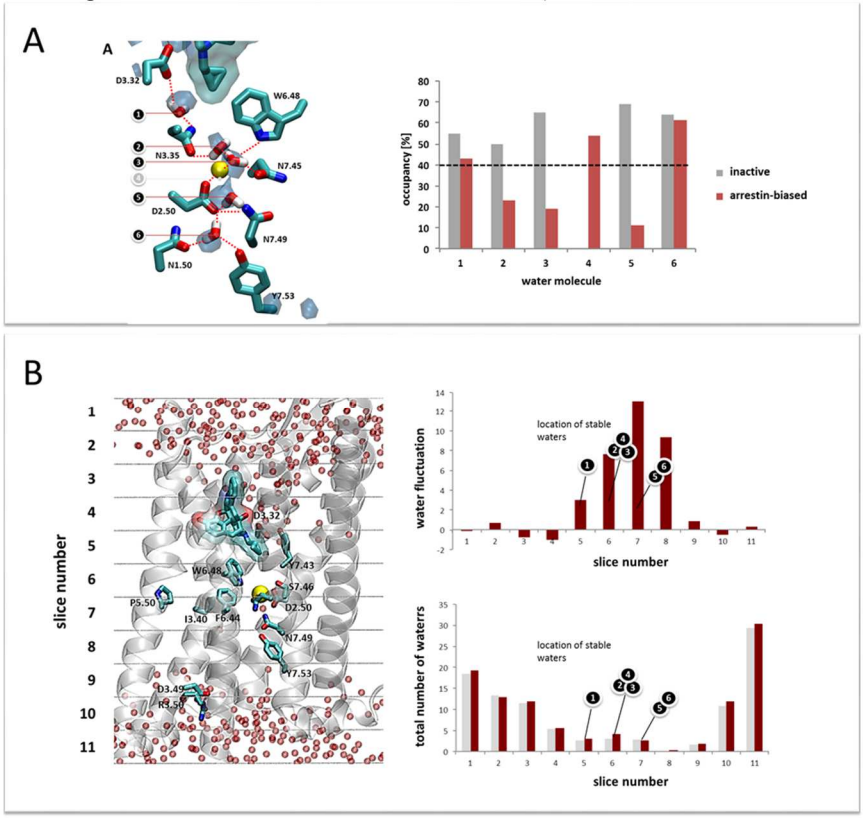

Figure S4 *Occupancy of water molecules in the connector region of the δOR*
*(**A**) The number of water molecule corresponds to its position in Figure 2 in the main text. In (**B**) we show the average number of waters and water fluctuation per slice.*

Hydrogen bonding network

Flare plots reveal general less inter-helical interactions in the mutated receptor (Figure S5B) compared to the WT receptor (Figure S5A). We can see that direct polar interactions between D2.50 and residue N7.49 and S7.46 arent maintained in the β-arr biased receptor (Figure 2C). Lack of those interactions likely contributes to increased fluctuations observed in the lower part of TM7. In the upper part we see that the polar bond between Y7.53 and D3.32 is less stable in the WT receptor. This is in line with our observation, that this conserved ionic lock is more often broken in the mutated receptor (Figure 2E, plot 1). We also observe a general decrease of inter-helical interactions in the β-arr biased receptor (i.e. interactions between TM2 and TM3, or TM3 and TM4). Such a result highlights the importance of the sodium ion, in stabilizing the interaction network of the δOR.

Curiously, we also observe differences in stability of intra-helical interactions between the studied systems. Intra-helical interactions are primarily interactions between backbone oxygens and nitrogens that stabilize the helical conformation. Thus, the observed changes may correspond to conformation differences between the studied receptors. We can observe pronounced differences in TM7 in respect ot those interractions. This changes can be related to difference in fluctuations (Figure 1C) and different population of macrostates for this regiond (Figure S7) observed in the D2.50A receptor.

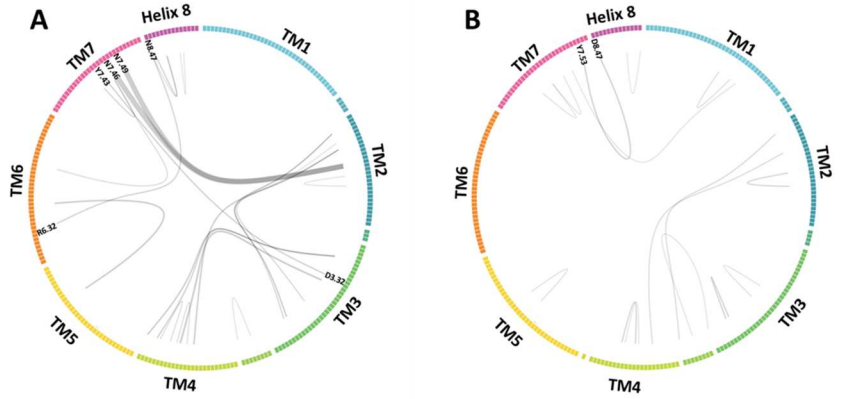

Figure S5 *Differences in the intra- and interhelical hydrogen bonding network for inactive WT (**A**) and β-arr biased (**B**) δOR. To obtain the graphs, we have generated interaction frequencies for both the WT and D2.50A δOR, and then substracted the resulting*

*frequencies between the systems as follows: WT receptor (Δfrequency = frequency$_{inactive}$ – frequency$_{β\text{-}arr\ biased}$) (A) and β-arr biased δOR: (Δfrequency = frequency$_{β\text{-}arr\ biased}$ – frequency$_{inactive}$). The graphs are plotted with a threshold of Δfrequency > 10%. Line thickness relates to the degree of interaction difference between the WT (A) and β-arr biased δOR (**B**)*

Y7.53 forms a water mediated bond with N1.50

In the inactive δOR[6,7] as well as in the closely related inactive μOR structure,[8] Y7.53 forms a water mediated bond with the highly conserved N1.50. An open state of this lock has been related to receptor activation in the μOR.[9] (Figure S5)

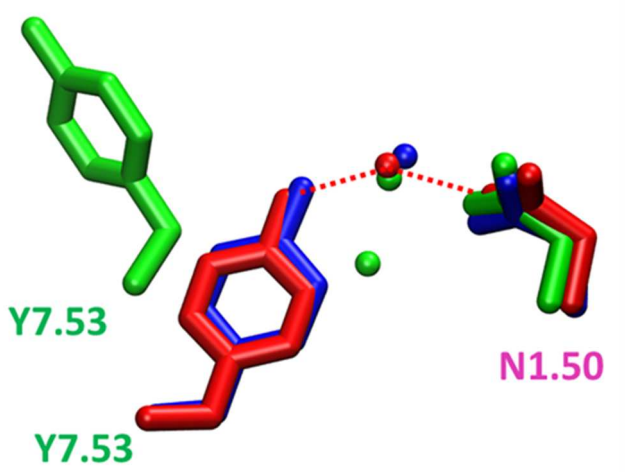

Figure S6 *Conservation of the lock between Y7.53 and N1.50 in opioid receptors mediated by a water molecule.*
Superimposition of the crystal structures of the inactive δ-opioid receptor (PDB code: 4N6H, colored blue), inactive μ-opioid receptor (PDB code: 4DKL, colored red), and active μ-opioid receptor (PDB code: 5C1M – colored green). Crystallized waters within 5Å distance of N1.50 are displayed as spheres.

Metastable states during receptor fluctuation detected via MSM analysis

Previous analysis showed that arrestin-bias is related to higher fluctuation in particular TM7 (Figure 2, main text). In order to explore potential metastable states and their transitions during receptor fluctuation, we performed Markov State Models (MSMs)

analysis on φ and Ψ dihedral angles of δOR residues Y7.43 - L7.56 (Figure S6A, see also experimental section). MSM analysis and PCCA+ yield 7 macrostates for WT δOR and 11 macrostates for the arrestin-biased δOR (D2.50A mutant). Most relevant macrostates in terms of frequency (state 1 to 5) and net fluxes suggested by Transition Pathway Theory (TPT) analysis (see tables S3, S4, S5) from state 1 to 3 and 5 are shown in Figure S7B. We can observe that the most stable state 1 in the WT receptor is more stable than the arrestin-biased receptor (WT/β-arr-Bias: 59%/34%). In contrast, states 2 (WT/β-arr-Bias: 3%/11%) and 4 (WT/β-arr-Bias: 20%/16%) become more stable in the arrestin-biased receptor.

Importantly, new states 3 and 5 appear exclusively in arrestin-biased δOR. These are characterized by helix movement and rotation of residues F7.44 – F7.55 with a pronounced conformational change in Y7.53. This residue is part of the NPXXY motif. Interestingly, the observed anti-clockwise rotation in the arrestin-biased δOR (D2.50A mutant) is also observed in rhodopsin when coupling to arrestin (Figure S7C). Note that state 4 and 5 together count for 9 % of simulation data in the arrestin-biased δOR while these states have not been found in the WT δOR. Considering the total analyzed simulation time of 12.8 μs obtained from 100 replicates, state 4 and 5 occur for a significant time of 1.2 μs for the arrestin-biased δOR (D2.50A mutant).

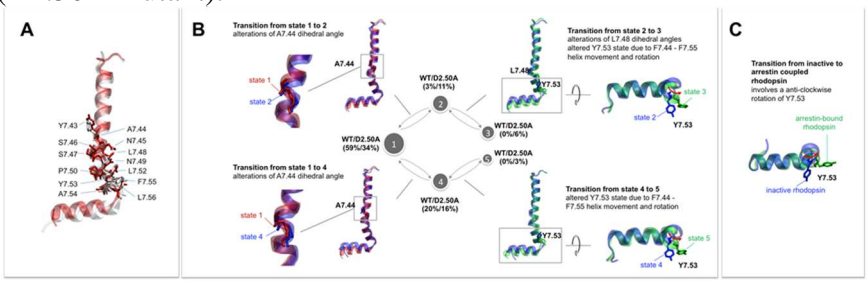

Figure S7 *Metastable states of TM7 detected during receptor fluctuation via MSM analysis.*
*δOR residues Y7.43 - L7.56 used for MSM analysis are labelled (**A**). Most relevant macrostates based on frequency (state 1 to 5) and pathways net fluxes suggested by TPT analysis (**B**). Superimposition of the crystal structures of inactive rhodopsin (PDB code: 1F88) and arrestin coupled rhodopsin (PDB code: 4ZWJ) (**C**).*

Table S2 *Impact of TM2 and TM7 mutation on the signaling profile of naltrindole.*

	β-arrestin activation Emax (% of BW373U86) ± SEM	β-arrestin activation EC50 (nM)	$G\alpha_i$ activation Emax (% of BW373U86) ± SEM	$G\alpha_i$ activation EC50 (nM)
WT	N/A[a]	N/A[a]	53.4 ± 2,8	21.9
D2.50A	64.3 ± 1	4.2	N/A[a]	N/A[a]
N7.45A	45 ±1	50	N/A[a]	N/A[a]
N7.49A	25.5 ± 1,4	36.7	N/A[a]	N/A[a]

[a] "N/A" indicated that no activation was observed or the ligand concentration dependence curve lacked a sigmoidal characteristic

Experimental Procedures

System preparation

The systems were generated using CHARMM-GUI.[10,11] We have used the crystal structure of δ-opioid receptor in complex with naltrindole (PDB code: 4N6H). To generate the mutated D2.50A δ-opioid receptor, we have inserted the mutation using the CHARMM-GUI panel. A sodium ion was placed in the allosteric binding site of the wild-type receptor. It was not placed in the D2.50A receptor, as mutational data show, that this mutation makes the receptor sodium insensitive.[6] The receptor was embedded in a ~ 80 x 80Å POPC bilayer and solvated with TIP3 water molecules. The ionic strength of the solution was kept at a 0.15 M with NaCl ions. Parameters for the simulation were obtained from the CHARMM36 forcefield.[12] Parameters for the ligand were assigned from the CGenFF forcefield automatically by the ParamChem tool implemented in CHARMM-GUI.[13,14]

Molecular dynamic simulations

The systems were first equilibrated in conditions of constant pressure (NPT, 1.01325 bar) for 20 ns, preceeded by an initial 1000 step minimization. After the NPT step we have carried out simulations in conditions of constant volume (NVT) of the system for 600 ns in 4 replicates. The simulations were run in ACEMD.[15] In both steps we used a time-step of 4 fs. Such a time-step was possible due to the hydrogen mass repartitioning scheme being employed in Acemd.[16]

A non-bonded interaction cutoff was set at 9 Å. A smooth switching function for the cut-off was applied, starting at 7.5 Å. The size of the cell was set to prevent non-bonding interactions between the protein and its periodic boundary image. Long-distance electrostatic forces were calculated using the Particle Mesh Ewald algorithm. The algorithm had grid spacing of 1 Å. The bond lengths of hydrogen atoms were kept constrained using the RATTLE algorithm. Simulations were carried out at a temperature of 300K.

Water fluctuation analysis

To analyze fluctuations, the receptor was aligned to the structure available in the OPM database.[17] For analysis only the area corresponding to the internal water channel of the protein (x>-4 and x <10 and y > -12 and y < 12) was taken into account. The area was divided into 5Å slices based on the value of the Z coordinate, with the eleventh slice starting at Z=-27,5 and ending at Z=-22,5. To quantify water fluctuations, the number of waters that either enter or exit the studied area between two subesequent frames was measured (for this analysis we we have strided the simulations, so that there is a 0,4ns time skip between frames). To simplify quantification, we only considered the oxygen atom, for describing the position of a water molecule. We divided the obtained fluctuations, by the average amount of water present in the slice in the two frames used to compute fluctuations. By averaging the values obtained from all of the coordinates, we get the number of fluctuations in a slice, per water molecule occurring over 0,4ns of the simulation. The values were then multiplied, to obtain the average number of fluctuations per slice that occur in 100ns.

Flare plot analysis

To generate flare plots (Figure 2AB, and Figure S5) we have used the tool developed by Dr. Fonseca and Dr Venkatakishnan (https://github.com/RasmusFonseca/EvoBundle; http://rasmusfonseca.github.io/EvoBundle/gpcr_demo2/). Flare plots are based on the computation of hydrogen bonds by means of the MDTraj Python library.[18] Hydrogen bonds are identified as any combination of donor atoms (NH or OH) and acceptor atoms (N or O) which have a donor-acceptor distance < 2.5A and the angle formed between the acceptor atom, the hydrogen atom and the atom covalently bound to the polar hydrogen has a value higher than 120°.

Markov State Models

Sines and cosines of φ and Ψ dihedral angles of arrestin-biased δOR and WT δOR residues Y7.43 - L7.56 for the whole 100 replicates of 128 ns per system were used as raw input data for dimensionality reduction. Raw data from both arrestin-biased δOR and WT δOR was processed together by Time-lagged Independent Component Analysis (TICA)[19-21] with a lag-time 0.2 ns yielding the first three time-lagged Independent Coordinates (tIC) for both systems that summarized the slowest processes of the system accounting for a total kinetic variability of 52%. The three tICs of each system were clustered independently to 1000 approx. discretized states by mini-batch K-means clustering.[22] Transition matrixes were estimated by maximum likelihood method considering a lag-time of 5 ns. Then, several macrostates were obtained by Robust Perron Cluster Analysis (PCCA+) for both systems.[23] Furthermore, Transition Pathway Theory (TPT)[24-26] analysis was perform to obtain a coarse-grained model for the transition between macrostates. Software used was HTMD 1.9.4[27] for MD data processing, MSM estimation and PCCA+ and PyEMMA 2.4[28] for TPT analysis.

Markov state model estimation and TPT analysis:

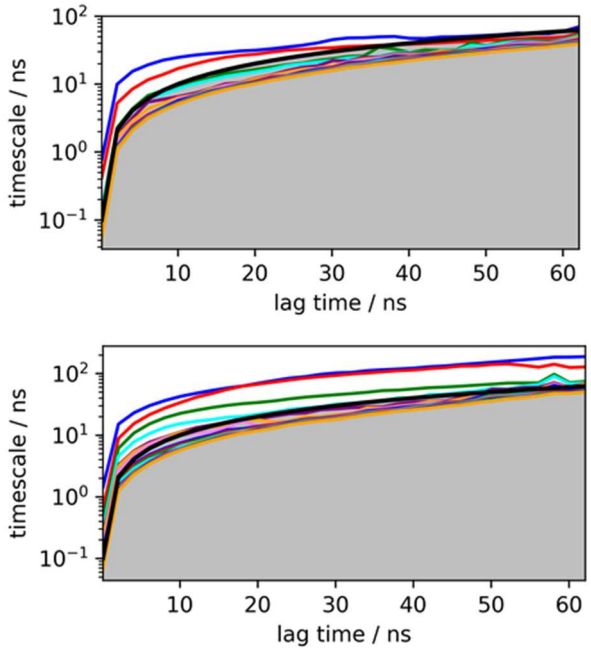

Figure S8 *20 first implied timescales computed for every 2 ns as a function of the lag time.*
Grey area and the limiting black line is defined by lag time > timescale and represent the area where the processes under investigation have already decayed and the estimation is not reliable. Left: Implied timescales of the markov model estimated from WT δOR simulations. Right: Implied timescales of the markov model estimated from WT δOR simulations arrestin-biased δOR. Nearly constant timescales show process markovianity.

Table S3. *Most relevant net fluxes of direct transitions between states in the pathways from state 1 to 3 and 5 obtained by TPT analysis for arrestin-biased δOR.*

State transitions	Net flux (10-5 transitions/ lag time*)	Transition time (1/Net flux, μs)
1→3 pathways		
1→2	5.35	093.30
2→3	7.63	065.50
1→4	2.51	198.88
4→2	1.51	331.91
4→3	1.03	484.93
1→5 pathways		
1→4	4.08	103.46
4→5	4.83	103.46
1→5	1.12	448.20
1→2	0.93	535.00
2→4	0.69	726.28

*Lag time = 5 ns

Table S4. *Most relevant net fluxes of direct transitions between states in the pathways from state 1 to 2 and 4 obtained by TPT analysis for WT δOR.*

State transitions	Net flux (10^{-5} transitions/ lag time*)	Transition time (1/Net flux, μs)
1→2 pathways		
1→2	12.18	041.06
1→4	06.83	073.26
4→2	06.84	073.10
1→4 pathways		
1→4	77.37	006.46
1→2	04.96	100.76
2→4	04.95	101.05

*Lag time = 5 ns

Table S5. Total transition rates of the different patways analized by TPT analysis starting from state 1.

Pathways	Total transition rate (k_{AB}) (10^{-5} transitions/ lag time*)	MFPT† (μs)
1→3 arrestin-biased δOR	09.52	52.54
1→5 arrestin-biased δOR	06.93	72.18
1→3+5 arrestin-biased δOR	16.00	31.26
1→2 WT δOR	19.59	25.52
1→4 WT δOR	89.75	05.57

*Lag time = 5 ns

†MFPT = Mean First Passage Time. MFPT = 1/ k_{AB}

References

[1] S. Yuan, S. Filipek, K. Palczewski, H. Vogel, Nat. Commun. 2014, 5, 4733.
[2] W. L. Jorgensen, J. Am. Chem. Soc. 1981, 103, 335–340.
[3] D. J. Huggins, J. Chem. Phys. 2012, 136, 1–30.
[4] M. Holz, S. R. Heil, A. Sacco, Phys. Chem. Chem. Phys. 2000, 2, 4740–4742.
[5] P. Florová, P. Sklenovský, P. Banáš, M. Otyepka, J. Chem. Theory Comput. 2010, 6, 3569–3579.
[6] G. Fenalti, P. M. Giguere, V. Katritch, X.-P. Huang, A. a Thompson, V. Cherezov, B. L. Roth, R. C. Stevens, Nature 2014, 506, 191–196.
[7] S. Granier, A. Manglik, A. C. Kruse, T. S. Kobilka, F. S. Thian, W. I. Weis, B. K. Kobilka, Nature 2012, 485, 400–4.
[8] A. Manglik, A. C. Kruse, T. S. Kobilka, F. S. Thian, J. M. Mathiesen, R. K. Sunahara, L. Pardo, W. I. Weis, B. K. Kobilka, S. Granier, Nature 2012, 485, 321–6.
[9] W. Huang, A. Manglik, a J. Venkatakrishnan, T. Laeremans, E. N. Feinberg, A. L. Sanborn, P. Gmeiner, H. E. Kato, K. E. Livingston, T. S. Thorsen, et al., Nature 2015, 524, 315–21.
[10] J. Lee, X. Cheng, J. M. Swails, M. S. Yeom, P. K. Eastman, J. A. Lemkul, S. Wei, J. Buckner, J. C. Jeong, Y. Qi, et al., J. Chem. Theory Comput. 2016, 12, 405–413.
[11] E. L. Wu, X. Cheng, S. Jo, H. Rui, K. C. Song, E. M. Dávila-Contreras, Y. Qi, J. Lee, V. Monje-Galvan, R. M. Venable, et al., J. Comput. Chem. 2014, 35, 1997–2004.
[12] J. B. Klauda, R. M. Venable, J. A. Freites, J. W. O'Connor, D. J. Tobias, C. Mondragon-Ramirez, I. Vorobyov, A. D. MacKerell, R. W. Pastor, J. Phys. Chem. B 2010, 114, 7830–7843.
[13] K. Vanommeslaeghe, E. Hatcher, C. Acharya, S. Kundu, S. Zhong, J. Shim, E. Darian, O. Guvench, P. Lopes, I. Vorobyov, et al., J. Comput. Chem. 2010, 31, 671–690.
[14] W. Yu, X. He, K. Vanommeslaeghe, A. D. MacKerell, J. Comput. Chem. 2012, 33, 2451–2468.
[15] M. J. Harvey, G. Giupponi, G. De Fabritiis, J. Chem. Theory Comput. 2009, 5, 1632–1639.
[16] K. A. Feenstra, B. Hess, H. J. C. Berendsen, J. Comput. Chem. 1999, 20, 786—798.
[17] M. A. Lomize, A. L. Lomize, I. D. Pogozheva, H. I. Mosberg, Bioinformatics 2006, 22, 623–625.

[18] R. T. McGibbon, K. A. Beauchamp, M. P. Harrigan, C. Klein, J. M. Swails, C. X. Hernández, C. R. Schwantes, L. P. Wang, T. J. Lane, V. S. Pande, Biophys. J. 2015, 109, 1528–1532.
[19] L. Molgedey, H. G. Schuster, Phys. Rev. Lett. 1994, 72, 3634–3637.
[20] C. R. Schwantes, V. S. Pande, J. Chem. Theory Comput. 2013, 9, 2000–2009.
[21] G. Pérez-Hernández, F. Paul, T. Giorgino, G. De Fabritiis, F. Noé, J. Chem. Phys. 2013, 139, 15102.
[22] D. Sculley, D., in Proc. 19th Int. Conf. World Wide Web - WWW '10, ACM Press, New York, New York, USA, 2010, p. 1177.
[23] S. Röblitz, M. Weber, Adv. Data Anal. Classif. 2013, 7, 147–179.
[24] W. E., E. Vanden-Eijnden, J. Stat. Phys. 2006, 123, 503–523.
[25] P. Metzner, C. Schütte, E. Vanden-Eijnden, Multiscale Model. Simul. 2009, 7, 1192–1219.
[26] F. Noé, C. Schütte, E. Vanden-Eijnden, L. Reich, T. R. Weikl, Proc. Natl. Acad. Sci. U. S. A. 2009, 106, 19011–6.
[27] S. Doerr, M. J. Harvey, F. Noé, G. De Fabritiis, J. Chem. Theory Comput. 2016, 12, 1845–52.
[28] M. K. Scherer, B. Trendelkamp-Schroer, F. Paul, G. Pérez-Hernández, M. Hoffmann, N. Plattner, C. Wehmeyer, J.-H. Prinz, F. Noé, J. Chem. Theory Comput. 2015, 11, 5525–42.

3.3 Concerted action of receptor phosphorylation sites govern β-arrestin recruitment, trafficking and signaling

In this chapter, we present our work in form of a journal article

Summary:
In this article, we study how distinct phosphorylation sites impact the stability and physiological result of arrestin interaction. For this, we use the vasopressin 2 (V_2) receptor as a model protein and generate multiple mutants of the phosporylatable c-terminal tail. The mutations prevent phosphorylation of each site, allowing us to effectively evaluate the impact of each position.

The effect of every phosphorylation site on the physiological response was studied using extensive biological assays. In parallel the structure of every mutant-arrestin complex was evaluated using molecular dynamics simulations. Interestingly, loss of one of those sites (T^{360}) was shown, to have a much more profound impact on arrestin coupling as well as signaling response. Simulations reveal a potential structural mechanism that might explain this phenomenon.

Our results shed light on how interactions with the C-tail promote a specific arrestin downstream response. Seeing the high degree of conservation of position 360, this data might be transferred to other GPCRs, as well as used for the design of drugs that inhibit this interaction, mediating the arrestin response in a tailored way.

The PhD candidate was responsible for all the computational work carried out in this study, as well as writing parts of the manuscript concerning the computational work.

Concerted action of receptor phosphorylation sites govern β-arrestin recruitment, trafficking and signaling

Hemlata Dwivedi[1#], Madhu Chaturvedi[1#], Mithu Baidya[1#], Tomasz Maciej Stępniewski[2], Shubhi Pandey[1], Jagannath Maharana[1], Jana Selent[2]* and Arun K. Shukla[1]*
#equal contribution

[1]Department of Biological Sciences and Bioengineering, Indian Institute of Technology, Kanpur 208016, India;
[2]Research Programme on Biomedical Informatics (GRIB), Department of Experimental and Health Sciences of Pompeu Fabra University (UPF)-Hospital del Mar Medical Research Institute (IMIM), 08003 Barcelona, Spain.

*Corresponding authors:
e-mail: arshukla@iitk.ac.in
e-mail: jana.selent@upf.edu

Keywords: GPCR, β-arrestins, phosphorylation, biased agonism, cellular signaling, vasopressin receptor

Abstract
Interaction with β-arrestins (βarrs) critically regulates downstream signaling and trafficking of GPCRs. Agonist-induced receptor phosphorylation is a key determinant of GPCR-βarr interaction and different phosphorylation patterns impart distinct βarr conformations leading to specific functional outcomes. It is generally believed that collective receptor phosphorylation, especially the clusters of phosporylatable residues in the carboxyl-terminus, determine the strength and the trafficking patterns of receptor-βarr complexes. Contrary to this notion, we discover using the human vasopressin receptor (V_2R) as a model system that several phospho-sites, positioned either individually or in clusters, work in a concerted fashion to regulated agonist-induced βarr recruitment, trafficking and ERK MAP kinase activation. Surprisingly, we also discover that even single phospho-sites, which are specifically positioned to cross-talk with key residues in βarrs, can have a decisive contribution in βarr recruitment and functional consequences. Structural analysis and molecular dynamics simulation provide mechanistic insights into how specific phospho-sites contribute towards the stability of receptor-βarr interaction and regulate the orientation of the lariat loop and inter-domain rotation in βarrs. Taken together, our findings reveal how specific phospho-sites contribute towards the stability and functionality of receptor-βarr complexes, and therefore, provide important insights to refine the conceptual framework of GPCR-βarr interaction.

Due to copy-right related issues, we present only the computational results of the paper with a short summary of obtained *in vitro* results.

Introduction

G protein-coupled receptors (GPCRs) receive a diverse array of signals from the extracellular milieu and relay them across the cell membrane and thereby play an important role in nearly every cellular and physiological event in human biology [1]. Upon agonist-activation, GPCRs couple to, and activate heterotrimeric G-proteins resulting in the generation of second messengers and downstream signaling [2]. Subsequently, they are phosphorylated in their carboxyl-terminus and intracellular loops by GRKs (GPCR kinases) which initiates the recruitment of multifunctional proteins called β-arrestins (βarrs) [3]. It was originally conceived that binding of βarrs excludes further coupling of G-proteins to activated receptors, leading to receptor desensitization. However, recent studies have also demonstrated the formation of GPCR-G-protein-βarr megaplexes both *in-vitro* and in the cellular context [4]. In addition, βarrs also direct receptor endocytosis through clathrin-dependent mechanism and contribute in downstream signaling pathways through their scaffolding capabilities of various signaling partners [5,6].

While several high-resolution structures are now available for GPCR-G-protein complexes which have allowed us to decipher their interaction interfaces and coupling mechanisms, structural information on GPCR-βarr complexes remains rather scarce [7,8]. In the current framework, receptor activation and phosphorylation are considered two major determinants of βarr-recruitment where the phosphorylated receptor tail (i.e. the carboxyl-terminus) engages with the N-domain of βarrs and the activated receptor core interacts with various loops in βarrs [9,10]. It is generally believed that the cumulative phosphorylation of the receptors determines the affinity of βarr-interaction and the stability of receptor-βarr complexes which in turn govern their trafficking and signaling patterns. GPCRs are typically categorized into two broad classes, class A and B, based on the stability of their interaction with βarrs and trafficking patterns [11].

Typically, class B receptors such as angiotensin receptor and vasopressin receptor harbor clusters of Ser/Thr which are conceived to give rise to their stable interaction with βarrs and trafficking of receptor-βarr complexes through endosomal routes for ultimate degradation [12]. However, a systematic analysis of different phosphorylation sites, for example, in case of V_2R, present either as

a part of the phospho-site clusters or in isolation, on βarr interaction, trafficking and signaling has not been done. Furthermore, it has been well established that specific phosphorylation sites in the receptors are important for driving distinct βarr conformations and corresponding functional outcomes, a paradigm referred to as receptor "bar-code" [13,14]. Still however, the structural basis of how specific spatial positioning of different phosphorylation sites is structurally linked to βarr activation and conformation remains less understood. These questions represent a central knowledge gap in our current conceptual framework of GPCR-βarr interaction and thus, are important to investigate in order to better understand βarr-mediated signaling and regulation of GPCRs.

Although previous studies have utilized site-directed mutagenesis to decipher the contribution of receptor phosphorylation sites in βarr binding and trafficking, the lack of a high-resolution active βarr structure has restricted direct structural interpretation of the data. Recently determined crystal structure of V_2Rpp-βarr1 complex has revealed the interactions between the receptor-attached phosphates and Lys/Arg residues in βarrs [15], and therefore, it allows a direct structure-guided interrogation and structural correlation of phosphorylation sites in βarr-interaction and activation. Although V_2Rpp harbors eight phosphate groups, only five of them i.e. S357, T360, S362, S363 and S364 are directly involved in charge interactions with Lys/Arg in βarr1. In the context of V_2R, previous studies have focused primarily on mutation and/or deletion for phosphorylation site clusters e.g. T359/T360, S363/S363/S364 and T369/S370/S371, and the contribution of individual sites in βarr recruitment, trafficking and signaling has not been explored.

To address this knowledge gap, we have generated 6 different constructs of V_2R harboring different phosphorylation site point mutations. By carrying out multiple biological assay, we were able to assess the impact of each phosphorylation site on arrestin function.
We discover that specifically-positioned phosphorylation sites can significantly influence βarr recruitment, trafficking and signaling. Molecular dynamics simulation using V_2Rpp-βarr1 crystal structure as a template provides structural insights into how specific phosphorylation sites contribute towards the stability of βarr interaction and inter-domain rotation.

Results

In vitro results

The role of phosphorylation sites has been investigated with a series of V_2R constructs, in which C-tail phosphorylation sites were mutated into alanine (Fig 1B). Each construct presented a comparable surface-expression level, as revealed by a previously utilized protocol [17]. For each construct, we assessed βarr recruitment and receptor trafficking (Fig 1C).

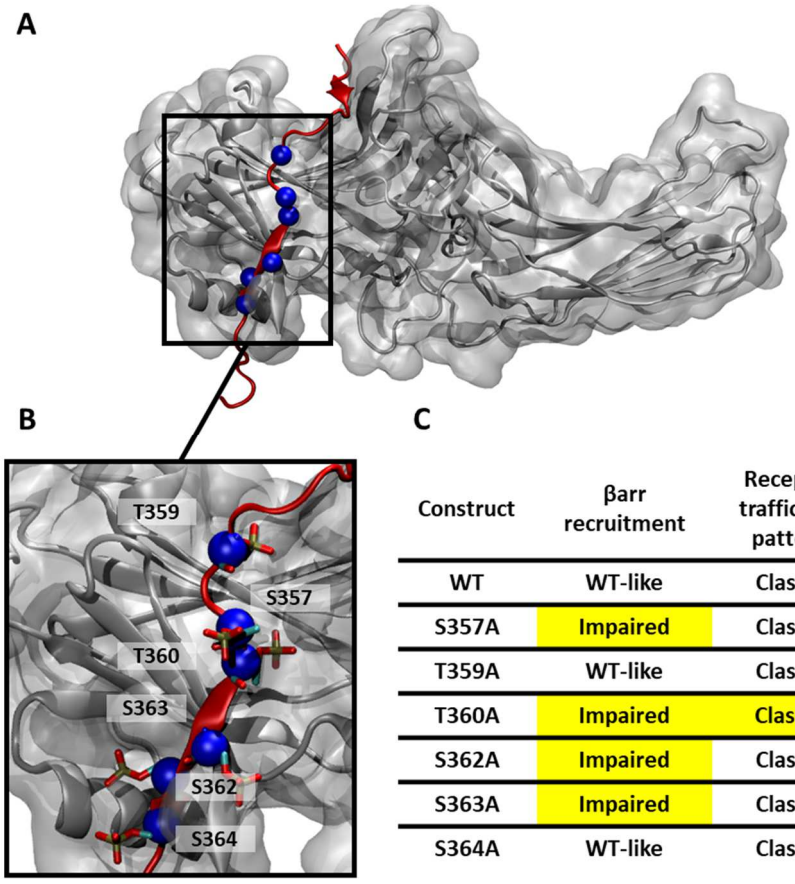

C

Construct	βarr recruitment	Receptor trafficking pattern
WT	WT-like	Class B
S357A	Impaired	Class B
T359A	WT-like	Class B
T360A	Impaired	Class A
S362A	Impaired	Class B
S363A	Impaired	Class B
S364A	WT-like	Class B

Figure 1 *Summary of analyzed experimental results.*
*(**A**) Structural depiction of βarr1 in complex with the V2Rpp WT. (**B**) Detailed representation of six mutated position in the V2R C-terminal tail (**C**) Functional impact of each mutation on the signaling response. Construct properties which are altered from the WT are highlighted in yellow..*

Remarkably, mutating one of the phosphorylation sites T360 not only impairs arrestin recruitment, but also changes the trafficking pattern of the V2R. We observe that its class B-like pattern is converted into a class A one involving a significant increase of the V2R concentration in the cell-membrane. Furthermore, additional experiments reveal that the T360A mutation impairs signaling within the ERK1/2 pathway. Taken together, this data highlights the key importance of position T360 in multiple arrestin-dependent processes.

Structural insights into βarr-recruitment and conformation.
In order to gain structural and mechanistic insights into the experimental findings, we employed molecular dynamics simulations using the V_2Rpp-βarr1 crystal structure as a template. We carried out classical unbiased simulations to monitor the dynamics of V_2Rpp in the context of phosphorylation site mutations. Here, a quantitative measure of V_2Rpp dynamics is obtained by computing the root mean square fluctuation (RMSF) per residue. We observe that the wild-type and mutated peptides exhibit an overall similar RMSF profiles (Figure S1). Expectedly, we observe higher RMSF at the N- (346 to 348) and the C-terminal ends (366 to 372) of the peptide, while two stretches in the middle which adopt an extended β-strand and pack against the β-strand I of βarr1 via backbone interactions display much lower RSMF profile (Figure S1).

In all the simulated systems T360 is repeatedly the most stable V2Rpp position. This suggests the importance of this residue, in stabilizing the V2Rpp-βarr1 complex. This hypothesis is supported by our biochemical data which shows that the mutation of T360 into Ala dramatically decreases βarr recruitment to the receptor. As indicated in Figure S1, T360 is a part of the extended β-strand in the middle of V2Rpp and it interacts with K294 in the lariat loop of βarr1 through a strong electrostatic interaction (Figure 2A). Structurally, T360 is at the center of a three-way connection between the N-domain, the V2Rpp and the C-domain of βarr1 through the T360-K294 ionic lock (Figure 2A). Thus, it is tempting to speculate that the T360-K294 ionic lock may be a crucial determinant for the βarr activation process which is linked to inter-domain rotation (inactive 0° and active 20°). To test this possibility, we assessed the inter-domain rotation angle of the βarr1 in complex with the V2Rpp WT

(Figure 2B). The observed rotation angle of 17° which is in line with previous simulation experiments from Latorraca et al. [16].

According to the conformational distribution, βarr1 is able to sample the whole conformational spectrum from active with high probability to inactive with low probability. Taking advantage of this, we computed the stability of the ionic lock (T360-K294) for different activation states corresponding to inter-domain rotation angle of -5 to 30 (Figure 2D). Interestingly, we observe that the ionic-lock stability directly correlates with inter-domain rotation angles showing a dramatic reduction of lock formation in inactive-like βarr1 states, i.e. inter-domain rotation angle < 11°. This highlights the role of the ionic lock as an important element in stabilizing the N- and the C-domain arrangement during βarr activation. In agreement with this notion, we uncover that the conformational distribution of βarr1 in complex with T360A mutant which lacks this ionic lock is shifted towards a more inactive-like conformations with an average inter-domain rotation angle of 11° compared to 17° in case of wild-type V2Rpp sequence (Figure 2C). Importantly, our previous experiments show that a T360Ala mutant impacts the trafficking pattern of βarrs compared to the V2Rpp WT. Ultimately, this suggests that the inter-domain rotation angle and thus different conformational states are directly related to the functional response of βarr1.

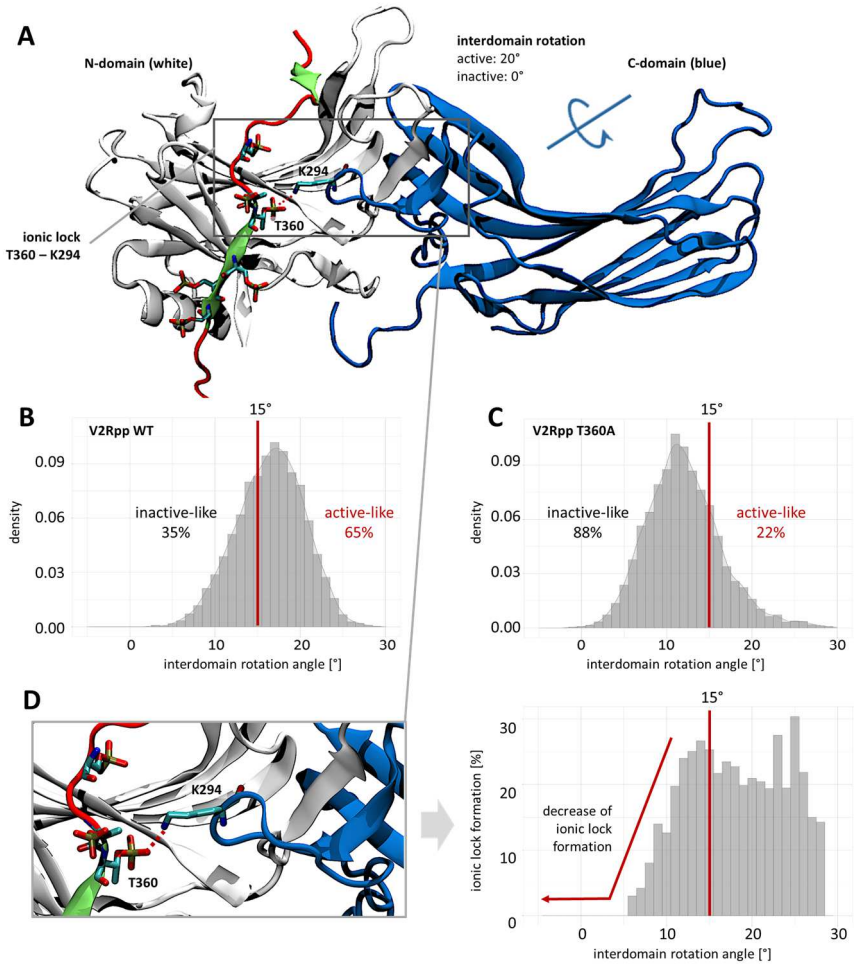

Figure 2 *Molecular dynamics simulation yields structural insights into βarr recruitment and conformation.*
*(**A**) Structural depiction of βarr1 in complex with the V2Rpp WT. (**B**) Interdomain rotation angle adopted by βarr1 in complex with the V2Rpp WT. We observe a conformational distribution with a peak at 17°. This is slightly lower than the rotation angle of the active state observed in the crystal structure (20°) and is in line with previous simulation experiments (Latorraca et al. Nature 2018). (**C**) Interdomain rotation angle adopted by βarr1 in complex with the V2Rpp T360A. The rotation angle is shifted to lower values with a peak at 11°. (**D**) The ionic lock between T360 and K294 links the N-domain to the C-domain via the V2Rpp. Its stability is a function of arrestin activation. Ionic lock formation is reduced in inactive-like (<11°) conformations.*

Discussion

GPCR phosphorylation is a key determinant of βarr interaction and activation leading to various regulatory and signaling outcomes. Thus, systematic investigation of specific contribution of receptor phosphorylation sites in overall βarr recruitment and functional outcomes is of paramount importance. V_2R has been one of the most extensively studied prototypical GPCRs in terms of βarr interaction, trafficking and signaling. Not only the contribution of different GRKs in phosphorylation of V_2R and subsequent ERK1/2 MAP kinase phosphorylation has been investigated in detail [18] but also there have been several studies to understand how the phosphorylated carboxyl-terminal peptide of V_2R (V2Rpp) activated βarrs *in-vitro* [18,19]. Moreover, the recently determined crystal structure of V_2Rpp-βarr1 complex now allows us to draw structural correlations using site-directed mutagenesis and biochemical data [15]. Therefore, V_2R is a suitable receptor system to decipher the role of different phosphorylation sites in βarr interaction and function.

V_2Rpp has a total of eight phosphorylation sites which include three isolated residues namely S347, S350 and S357, and five residues present as two distinct clusters namely T359/360 and S362/363/364. We observed that S357 mutation results in a decrease of βarr1/2 interaction but does not significantly affect the class B pattern of βarr trafficking. On the other hand, S347 and S350 appear to be dispensable for receptor-βarr interaction when mutated individually. In the T359/360 cluster, although T359 is not crucial for βarr-recruitment, the adjacent residue T360 appears to have a major contribution in receptor-βarr interaction and trafficking. T360Ala mutant exhibits not only weaker physical interaction but also dramatically alters the trafficking pattern of βarrs from class B to class A, and significantly diminishes agonist-induced ERK1/2 phosphorylation. These data demonstrate that even a single phosphorylation site may have decisive contribution in governing receptor-βarr interaction, and in turn driving βarr trafficking and ERK1/2 phosphorylation.

Previous studies using S362/363/364 cluster mutant has revealed its contribution in receptor phosphorylation and receptor trafficking [20] although a systematic analysis of βarr interaction and trafficking has not been carried out. Our data with isolated mutants of Ser present in this cluster reveal that S362 and S363 are important for physical

interaction with βarrs but S364 is mostly dispensable when tested individually.

So, how does this biochemical data fit in the structural framework? Using MD simulation on V_2Rpp-βrr1 structural template, we discover two major insights. First, T360 appears to be a key pivotal site for keeping V_2Rpp locked in the N-domain of βarr1. Second, it forms a salt-bridge interaction with K294 in the lariat loop of βarr1 which appears to be an important contributor in determining the extent of inter-domain rotation during the activation process. It is interesting that T359 which is right next to T360 points in a direction away from K294 and even after T360A mutation, it does not engage with K294 suggesting that its orientation is ill-suited for an interaction with the lariat loop. K294 is highly conserved across the different arrestins and species suggesting that its interaction with spatially positioned receptor phosphate may be a common mechanism for receptor interaction and activation. Moreover, as βarr trafficking pattern changes from class B to class A for T360 mutant, and the T360-K294 salt-bridge correlates with the inter-domain rotation, it is tempting to speculate that the extent of inter-domain rotation may also be directly connected with the trafficking pattern of βarrs for different receptors. Future studies designed to probe this possibility may uncover additional structural mechanisms determining the receptor-βarr interaction and ensuing trafficking patterns.

In conclusion, our data uncovers how a phosphorylation site in the receptor may work as connecting point between the N-domain and the C-domain of βarrs, and thereby regulate the inter-domain rotation during the activation process. Our study therefore provides a missing piece in the paradigm of GPCR-βarr interaction using V_2R as a model system, and it also offers a framework that may potentially have general applicability for other GPCRs.

Materials and methods

Molecular dynamics simulations

System setup and simulation

To generate all simulated complexes, we used the structure of V2Rpp in complex with βarr1 (PDB code: 4JQI). The co-crystallized FAB30 antibody was removed and missing fragments in the βarr1 and V2Rpp structures were modelled using the loop modeler module available in the MOE package (https://www.chemcomp.com). The complexes were solvated (TIP3P water) and set to an ionic strength of 0.15 M sodium chloride. Simulation parameters were obtained from the Charmm36M forcefield. Systems generated this way were simulated using the ACEMD software [22]. To allow rearrangement of waters and side-chains, we carried out a 25 ns equilibration phase in NPT conditions with restraints applied to backbone atoms. The timestep was set at 2fs and the pressure was kept constant, using the Berendsen barostat. After NPT equilibration, systems were subjected to production runs (NVT ensemble) for 1 μs in 4 parallel runs. Simulation runs of the WT, and 360A systems were extended to 2 μs, amassing a total of 8 μs per system. For each NVT run, we employed a 4 fs timestep. In all runs, temperature was kept at 300 K using the Langevin thermostat and hydrogen bonds were restrained using the RATTLE algorithm. Non-bonded interactions were cut-off at 9 Å with a smooth switching function applied at 7.5 Å.

Analysis

To assess C-terminal tail stability, we aligned the system using backbone atoms of the arrestin. Afterwards RMSF values were calculated for the Cα atoms of the C-terminal tail. The interdomain rotation angle was used as a metric to assess the activation state of βarr1. We computed the displacement of the C-domain relative to the N-domain between the inactive (PDB code: 1G4R) and active βarr1 crystal structures (PDB code: 4JQI) as previously described [21]. The corresponding script was kindly provided by Naomi Latorraca. Using obtained values of the rotational angles, we divided the simulation frames into groups with a bin width of 1. For each bin of rotation angle, we assessed the stability of the ionic lock between residue T^{360} of the peptide, and K294 of the lariat loop. We considered the salt bridge to be formed if the distance between heavy polar atoms of those residues was less than 4 Å.

Acknowledgements
Research in Dr. Shukla's laboratory is supported by the Intermediate Fellowship of the Wellcome Trust/DBT India Alliance (IA/I/14/1/501285) awarded to AKS, Innovative Young Biotechnologist Award from the Department of Biotechnology (DBT) (BT/08/IYBA/2014-3), Science and Engineering Research Board (EMR/2017/003804), Young Scientist Award from the Lady TATA Memorial Trust, Department of Science and Technology and the Indian Institute of Technology, Kanpur. Dr. Shukla is an Intermediate Fellow of Wellcome Trust/DBT India Alliance (IA/I/14/1/501285) and EMBO Young Investigator. Dr. Selent's laboratory acknowledges support from the Instituto de Salud Carlos III FEDER (PI15/00460 and PI18/00094). TMS acknowledges support from Nacional Center of Science, Poland, grant 2017/27/N/NZ2/02571. We thank Drs. Eshan Ghosh and Punita Kumari for their assistance in generation and characterization of some of the V_2R mutants.

Authors' contribution
HD and MC carried out the surface expression, co-IP and ERK assays; MB carried out the confocal microscopy assisted by MC; JM assisted with structural analysis of V2Rpp-βarr1 complex; TMS carried out the MD simulation experiments under the supervision of JS; AKS supervised the overall project. All authors contributed to writing and editing of the manuscript.

References

1. Insel PA, et al. (2015) G Protein-Coupled Receptor (GPCR) Expression in Native Cells: "Novel" endoGPCRs as Physiologic Regulators and Therapeutic Targets. Mol Pharmacol 88(1):181-187.
2. Rosenbaum DM, Rasmussen SG, & Kobilka BK (2009) The structure and function of G-protein-coupled receptors. Nature 459(7245):356-363.
3. Pierce KL, Premont RT, & Lefkowitz RJ (2002) Seven-transmembrane receptors. Nat Rev Mol Cell Biol 3(9):639-650.
4. Thomsen ARB, et al. (2016) GPCR-G Protein-beta-Arrestin Super-Complex Mediates Sustained G Protein Signaling. Cell 166(4):907-919.
5. Kang DS, Tian X, & Benovic JL (2014) Role of beta-arrestins and arrestin domain-containing proteins in G protein-coupled receptor trafficking. Curr Opin Cell Biol 27:63-71.
6. Lefkowitz RJ & Shenoy SK (2005) Transduction of receptor signals by beta-arrestins. Science 308(5721):512-517.
7. Ghosh E, Kumari P, Jaiman D, & Shukla AK (2015) Methodological advances: the unsung heroes of the GPCR structural revolution. Nat Rev Mol Cell Biol 16(2):69-81.
8. Baidya M, Dwivedi H, & Shukla AK (2017) Frozen in action: cryo-EM structure of a GPCR-G-protein complex. Nat Struct Mol Biol 24(6):500-502.
9. Shukla AK, et al. (2014) Visualization of arrestin recruitment by a G-protein-coupled receptor. Nature 512(7513):218-222.
10. Ranjan R, Dwivedi H, Baidya M, Kumar M, & Shukla AK (2017) Novel Structural Insights into GPCR-beta-Arrestin Interaction and Signaling. Trends Cell Biol 27(11):851-862.
11. Oakley RH, Laporte SA, Holt JA, Caron MG, & Barak LS (2000) Differential affinities of visual arrestin, beta arrestin1, and beta arrestin2 for G protein-coupled receptors delineate two major classes of receptors. J Biol Chem 275(22):17201-17210.
12. Oakley RH, Laporte SA, Holt JA, Barak LS, & Caron MG (2001) Molecular determinants underlying the formation of stable intracellular G protein-coupled receptor-beta-arrestin complexes after receptor endocytosis*. J Biol Chem 276(22):19452-19460.
13. Nobles KN, et al. (2011) Distinct phosphorylation sites on the beta(2)-adrenergic receptor establish a barcode that encodes differential functions of beta-arrestin. Sci Signal 4(185):ra51.

14. Shukla AK, Singh G, & Ghosh E (2014) Emerging structural insights into biased GPCR signaling. Trends Biochem Sci 39(12):594-602.
15. Shukla AK, et al. (2013) Structure of active beta-arrestin-1 bound to a G-protein-coupled receptor phosphopeptide. Nature 497(7447):137-141.
16. Latorraca, N. R., Wang, J. K., Bauer, B., Townshend, R. J., Hollingsworth, S. A., Olivieri, J. E., ... & Dror, R. O. (2018). Molecular mechanism of GPCR-mediated arrestin activation. Nature, 557(7705), 452.
17. Pandey S, Roy D, & Shukla AK (2019) Measuring surface expression and endocytosis of GPCRs using whole-cell ELISA. Methods Cell Biol 149:131-140.
18. Ren XR, et al. (2005) Different G protein-coupled receptor kinases govern G protein and beta-arrestin-mediated signaling of V2 vasopressin receptor. Proc Natl Acad Sci U S A 102(5):1448-1453.
19. Xiao K, Shenoy SK, Nobles K, & Lefkowitz RJ (2004) Activation-dependent conformational changes in {beta}-arrestin 2. J Biol Chem 279(53):55744-55753.
20. Nobles KN, Guan Z, Xiao K, Oas TG, & Lefkowitz RJ (2007) The active conformation of beta-arrestin1: direct evidence for the phosphate sensor in the N-domain and conformational differences in the active states of beta-arrestins1 and -2. J Biol Chem 282(29):21370-21381.
21. Innamorati G, Sadeghi HM, Tran NT, & Birnbaumer M (1998) A serine cluster prevents recycling of the V2 vasopressin receptor. Proc Natl Acad Sci U S A 95(5):2222-2226.
22. Harvey, M. J., Giupponi, G., & Fabritiis, G. D. (2009). ACEMD: accelerating biomolecular dynamics in the microsecond time scale. Journal of chemical theory and computation, 5(6), 1632-1639.

Supplementary information

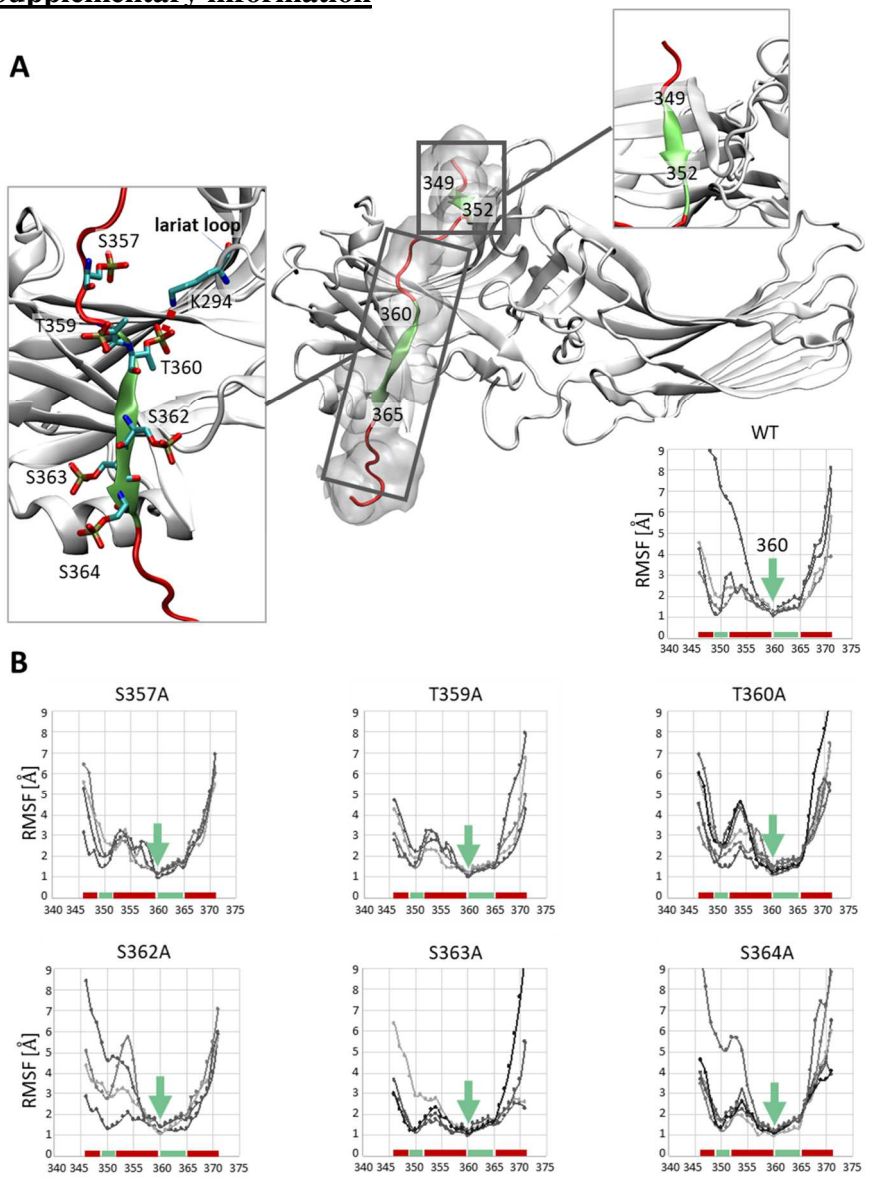

Figure S1 *Stability of the C-terminal peptides in complex with βarr1 (**A**). Representation of the c-tail/βarr1 complex (**B**).Per-residue stability (calculated as RMSF of the Cα) of the WT and mutated C-terminal complexes*

3.4 Palmitoylation of cysteine 415 of CB1 receptor affects ligand-stimulated internalization and selective interaction with membrane cholesterol and caveolin 1

Summary:
In this article we study the effect of palmitoylation of helix 8 on the CB1 receptor. Experimental results show that loss of this modification severely downregulates coupling of caveolin 1 to the receptor. Interestingly, our MD experiments reveal that palmitoylation stabilizes helix 8 in a helical conformation, likely altering the coupling interface of this receptor. Such changes in the coupling interface could explain how palmitoylation promotes interactions with caveolin 1.

Additionally, we find, that palmitoylation promotes interaction of the receptor with cholesterol. This could explain, why palmitoylated receptor is primarily localized in cholesterol-rich lipid rafts, in contrast to the unpalmitoylated receptor. To summarize, our data provides a possible structural explanation, into how palmitoylation modulates GPCR function.

The PhD candidate participated in designing, carrying out and analyzing all of the computational experiments, as well as in writing the manuscript.

Oddi S, Stepniewski TM, Totaro A, Selent J, Scipioni L, Dufrusine B, et al. Palmitoylation of cysteine 415 of CB 1 receptor affects ligand-stimulated internalization and selective interaction with membrane cholesterol and caveolin 1. Biochimica et biophysica acta Molecular and cell biology of lipids. 2017;1862(5):523–32. DOI: 10.1016/ j.bbalip.2017.02.004

Chapter 4
Discussion

As previously discussed, GPCRs are focal players in the process of neurotransmission, and attractive targets to understand as well as treat multiple CNS disorders. However, those receptors are intricate signaling machines, regulated by complex phenomena at multiple levels of action (e.g. ligand-receptor interactions, event in the allosteric network or post-translational modifications). To fully appreciate their activity, a multidisciplinary approach is necessary, combining biochemical assays with structural studies.

In **publication 3.1** we aimed to better understand functional selectivity within monoaminergic neurotransmitter receptors. We were motivated by the fact, that those receptors are important pharmacological targets, and their functionally selective ligands show great promise as safer and more efficient drugs. Our investigation revealed a conserved interaction pattern, that appears to be related to a specific signaling response within monoamine neurotransmitter receptors. This finding is an important contribution to the understanding of GPCRs, being to our knowledge the second study[175] that identifies a structural phenomenon connected to functional selectivity that is conserved within several receptors.

The presented results also open several questions. Most importantly, ligand kinetics (e.g. the association and dissociation rate) can play a role in signaling bias.[176] In this context it would be interesting to evaluate, if and to which extent the observed ligand-receptor interaction patterns contribute to a coupling outcome by having a conserved effect on ligand kinetics (i.e. ligand that interact with both TM5 and TM6 have a longer residence time, which is a necessary factor for the coupling of β-arr2).

Furthermore, although we studied the coupling of multiple downstream components, in the future it would be prudent to include additional G-proteins, as well as βarr1, which would allow to fully explore the complexity of the studied ligands. Finally, seeing that in this study we identified several signaling probes of the dopamine 2 receptor, it would be interesting to extensively sample how each of

the ligands engages the GPCR allosteric network, and how changes within this pattern are related to a specific response.

Finally the presented data provides tools to interrogate signaling pathways within various receptors in animal models of disease. For example, according to the presented data genetically modifying a mouse, to have an un-polar residue in position 6.55 of the serotonin 2A receptor, would likely result in an animal which has a reduced capability to couple arrestin to this receptor. Such a mice-model would offer the possibility to study the involvement of this interaction in the development and progression of multiple diseases (e.g. affective and psychotic).

Although we did not study in detail the allosteric network in the previous paper, we thoroughly investigated it in **publication 3.2**. There, using the wealth of previously generated structural and functional data, we propose a mechanism how a set of mutations induces arrestin bias in the δOR-naltrindole complex. Our simulations show, that in this system, breakage of interactions between TM2 and TM7 results in arrestin bias. Structural insights from this study can be further verified by additional experiments, i.e. NMR studies or other mutations tailored to destabilize TM7.

It would be tempting to speculate that results obtained here, can be extrapolated to other receptors and ligands (i.e. increasing the mobility of TM7 will always result in promoting arrestin coupling). However experimental data shows that the mutation effect in the δOR is highly ligand specific, i.e. the same mutation of the δOR in complex with the agonist Deltorphin II, induces G-protein bias.[177] This highlights the intrinsicness of the GPCR allosteric network, and that it always needs to be studied in relation to a set of specific conditions (the bound ligand, membrane environment etc.). However, the results of this study, appear to apply for multiple antagonists of the δOR.[177] As such engineering molecules with a δOR antagonist scaffold that induce conformational changes in TM7, might be a path to obtain β-arrestin bias within this receptor. In fact, interactions with TM7 have been postulated as contributing to arrestin bias within various GPCRs.[178]

Finally, this study demonstrated, that important structural changes in GPCRs can be observed as early as within the first 128 ns of simulations. The typical approach, when studying GPCRs with MD is to run few extended simulations. However, by concatenating multiple relatively short runs, we were able to identify small conformational changes, that appear to well capture the initial mechanism of βarr bias in the studied system. In the case of this study, multiple short runs were more informative, than several extended ones. As such, it would be interesting to evaluate, in which computational problems this methodology would be superior to the standard way fo running GPCR unbiased MDs.

In **publication 3.3** we aimed to understand how a specific phosphorylation pattern of the C-terminal tail contributes to the structural and functional features of GPCR-arrestin interactions. By using unbiased MD, we observe, how T^{360} by interacting with polar residues in the lariat loop of βarr1, induces a specific structural state which appears to contribute to the signaling response.

The implication of the lariat loop in stabilizing arrestin conformations have been previously speculated by other research teams.[179] An interesting development of this study, would be to further analyze the arrestin-receptor complex with more structural methods i.e. FRET[180] or NMR.[147] A potential limitation of the study is also the starting structure used in MD simulations. The input structure was the crystallized complex of βarr1 with the C-terminal tail of vasopressin 2 receptor. Although nanobody experiments confirm that arrestin is in a similar conformation as with the high affinity receptor complex, it is not possible to exclude that in the actual arrestin-receptor complex the C-terminal tail might be in a slightly different conformation. Finally, further experiments (e.g. mutations within arrestin) are necessary to confirm structural phenomena observed in our study.

Lastly, seeing that a phosphorylatable residue in a position corresponding to that of T360 is conserved among GPCRs, it would be interesting to evaluate whether the results obtained for this residue in V2R (structural and functional) are conserved among other receptors.

In the last article, **publication 3.4** we attempt to structurally rationalize some of the physiological effects induced by palmitoylation on CB_1-the most prominently expressed receptor in the human brain. *In vitro* experiments demonstrate that this modification promotes interaction with caveolin 1. Our structural data highlights that the palmitoylation stabilizes helix 8 in a helical conformation. Thus, a potential explanation, is that helix 8 forms part of the coupling interface with caveolin 1. Destabilization of this interface would likely inhibit caveolin 1 coupling. This hypothesis however needs to be further confirmed.

MD simulations also show, that palmitoylation promotes interaction of the receptor with cholesterol. To our knowledge, this is the first study that demonstrates this effect of palmitoylation. This result goes in line with functional studies, that prove the preferential residence of palmitoylated CB_1 in cholesterol rich lipid rafts. Additional insight on how palmitoylation promotes the residence of CB1 in lipid rafts could be obtained from multiscale simulations, i.e. coarse-grained molecular dynamics. By using a reduced representation of the receptor, water as well as lipid membranes it would be possible to sample the localization of the palmitoylated and unpalmitoylated receptor in a large multicomponent membrane with regions corresponding to lipid rafts, and regions corresponding to a standard POPC membrane. A similar approach has been successfully applied in a study of lipid-dependent GPCR oligomerisation.[181]

In summary, in this thesis we demonstrate how by combining various computational techniques in tandem with experimental data, it is possible to shed light on the functionality of GPCRs involved in neurotransmission. This work highlights the importance of collaboration and a multi-professional team to answer scientific questions.

Although computational methods present undoubtable advantages, it, it is also important to recognize their limitations. Molecular dynamics, albeit a powerful tool, is a numerical model of biological events. As such, they do not take into account various phenomena in GPCR functionality, such as changes of protonation or friction. Furthermore, when simulating molecules not included in forcefields, one has to generate new parameters for them. Despite the development of automated protocols (e.g.

http://www.paramchem.org, http://www.swissparam.ch), this is a difficult task that comes with a moderate degree of error. Additional constraints arise from limited computational resources. The current simulation timescale is not enough to observe extended processes, like receptor activation, or arrestin recruitment. Furthermore, although methods exist, to ensure proper statistical sampling of a process[182], they either require extended computational time, or identifying several structural events that can be used to adequately describe the process. Those and multiple other issues, will likely be addressed to some extent by developments of computational hardware, that will allow simulating bigger systems, for larger timescales using more realistic structural descriptors.

Chapter 5
Conclusions

1. Monoaminergic neurotransmitters primarily form polar interactions with TM5 and TM6 of their respective receptors. Exclusive interactions with TM5 leads to G-protein bias (particularly G_{oB}).

2. The D2.50A mutation appears to induce βarr bias in the δ-opioid receptor-naltrindole complex by allowing conformational flexibility of TM7. These results are in line with NMR data.

3. The phosphorylated residue T^{360} in the V_2 receptor C-terminal tail, plays an important role in receptor-arrestin interactions, promoting arrestin recruitment, receptor internalization as well as ERK signaling. MD simulations reveal that T^{360} forms a salt-bridge with a polar residue of the lariat loop of βarr 1. The formation of this bridge correlates with a more active-like conformation of arrestin. Taken together, these results help unravel how a distinct phosphorylation pattern of the C-terminal tail contributes to a distinct arrestin conformation and in turn signaling response.

4. Palmitoylation of helix 8 the CB1 in receptor, stabilizes this fragment in the helical conformation, which affects the intracellular interface of CB1. This could potentially explain why only the palmitoylated receptor interacts with caveolin 1. Furthermore, this modification promotes the interaction of the receptor with cholesterol. This can at least partially explain, why the palmitoylated receptor is found primarily within cholesterol-rich lipid rafts.

Chapter 6
List of communications

Articles:

1. Stepniewski, T.M., Oddi, S., Totaro, A., Selent, J., Scipioni, L., Dufrusine, B., Fezza, F., Dainese, E. and Maccarrone, M., 2017. Palmitoylation of cysteine 415 of CB1 receptor affects ligand-stimulated internalization and selective interaction with membrane cholesterol and caveolin 1. *Biochimica et Biophysica Acta (BBA)-Molecular and Cell Biology of Lipids*, 1862(5), pp.523-532.

Chapter 7
Appendix: communications not included in thesis

This section lists other articles published while carrying out this thesis.

Articles:

1. Conformational sensors and domain-swapping reveal structural and functional differences between arrestin isoforms. Ghosh E, Dwivedi H, Baidya M, Srivastava A, Kumari P, Stepniewski T, Kim HY, Lee MH, Gastel JV, Chaturvedi M, Roy D, Pandey S, Maharana J, Ganzalez RY, Luttrell LM, Chung KY, Dutta S, Selent J and Shukla AK., 2019, *Cell Reports.*, epub ahead of print

2. Karoussiotis, C., Marti-Solano, M., Stepniewski, T.M., Symeonof, A., Selent, J. and Georgoussi, Z., 2019. A highly conserved δ-opioid receptor region determines RGS 4 interaction. *The FEBS Journal*., epub ahead of print

3. Ghosh, E., Dwivedi, H., Baidya, M., Srivastava, A., Kumari, P., Stepniewski, T., Kim, H.R., Lee, M.H., van Gastel, J., Chaturvedi, M. and Roy, D., 2019. Conformational sensors and domain-swapping reveal structural and functional differences between β-arrestin isoforms. *bioRxiv,* p.725622.

4. Baidya, M., Kumari, P., Dwivedi, H., Ghosh, E., Sokrat, B., Sposini, S., Pandey, S., Stepniewski, T., Selent, J., Hanyaloglu, A. and Bouvier, M., 2019. Genetically encoded intrabody sensors illuminate structural and functional diversity in GPCR-β-arrestin complexes. *bioRxiv*, p.651463.

5. Stepniewski, T.M., Torrens-Fontanals, M., Rodríguez-Espigares, I., Giorgino, T., Primdahl, K.G., Vik, A., Stenstrøm, Y., Selent, J. and Hansen, T.V., 2018. Synthesis, molecular modelling studies and biological evaluation of new oxoeicosanoid receptor 1 agonists. *Bioorganic & medicinal chemistry*, 26(12), p.3580-3587.

6. Oddi, S., Totaro, A., Scipioni, L., Dufrusine, B., Stepniewski, T.M., Selent, J., Maccarrone, M. and Dainese, E., 2018. Role of palmitoylation of cysteine 415 in functional coupling CB1 receptor to Gαi2 protein. *Biotechnology and applied biochemistry*, 65(1), p.16-20.

7. Azuaje, J., López, P., Iglesias, A., Rocío, A., Pérez-Rubio, J.M., García, D., Stępniewski, T.M., García-Mera, X., Brea, J.M., Selent, J. and Pérez, D., 2017. Development of Fluorescent Probes that Target Serotonin 5-HT 2B Receptors. Scientific reports, 7(1), p.10765.

Book chapters:

1. Torrens-Fontanals, M., Stepniewski, T.M., Rodríguez-Espigares, I. and Selent, J., 2018. Application of Biomolecular Simulations to G Protein–Coupled Receptors (GPCRs). In *Biomolecular Simulations in Structure-Based Drug Discovery*, p.205-223.

2. Kaczor, A.A., Bartuzi, D., Stępniewski, T.M., Matosiuk, D. and Selent, J., 2018. Protein–Protein Docking in Drug Design and Discovery. In *Computational Drug Discovery and Design*, p. 285-305.

3. Rodríguez-Espigares, I., Kaczor, A.A., Stepniewski, T.M. and Selent, J., 2018. Challenges and Opportunities in Drug Discovery of Biased Ligands. In *Computational Methods for GPCR Drug Discovery*, p. 321-334.

Bibliography

1. Bennett, M. V. L. & Zukin, R. S. Electrical Coupling and Neuronal Synchronization in the Mammalian Brain. *Neuron* (2004). doi:10.1016/S0896-6273(04)00043-1
2. Greengard, P. The neurobiology of slow synaptic transmission. *Science* (2001). doi:10.1126/science.294.5544.1024
3. Connors, B. W. & Long, M. A. ELECTRICAL SYNAPSES IN THE MAMMALIAN BRAIN. *Annu. Rev. Neurosci.* (2004). doi:10.1146/annurev.neuro.26.041002.131128
4. Huang, Y. & Thathiah, A. Regulation of neuronal communication by G protein-coupled receptors. *FEBS Letters* (2015). doi:10.1016/j.febslet.2015.05.007
5. Russo, A. F. Overview of Neuropeptides: Awakening the Senses? *Headache* (2017). doi:10.1111/head.13084
6. Purves, D. *et al. Neuroscience 4th edition*. *4th edition* (2008).
7. Wang, H. & Zhuo, M. Group I metabotropic glutamate receptor-mediated gene transcription and implications for synaptic plasticity and diseases. *Front. Pharmacol.* (2012). doi:10.3389/fphar.2012.00189
8. Van Rossum, D. & Hanisch, U. K. Cytoskeletal dynamics in dendritic spines: Direct modulation by glutamate receptors? *Trends in Neurosciences* (1999). doi:10.1016/S0166-2236(99)01404-6
9. Holz, R. W. & Fisher, S. K. Synaptic Transmission and Cellular Signaling: An Overview. in *Basic Neurochemistry* (2012). doi:10.1016/B978-0-12-374947-5.00012-2
10. Lefkowitz, R. J. A brief history of G-protein coupled receptors (Nobel Lecture). *Angewandte Chemie - International Edition* (2013). doi:10.1002/anie.201301924
11. Jong, Y. J. I., Harmon, S. K. & O'Malley, K. L. Intracellular GPCRs Play Key Roles in Synaptic Plasticity. *ACS Chemical Neuroscience* (2018). doi:10.1021/acschemneuro.7b00516
12. Abrol, R., Kim, S. K., Bray, J. K., Griffith, A. R. & Goddard, W. A. Characterizing and predicting the functional and conformational diversity of seven-transmembrane proteins. *Methods* (2011). doi:10.1016/j.ymeth.2011.12.005
13. Kolakowski, L. F. GCRDb: A G-protein-coupled receptor database. *Receptors and Channels* (1994).

14. Taddese, B. *et al.* Do plants contain G protein-coupled receptors? *Plant Physiol.* (2014). doi:10.1104/pp.113.228874
15. Brown, N. A., Schrevens, S., Van Dijck, P. & Goldman, G. H. Fungal G-protein-coupled receptors: Mediators of pathogenesis and targets for disease control. *Nature Microbiology* (2018). doi:10.1038/s41564-018-0127-5
16. Kim, J. Y., Van Haastert, P. & Devreotes, P. N. Social senses: G-protein-coupled receptor signaling pathways in Dictyostelium discoideum. *Chemistry and Biology* (1996). doi:10.1016/S1074-5521(96)90103-9
17. Sriram, K. & Insel, P. A. G protein-coupled receptors as targets for approved drugs: How many targets and how many drugs? in *Molecular Pharmacology* (2018). doi:10.1124/mol.117.111062
18. Oprea, T. I. *et al.* Unexplored therapeutic opportunities in the human genome. *Nature Reviews Drug Discovery* (2018). doi:10.1038/nrd.2018.14
19. Vassilatis, D. K. *et al.* The G protein-coupled receptor repertoires of human and mouse. *Proc. Natl. Acad. Sci. U. S. A.* (2003). doi:10.1073/pnas.0230374100
20. Wise, A., Gearing, K. & Rees, S. Target validation of G-protein coupled receptors. *Drug Discovery Today* (2002). doi:10.1016/S1359-6446(01)02131-6
21. Wacker, D., Stevens, R. C. & Roth, B. L. How Ligands Illuminate GPCR Molecular Pharmacology. *Cell* **170**, 414–427 (2017).
22. Latorraca, N. R., Venkatakrishnan, A. J. & Dror, R. O. GPCR Dynamics: Structures in Motion. *Chem. Rev.* acs.chemrev.6b00177 (2016). doi:10.1021/acs.chemrev.6b00177
23. Rodríguez-Espigares, I., Kaczor, A. A. & Selent, J. *In silico* Exploration of the Conformational Universe of GPCRs. *Mol. Inform.* **35**, 227–237 (2016).
24. Samama, P., Cotecchia, S., Costa, T. & Lefkowitz, R. J. A mutation-induced activated state of the β2-adrenergic receptor. Extending the ternary complex model. *J. Biol. Chem.* (1993).
25. Kenakin, T. & Miller, L. J. Seven Transmembrane Receptors as Shapeshifting Proteins: The Impact of Allosteric Modulation and Functional Selectivity on New Drug Discovery. *Pharmacol. Rev.* **62**, 265–304 (2010).

26. Maurice, P. *et al.* GPCR-Interacting Proteins, Major Players of GPCR Function. in *Advances in Pharmacology* (2011). doi:10.1016/B978-0-12-385952-5.00001-4
27. Birnbaumer, L., Abramowitz, J. & Brown, A. M. Receptor-effector coupling by G proteins. *BBA - Reviews on Biomembranes* (1990). doi:10.1016/0304-4157(90)90007-Y
28. Colicelli, J. Human RAS superfamily proteins and related GTPases. *Science's STKE : signal transduction knowledge environment* (2004).
29. Yuen, J. W. F. *et al.* Activation of STAT3 by specific Gα subunits and multiple Gβγ dimers. *Int. J. Biochem. Cell Biol.* (2010). doi:10.1016/j.biocel.2010.03.017
30. Marrari, Y., Crouthamel, M., Irannejad, R. & Wedegaertner, P. B. Assembly and trafficking of heterotrimeric G proteins. *Biochemistry* (2007). doi:10.1021/bi700338m
31. Hurowitz, E. H. *et al.* Genomic characterization of the human heterotrimeric G protein alpha, beta, and gamma subunit genes. *DNA Res.* (2000).
32. Robishaw, J. D. & Berlot, C. H. Translating G protein subunit diversity into functional specificity. *Current Opinion in Cell Biology* (2004). doi:10.1016/j.ceb.2004.02.007
33. Neves, S. R., Ram, P. T. & Iyengar, R. G protein pathways. *Science* (2002). doi:10.1126/science.1071550
34. Godinho, R. O., Duarte, T. & Pacini, E. S. A. New perspectives in signaling mediated by receptors coupled to stimulatory G protein: The emerging significance of cAMP effux and extracellular cAMP-adenosine pathway. *Frontiers in Pharmacology* (2015). doi:10.3389/fphar.2015.00058
35. Gilman, A. G. G proteins: transducers of receptor-generated signals. *Annual review of biochemistry* **56**, 615–649 (1987).
36. Mizuno, N. & Itoh, H. Functions and regulatory mechanisms of Gq-signaling pathways. *NeuroSignals* (2009). doi:10.1159/000186689
37. Dhanasekaran, N. & Dermott, J. M. Signaling by the G12 class of G proteins. *Cellular Signalling* (1996). doi:10.1016/0898-6568(96)00048-4
38. Stephens, G. J. G-protein-coupled-receptor-mediated presynaptic inhibition in the cerebellum. *Trends in Pharmacological Sciences* (2009). doi:10.1016/j.tips.2009.05.008
39. Krasel, C. & Lohse, M. J. G protein coupled receptor kinases.

in *xPharm: The Comprehensive Pharmacology Reference* (2007). doi:10.1016/B978-008055232-3.63085-5

40. Gurevich, V. V. & Gurevich, E. V. The structural basis of arrestin-mediated regulation of G-protein-coupled receptors. *Pharmacology and Therapeutics* (2006). doi:10.1016/j.pharmthera.2005.09.008
41. Scheerer, P. & Sommer, M. E. Structural mechanism of arrestin activation. *Current Opinion in Structural Biology* (2017). doi:10.1016/j.sbi.2017.05.001
42. Luttrell, L. M. & Miller, W. E. Arrestins as regulators of kinases and phosphatases. in *Progress in Molecular Biology and Translational Science* (2013). doi:10.1016/B978-0-12-394440-5.00005-X
43. Grundmann, M. *et al.* Lack of beta-arrestin signaling in the absence of active G proteins. *Nat. Commun.* (2018). doi:10.1038/s41467-017-02661-3
44. Craft, C. M., Whitmore, D. H. & Wiechmann, A. F. Cone arrestin identified by targeting expression of a functional family. *J. Biol. Chem.* (1994).
45. Smith, J. S. & Rajagopal, S. The β-Arrestins: Multifunctional regulators of G protein-coupled receptors. *J. Biol. Chem.* (2016). doi:10.1074/jbc.R115.713313
46. Love, T. M. Oxytocin, motivation and the role of dopamine. *Pharmacology Biochemistry and Behavior* (2014). doi:10.1016/j.pbb.2013.06.011
47. Hen, R. & Nautiyal, K. M. Serotonin receptors in depression: From A to B. *F1000Research* (2017). doi:10.12688/f1000research.9736.1
48. Bowers, M. E., Choi, D. C. & Ressler, K. J. Neuropeptide regulation of fear and anxiety: Implications of cholecystokinin, endogenous opioids, and neuropeptide Y. *Physiol. Behav.* (2012). doi:10.1016/j.physbeh.2012.03.004
49. Leung, C. C. Y. & Wong, Y. H. Role of G protein-coupled receptors in the regulation of structural plasticity and cognitive function. *Molecules* (2017). doi:10.3390/molecules22071239
50. Beaulieu, J. M. & Gainetdinov, R. R. The physiology, signaling, and pharmacology of dopamine receptors. *Pharmacological Reviews* (2011). doi:10.1124/pr.110.002642
51. Jaber, M., Robinson, S. W., Missale, C. & Caron, M. G. Dopamine receptors and brain function. *Neuropharmacology* (1996). doi:10.1016/S0028-3908(96)00100-1

52. Levey, A. I. *et al.* Localization of D1 and D2 dopamine receptors in brain with subtype-specific antibodies. *Proc. Natl. Acad. Sci. U. S. A.* (1993). doi:10.1073/pnas.90.19.8861
53. Ryczko, D. & Dubuc, R. Dopamine and the brainstem locomotor networks: From lamprey to human. *Frontiers in Neuroscience* (2017). doi:10.3389/fnins.2017.00295
54. Bressan, R. A. & Crippa, J. A. The role of dopamine in reward and pleasure behaviour - Review of data from preclinical research. *Acta Psychiatrica Scandinavica, Supplement* (2005).
55. Puig, M. V., Rose, J., Schmidt, R. & Freund, N. Dopamine modulation of learning and memory in the prefrontal cortex: Insights from studies in primates, rodents, and birds. *Frontiers in Neural Circuits* (2014). doi:10.3389/fncir.2014.00093
56. Volkow, N. D. & Morales, M. The Brain on Drugs: From Reward to Addiction. *Cell* (2015). doi:10.1016/j.cell.2015.07.046
57. Elsworth, J. D. & Roth, R. H. Dopamine synthesis, uptake, metabolism, and receptors: Relevance to gene therapy of Parkinson's disease. *Exp. Neurol.* (1997). doi:10.1006/exnr.1996.6379
58. Ashok, A. H. *et al.* The dopamine hypothesis of bipolar affective disorder: The state of the art and implications for treatment. *Molecular Psychiatry* (2017). doi:10.1038/mp.2017.16
59. Masri, B. *et al.* Antagonism of dopamine D2 receptor/β-arrestin 2 interaction is a common property of clinically effective antipsychotics. *Proc. Natl. Acad. Sci. U. S. A.* (2008). doi:10.1073/pnas.0803522105
60. Pupo, A. S. & Minneman, K. P. Adrenergic Pharmacology: Focus on the Central Nervous System. *CNS Spectr.* **6**, 656–662 (2001).
61. Robertson, D. The Adrenergic Receptor in the 21st Century. *Br. J. Clin. Pharmacol.* (2006). doi:10.1111/j.1365-2125.2006.02645.x
62. Sirviö, J. & MacDonald, E. Central α1-adrenoceptors: Their role in the modulation of attention and memory formation. *Pharmacology and Therapeutics* (1999). doi:10.1016/S0163-7258(99)00017-0
63. Heneka, M. T. *et al.* Noradrenergic Depletion Potentiates β-Amyloid-Induced Cortical Inflammation: Implications for Alzheimer's Disease. *J. Neurosci.* (2002).

64. Berridge, C. W. & Waterhouse, B. D. The locus coeruleus-noradrenergic system: Modulation of behavioral state and state-dependent cognitive processes. *Brain Research Reviews* (2003). doi:10.1016/S0165-0173(03)00143-7
65. Maletic, V., Eramo, A., Gwin, K., Offord, S. J. & Duffy, R. A. The role of norepinephrine and its α-adrenergic receptors in the pathophysiology and treatment of major depressive disorder and schizophrenia: A systematic Review. *Frontiers in Psychiatry* (2017). doi:10.3389/fpsyt.2017.00042
66. Cheng, J. T. & Kuo, D. Y. Both α1-adrenergic and D1-dopaminergic neurotransmissions are involved in phenylpropanolamine-mediated feeding suppression in mice. *Neurosci. Lett.* (2003). doi:10.1016/S0304-3940(03)00637-2
67. Khan, Z. P., Ferguson, C. N. & Jones, R. M. Alpha-2 and imidazoline receptor agonists. Their pharmacology and therapeutic role. *Anaesthesia* (1999). doi:10.1046/j.1365-2044.1999.00659.x
68. Cottingham, C. & Wang, Q. α2 adrenergic receptor dysregulation in depressive disorders: Implications for the neurobiology of depression and antidepressant therapy. *Neuroscience and Biobehavioral Reviews* (2012). doi:10.1016/j.neubiorev.2012.07.011
69. Dahlström, A. & Fuxe, K. Localization of monoamines in the lower brain stem. *Experientia* (1964). doi:10.1007/BF02147990
70. Berger, M., Gray, J. A. & Roth, B. L. The Expanded Biology of Serotonin. *Annu. Rev. Med.* (2009). doi:10.1146/annurev.med.60.042307.110802
71. Wirth, A., Holst, K. & Ponimaskin, E. How serotonin receptors regulate morphogenic signalling in neurons. *Progress in Neurobiology* (2017). doi:10.1016/j.pneurobio.2016.03.007
72. Barnes, N. M. & Sharp, T. A review of central 5-HT receptors and their function. *Neuropharmacology* (1999). doi:10.1016/S0028-3908(99)00010-6
73. Meeter, M., Talamini, L., Schmitt, J. A. J. & Riedel, W. J. Effects of 5-HT on memory and the hippocampus: Model and data. *Neuropsychopharmacology* (2006). doi:10.1038/sj.npp.1300869
74. Schiapparelli, L., Del Río, J. & Frechilla, D. Serotonin 5-HT1A receptor blockade enhances Ca 2+/calmodulin-

dependent protein kinase II function and membrane expression of AMPA receptor subunits in the rat hippocampus: Implications for memory formation. *J. Neurochem.* (2005). doi:10.1111/j.1471-4159.2005.03193.x

75. Lesch, K. P. *et al.* Association of anxiety-related traits with a polymorphism in the serotonin transporter gene regulatory region. *Science (80-.).* (1996). doi:10.1126/science.274.5292.1527
76. Żmudzka, E., Sałaciak, K., Sapa, J. & Pytka, K. Serotonin receptors in depression and anxiety: Insights from animal studies. *Life Sciences* (2018). doi:10.1016/j.lfs.2018.08.050
77. Leibowitz, S. F. The Role of Serotonin in Eating Disorders. *Drugs* (1990). doi:10.2165/00003495-199000393-00005
78. Yohn, C. N., Gergues, M. M. & Samuels, B. A. The role of 5-HT receptors in depression Tim Bliss. *Molecular Brain* (2017). doi:10.1186/s13041-017-0306-y
79. Blier, P. & de Montigny, C. Serotonin and drug-induced therapeutic responses in major depression, obsessive-compulsive and panic disorders. *Neuropsychopharmacology* (1999). doi:10.1016/S0893-133X(99)00036-6
80. Negro, A., Koverech, A. & Martelletti, P. Serotonin receptor agonists in the acute treatment of migraine: A review on their therapeutic potential. *Journal of Pain Research* (2018). doi:10.2147/JPR.S132833
81. Meltzer, H. Y. & Massey, B. W. The role of serotonin receptors in the action of atypical antipsychotic drugs. *Current Opinion in Pharmacology* (2011). doi:10.1016/j.coph.2011.02.007
82. Vollenweider, F. X., Vollenweider-Scherpenhuyzen, M. F. I., Bäbler, A., Vogel, H. & Hell, D. Psilocybin induces schizophrenia-like psychosis in humans via a serotonin-2 agonist action. *Neuroreport* (1998). doi:10.1097/00001756-199812010-00024
83. Santini, M. A. *et al.* Enhanced prefrontal serotonin 2A receptor signaling in the subchronic phencyclidine mouse model of schizophrenia. *J. Neurosci. Res.* (2013). doi:10.1002/jnr.23198
84. Miyamoto, S., Miyake, N., Jarskog, L. F., Fleischhacker, W. W. & Lieberman, J. A. Pharmacological treatment of schizophrenia: A critical review of the pharmacology and clinical effects of current and future therapeutic agents.

Molecular Psychiatry (2012). doi:10.1038/mp.2012.47
85. Valentino, R. J. & Volkow, N. D. Untangling the complexity of opioid receptor function. *Neuropsychopharmacology* (2018). doi:10.1038/s41386-018-0225-3
86. Waldhoer, M., Bartlett, S. E. & Whistler, J. L. ECEPTORS Maria Waldhoer, Selena E. Bartlett, and Jennifer L. Whistler. (2004). doi:10.1146/annurev.biochem.73.011303.073940
87. Peciña, M. *et al.* Endogenous opioid system dysregulation in depression: implications for new therapeutic approaches. *Molecular Psychiatry* (2019). doi:10.1038/s41380-018-0117-2
88. Law, P. Y. & Loh, H. H. Opioid Receptors. in *Encyclopedia of Biological Chemistry: Second Edition* (2013). doi:10.1016/B978-0-12-378630-2.00347-9
89. Matthes, H. W. D. *et al.* Loss of morphine-induced analgesia, reward effect and withdrawal symptoms in mice lacking the μ-opioid-receptor gene. *Nature* (1996).
90. Zadina, J. E., Harrison, L. M., Ge, L. J., Kastin, A. J. & Chang, S. L. Differential regulation of mu and delta opiate receptors by morphine, selective agonists and antagonists and differentiating agents in SH-SY5Y human neuroblastoma cells. *J. Pharmacol. Exp. Ther.* (1994).
91. Trescot, A. M., Datta, S., Lee, M. & Hans, H. Opioid pharmacology. *Pain Physician* (2008).
92. Siuda, E. R., Carr, R., Rominger, D. H. & Violin, J. D. Biased mu-opioid receptor ligands: a promising new generation of pain therapeutics. *Current Opinion in Pharmacology* (2017). doi:10.1016/j.coph.2016.11.007
93. Herkenham, M. *et al.* Characterization and localization of cannabinoid receptors in rat brain: A quantitative in vitro autoradiographic study. *J. Neurosci.* (1991).
94. Schlicker, E. & Kathmann, M. Modulation of transmitter release via presynaptic cannabinoid receptors. *Trends in Pharmacological Sciences* (2001). doi:10.1016/S0165-6147(00)01805-8
95. Hampson, R. E. & Deadwyler, S. A. Cannabinoids, hippocampal function and memory. *Life Sci.* (1999). doi:10.1016/S0024-3205(99)00294-5
96. Hill, M. N. *et al.* Endogenous cannabinoid signaling is essential for stress adaptation. *Proc. Natl. Acad. Sci. U. S. A.* (2010). doi:10.1073/pnas.0914661107

97. Starowicz, K., Malek, N. & Przewlocka, B. Cannabinoid receptors and pain. *Wiley Interdiscip. Rev. Membr. Transp. Signal.* (2013). doi:10.1002/wmts.83
98. Perucca, E. Cannabinoids in the Treatment of Epilepsy: Hard Evidence at Last? *J. Epilepsy Res.* (2017). doi:10.14581/jer.17012
99. Guggenhuber, S., Monory, K., Lutz, B. & Klugmann, M. AAV vector-mediated overexpression of CB1 cannabinoid receptor in pyramidal neurons of the hippocampus protects against seizure-induced excitoxicity. *PLoS One* (2010). doi:10.1371/journal.pone.0015707
100. Rubino, T., Zamberletti, E. & Parolaro, D. Endocannabinoids and mental disorders. in *Handbook of Experimental Pharmacology* (2015). doi:10.1007/978-3-319-20825-1_9
101. Ashton, C. H., Moore, P. B., Gallagher, P. & Young, A. H. Cannabinoids in bipolar affective disorder: A review and discussion of their therapeutic potential. *Journal of Psychopharmacology* (2005). doi:10.1177/0269881105051541
102. Ortega-Alvaro, A., Aracil-Fernández, A., García-Gutiérrez, M. S., Navarrete, F. & Manzanares, J. Deletion of CB2 cannabinoid receptor induces schizophrenia-related behaviors in mice. *Neuropsychopharmacology* (2011). doi:10.1038/npp.2011.34
103. Wei, H. *et al.* Independent β-arrestin 2 and G protein-mediated pathways for angiotensin II activation of extracellular signal-regulated kinases 1 and 2. *Proc. Natl. Acad. Sci. U. S. A.* (2003). doi:10.1073/pnas.1834556100
104. Azzi, M. *et al.* β-arrestin-mediated activation of MAPK by inverse agonists reveals distinct active conformations for G protein-coupled receptors. *Proc. Natl. Acad. Sci. U. S. A.* (2003). doi:10.1073/pnas.1936664100
105. Kenakin, T. Collateral efficacy in drug discovery: taking advantage of the good (allosteric) nature of 7TM receptors. *Trends in Pharmacological Sciences* (2007). doi:10.1016/j.tips.2007.06.009
106. Kobilka, B. K. & Deupi, X. Conformational complexity of G-protein-coupled receptors. *Trends in Pharmacological Sciences* (2007). doi:10.1016/j.tips.2007.06.003
107. Michel, M. C. & Charlton, S. J. Biased agonism in drug discovery-is it too soon to choose a path? in *Molecular*

Pharmacology (2018). doi:10.1124/mol.117.110890
108. Komatsu, H., Fukuchi, M. & Habata, Y. Potential Utility of Biased GPCR Signaling for Treatment of Psychiatric Disorders. *Int. J. Mol. Sci.* (2019). doi:10.3390/ijms20133207
109. Senese, N. B., Rasenick, M. M. & Traynor, J. R. The role of G-proteins and G-protein regulating proteins in depressive disorders. *Frontiers in Pharmacology* (2018). doi:10.3389/fphar.2018.01289
110. Komatsu, H. Novel therapeutic GPCRS for psychiatric disorders. *Int. J. Mol. Sci.* (2015). doi:10.3390/ijms160614109
111. Catapano, L. A. & Manji, H. K. G protein-coupled receptors in major psychiatric disorders. *Biochimica et Biophysica Acta - Biomembranes* (2007). doi:10.1016/j.bbamem.2006.09.025
112. Vaidehi, N., Brown, J. T., Goddard, W. A. & Mailman, R. B. ScienceDirect.com - Neuropharmacology - Functional selectivity of dopamine D1 receptor agonists in regulating the fate of internalized receptors. … (2007).
113. Hill, S. J. *et al.* International union of pharmacology. XIII. Classification of histamine receptors. *Pharmacological Reviews* (1997).
114. Poulin, B. *et al.* The M3-muscarinic receptor regulates learning and memory in a receptor phosphorylation/arrestin-dependent manner. *Proc. Natl. Acad. Sci. U. S. A.* (2010). doi:10.1073/pnas.0914801107
115. Gromada, J. & Hughes, T. E. Ringing the dinner bell for insulin: Muscarinic M3 receptor activity in the control of pancreatic β cell function. *Cell Metabolism* (2006). doi:10.1016/j.cmet.2006.05.004
116. Porter-Stransky, K. A. & Weinshenker, D. Arresting the Development of Addiction: The Role of β-Arrestin 2 in Drug Abuse. *Journal of Pharmacology and Experimental Therapeutics* (2017). doi:10.1124/jpet.117.240622
117. Raehal, K. M. & Bohn, L. M. β-arrestins: Regulatory role and therapeutic potential in opioid and cannabinoid receptor-mediated analgesia. *Handb. Exp. Pharmacol.* (2014). doi:10.1007/978-3-642-41199-1_22
118. Broom, D. C. *et al.* Convulsant activity of a non-peptidic δ-opioid receptor agonist is not required for its antidepressant-like effects in Sprague-Dawley rats. *Psychopharmacology (Berl).* (2002). doi:10.1007/s00213-002-1179-y
119. Brust, T. F. *et al.* Biased agonists of the kappa opioid receptor

suppress pain and itch without causing sedation or dysphoria. *Sci. Signal.* (2016). doi:10.1126/scisignal.aai8441

120. González-Maeso, J. *et al.* Hallucinogens Recruit Specific Cortical 5-HT 2A Receptor-Mediated Signaling Pathways to Affect Behavior. *Neuron* (2007). doi:10.1016/j.neuron.2007.01.008
121. Seyedabadi, M., Ghahremani, M. H. & Albert, P. R. Biased signaling of G protein coupled receptors (GPCRs): Molecular determinants of GPCR/transducer selectivity and therapeutic potential. *Pharmacol. Ther.* **200**, 148–178 (2019).
122. Wisler, J. W. *et al.* A unique mechanism of β-blocker action: Carvedilol stimulates β-arrestin signaling. *Proc. Natl. Acad. Sci. U. S. A.* (2007). doi:10.1073/pnas.0707936104
123. Baker, D. E. Loperamide: A pharmacological review. *Reviews in Gastroenterological Disorders* (2007).
124. Urban, J. D., Vargas, G. A., Von Zastrow, M. & Mailman, R. B. Aripiprazole has functionally selective actions at dopamine D2 receptor-mediated signaling pathways. *Neuropsychopharmacology* (2007). doi:10.1038/sj.npp.1301071
125. Ok, H. G. *et al.* Can oliceridine (TRV130), an ideal novel μ receptor G protein pathway selective (μ-GPS) modulator, provide analgesia without opioid-related adverse reactions? *Korean Journal of Pain* (2018). doi:10.3344/kjp.2018.31.2.73
126. A.L., C. *et al.* TRV250: A novel biased ligand at the delta receptor for the potential treatment of migraine. *Headache* (2015).
127. Boerrigter, G. *et al.* Cardiorenal actions of TRV120027, a novel ß-arrestin-biased ligand at the angiotensin II type i receptor, in healthy and heart failure canines: A novel therapeutic strategy for acute heart failure. *Circ. Hear. Fail.* **4**, 770–778 (2011).
128. Kooistra, A. J., Kuhne, S., De Esch, I. J. P., Leurs, R. & De Graaf, C. A structural chemogenomics analysis of aminergic GPCRs: Lessons for histamine receptor ligand design. *Br. J. Pharmacol.* **170**, 101–126 (2013).
129. Erlandson, S. C., Mcmahon, C. & Kruse, A. C. Annual Review of Biophysics Structural Basis for G Protein-Coupled Receptor Signaling. 1–18 (2018). doi:10.1146/annurev-biophys
130. Yuan, S., Hu, Z., Filipek, S. & Vogel, H. W2466.48 opens a

gate for a continuous intrinsic water pathway during activation of the adenosine A2A receptor. *Angew. Chemie - Int. Ed.* (2015). doi:10.1002/anie.201409679

131. Yuan, S., Filipek, S., Palczewski, K. & Vogel, H. Activation of G-protein-coupled receptors correlates with the formation of a continuous internal water pathway. *Nat. Commun.* **5**, (2014).
132. Ballesteros, J. *et al.* Functional microdomains in G-protein-coupled receptors: The conserved arginine-cage motif in the gonadotropin-releasing hormone receptor. *J. Biol. Chem.* (1998). doi:10.1074/jbc.273.17.10445
133. Rasmussen, S. G. F. *et al.* Structure of a nanobody-stabilized active state of the β2 adrenoceptor. *Nature* (2011). doi:10.1038/nature09648
134. Liu, J. J., Horst, R., Katritch, V., Stevens, R. C. & Wüthrich, K. Biased signaling pathways in β2-adrenergic receptor characterized by 19F-NMR. *Science* **335**, 1106–10 (2012).
135. Isogai, S. *et al.* Backbone NMR reveals allosteric signal transduction networks in the β 1-adrenergic receptor. *Nature* **530**, 237–241 (2016).
136. Martí-Solano, M., Sanz, F., Pastor, M. & Selent, J. A dynamic view of molecular switch behavior at serotonin receptors: Implications for Functional selectivity. *PLoS One* **9**, (2014).
137. Xiao, K. & Liu, H. "Barcode" and Differential Effects of GPCR Phosphorylation by Different GRKs. in (2016). doi:10.1007/978-1-4939-3798-1_5
138. Ren, X. R. *et al.* Different G protein-coupled receptor kinases govern G protein and β-arrestin-mediated signaling of V2 vasopressin receptor. *Proc. Natl. Acad. Sci. U. S. A.* (2005). doi:10.1073/pnas.0409534102
139. Nobles, K. N. *et al.* Distinct phosphorylation sites on the β 2-adrenergic receptor establish a barcode that encodes differential functions of β-arrestin. *Sci. Signal.* (2011). doi:10.1126/scisignal.2001707
140. Busillo, J. M. *et al.* Site-specific phosphorylation of CXCR4 is dynamically regulated by multiple kinases and results in differential modulation of CXCR4 signaling. *J. Biol. Chem.* (2010). doi:10.1074/jbc.M109.091173
141. Liggett, S. B. Phosphorylation barcoding as a mechanism of directing GPCR signaling. *Science Signaling* (2011). doi:10.1126/scisignal.2002331

142. Butcher, A. J. *et al.* Differential G-protein-coupled receptor phosphorylation provides evidence for a signaling bar code. *J. Biol. Chem.* (2011). doi:10.1074/jbc.M110.154526
143. Kang, Y. *et al.* Crystal structure of rhodopsin bound to arrestin by femtosecond X-ray laser. *Nature* **523**, 561–7 (2015).
144. Shukla, A. K. *et al.* Structure of active β-arrestin-1 bound to a G-protein-coupled receptor phosphopeptide. *Nature* (2013). doi:10.1038/nature12120
145. Shukla, A. K. *et al.* Distinct conformational changes in β-arrestin report biased agonism at seven-transmembrane receptors. *Proc. Natl. Acad. Sci. U. S. A.* (2008). doi:10.1073/pnas.0804246105
146. Lee, M. H. *et al.* The conformational signature of β-arrestin2 predicts its trafficking and signalling functions. *Nature* (2016). doi:10.1038/nature17154
147. Mayer, D. *et al.* Distinct G protein-coupled receptor phosphorylation motifs modulate arrestin affinity and activation and global conformation. *Nat. Commun.* (2019). doi:10.1038/s41467-019-09204-y
148. Yang, F. *et al.* Phospho-selective mechanisms of arrestin conformations and functions revealed by unnatural amino acid incorporation and 19 F-NMR. *Nat. Commun.* (2015). doi:10.1038/ncomms9202
149. Yang, Z. *et al.* Phosphorylation of g protein-coupled receptors: From the barcode hypothesis to the flute model. *Molecular Pharmacology* (2017). doi:10.1124/mol.116.107839
150. Chini, B. & Parenti, M. G-protein-coupled receptors, cholesterol and palmitoylation: Facts about fats. *Journal of Molecular Endocrinology* (2009). doi:10.1677/JME-08-0114
151. Naumenko, V. S. & Ponimaskin, E. Palmitoylation as a functional regulator of neurotransmitter receptors. *Neural Plast.* (2018). doi:10.1155/2018/5701348
152. Probst, W. C., Snyder, L. A., Schuster, D. I., Brosius, J. & Sealfon, S. C. Sequence Alignment of the G-Protein Coupled Receptor Superfamily. *DNA Cell Biol.* (1992). doi:10.1089/dna.1992.11.1
153. Escribá, P. V., Wedegaertner, P. B., Goñi, F. M. & Vögler, O. Lipid-protein interactions in GPCR-associated signaling. *Biochimica et Biophysica Acta - Biomembranes* (2007). doi:10.1016/j.bbamem.2006.09.001
154. Cho, E. & Park, M. Palmitoylation in Alzheimer's disease and

other neurodegenerative diseases. *Pharmacological Research* (2016). doi:10.1016/j.phrs.2016.06.008
155. Oddi, S. *et al.* Effects of palmitoylation of Cys 415 in helix 8 of the CB 1 cannabinoid receptor on membrane localization and signalling. *Br. J. Pharmacol.* (2012). doi:10.1111/j.1476-5381.2011.01658.x
156. Liang, B. & Tamm, L. K. NMR as a tool to investigate the structure, dynamics and function of membrane proteins. *Nature Structural and Molecular Biology* (2016). doi:10.1038/nsmb.3226
157. Stenkamp, R. E., Teller, D. C. & Palczewski, K. Crystal structure of rhodopsin: A G-protein-coupled receptor. *ChemBioChem* (2002). doi:10.1002/1439-7633(20021004)3:10<963::AID-CBIC963>3.0.CO;2-9
158. Cherezov, V. *et al.* High-resolution crystal structure of an engineered human β2-adrenergic G protein-coupled receptor. *Science (80-.).* (2007). doi:10.1126/science.1150577
159. Rasmussen, S. G. F. *et al.* Crystal structure of the human β2 adrenergic G-protein-coupled receptor. *Nature* (2007). doi:10.1038/nature06325
160. Xiang, J. *et al.* Successful Strategies to Determine High-Resolution Structures of GPCRs. *Trends in Pharmacological Sciences* (2016). doi:10.1016/j.tips.2016.09.009
161. Michino, M. *et al.* Community-wide assessment of GPCR structure modelling and ligand docking: GPCR Dock 2008. *Nat. Rev. Drug Discov.* (2009). doi:10.1038/nrd2877
162. Kufareva, I. *et al.* Status of GPCR modeling and docking as reflected by community-wide GPCR Dock 2010 assessment. *Structure* **19**, 1108–1126 (2011).
163. Kufareva, I., Katritch, V., Participants of GPCR Dock 2013, Stevens, R. C. & Abagyan, R. Advances in GPCR modeling evaluated by the GPCR Dock 2013 assessment: meeting new challenges. *Structure* **22**, 1120–39 (2014).
164. Carlsson, J. *et al.* Ligand discovery from a dopamine D3 receptor homology model and crystal structure. *Nat. Chem. Biol.* (2011). doi:10.1038/nchembio.662
165. Torrens-Fontanals, M., Stepniewski, T. M., Rodríguez-Espigares, I., & Selent, J. Application of Biomolecular Simulations to G Protein–Coupled Receptors (GPCRs).e. in *Biomolecular Simulations in Structure-Based Drug Discovery* 205–223 (2018).

166. Laio, A. & Parrinello, M. Escaping free-energy minima. *Proc. Natl. Acad. Sci. U. S. A.* (2002). doi:10.1073/pnas.202427399
167. Barducci, A., Bonomi, M. & Parrinello, M. Metadynamics. *Wiley Interdisciplinary Reviews: Computational Molecular Science* **1**, 826–843 (2011).
168. Barducci, A., Bussi, G. & Parrinello, M. Well-tempered metadynamics: A smoothly converging and tunable free-energy method. *Phys. Rev. Lett.* **100**, (2008).
169. Saleh, N., Ibrahim, P., Saladino, G., Gervasio, F. L. & Clark, T. An Efficient Metadynamics-Based Protocol to Model the Binding Affinity and the Transition State Ensemble of G-Protein-Coupled Receptor Ligands. *J. Chem. Inf. Model.* **57**, 1210–1217 (2017).
170. Shang, Y. *et al.* Proposed Mode of Binding and Action of Positive Allosteric Modulators at Opioid Receptors. *ACS Chem. Biol.* **11**, 1220–1229 (2016).
171. Woodward, R., Coley, C., Daniell, S., Naylor, L. H. & Strange, P. G. Investigation of the role of conserved serine residues in the long form of the rat D2 dopamine receptor using site-directed mutagenesis. *J. Neurochem.* **66**, 394–402 (1996).
172. Fowler, J. C., Bhattacharya, S., Urban, J. D., Vaidehi, N. & Mailman, R. B. Receptor Conformations Involved in Dopamine D2L Receptor Functional Selectivity Induced by Selected Transmembrane-5 Serine Mutations. *Mol. Pharmacol.* **81**, 820–831 (2012).
173. Wiens, B. L., Nelson, C. S. & Neve, K. A. Contribution of Serine Residues to Constitutive and Agonist- Induced Signaling via the D 2S Dopamine Receptor : Evidence for Multiple , Agonist-Specific Active Conformations. *Mol. Pharmacol.* **444**, 435–444 (1998).
174. Cox, B. A., Henningsen, R. A., Spanoyannis, A., Neve, R. L. & Neve, K. A. Contributions of Conserved Serine Residues to the Interactions of Ligands with Dopamine D2 Receptors. *J. Neurochem.* **59**, 627–635 (1992).
175. McCorvy, J. D. *et al.* Structure-inspired design of β-arrestin-biased ligands for aminergic GPCRs. *Nat. Chem. Biol.* **14**, 126–134 (2018).
176. Herenbrink, C. K. *et al.* The role of kinetic context in apparent biased agonism at GPCRs. *Nat. Commun.* **7**, (2016).
177. Fenalti, G. *et al.* Molecular control of δ-opioid receptor signalling. *Nature* **506**, 191–196 (2014).

178. Shukla, A. K., Singh, G. & Ghosh, E. Emerging structural insights into biased GPCR signaling. *Trends in Biochemical Sciences* (2014). doi:10.1016/j.tibs.2014.10.001
179. Chen, Q. *et al.* Structural basis of arrestin-3 activation and signaling. *Nat. Commun.* (2017). doi:10.1038/s41467-017-01218-8
180. Lally, C. C. M., Bauer, B., Selent, J. & Sommer, M. E. C-edge loops of arrestin function as a membrane anchor. *Nat. Commun.* (2017). doi:10.1038/ncomms14258
181. Guixà-González, R. *et al.* Membrane omega-3 fatty acids modulate the oligomerisation kinetics of adenosine A2A and dopamine D2 receptors. *Sci. Rep.* **6**, 19839 (2016).
182. Chodera, J. D. & Noé, F. Markov state models of biomolecular conformational dynamics. *Current Opinion in Structural Biology* (2014). doi:10.1016/j.sbi.2014.04.002